TRAVEL TIME ESTIMATION ON URBAN ARTERIALS — A REAL TIME ASPECT

by

Jingcheng Wu

A Dissertation Submitted in

Partial Fulfillment of the

Requirements for the Degree of

Doctor of Philosophy

in Engineering

at

The University of Wisconsin — Milwaukee

December 2016

ABSTRACT

TRAVEL TIME ESTIMATION ON URBAN ARTERIALS — A REAL TIME ASPECT

by

Jingcheng Wu

The University of Wisconsin-Milwaukee, 2016
Under the Supervision of Professor Xiao Qin

This dissertation attempts to develop simple and direct approaches to estimate the vehicle queue length and travel time along signalized arterial links for real-time traffic operations. This dissertation is the first to demonstrate a process using vehicle trajectory data to generate detector volume, speed and time occupancy data, along with the generalized flow rate, density and space mean speed data. This approach minimizes detector over-counting and miss-counting issues. The detection zone can be of any shape or size and at any location along the trajectory. The relationships among detector volume, speed and time occupancy along signalized arterials are analyzed theoretically and experientially. If the generalized definitions of flow rate, density and space mean speed are used, the fundamental relationship, $v = ds$, holds valid in a signalized arterial environment. The fundamental relationship diagram plotted using field signalized arterial data has not been seen in any of the literatures reviewed.

Within the defined time-space region, the scatter diagram of the generalized density and the detector time occupancy presents a strong linear correlation. Simply converting detector volume

counts within one data collection time period to use as the generalized flow rate introduces estimation errors. There are two major reasons. The first is that vehicles don't completely cross the detector during the data collection time period. The second is that it assumes vehicles would evenly spread across the data collection time period when crossing the detection zone. Traffic flow intensity is introduced and defined within the time-space regions to provide much more accurate description of the traffic flow arrival and departure conditions.

This dissertation attempts to make improvements to the input-output technique for queue estimation along signalized links. Based on analyses of the theoretical and experiential cumulative input-output diagrams, also known as the Newell Curves, two major improvements are proposed to improve the performance of the input-output technique. The improvements take into account vehicles stop on top of detectors in the estimation, make necessary adjustments to detector vehicle counts, and introduce a reset mechanism to remove the accumulated estimation errors during a long time period. The improvements are tested using two sets of field data. One set of data are 10-second queue and virtual detector data generated using the Federal Highway Administration Next Generation Simulation Peachtree Street dataset. The other set of data are field manually collected 20-second queue, and loop detector vehicle count and time occupancy data at metered on-ramps. It is concluded that both improvements help to produce estimation results far better than the original input-output technique. With adjusted detector vehicle counts, the performance of the Kalman Filter queue estimation model is also improved.

A simple conservation law approach is developed to estimate travel time along signalized arterial links. Inputs used include the traffic flow intensity at input and out detectors, plus the initial

vehicle queue. The estimated travel time is tested with the field travel time data to evaluate the performance of the estimation. The developed model is also compared with the NCHRP Project 3-79 model and the Little's Law queueing theory model. The developed model performs much better for per short interval travel time estimation.

The proposed travel time estimation approach only uses the detector volume and time occupancy data. It does not rely on signal timing data to estimate the control delay or a delay model to estimate the queueing delay. In addition, neither roadway geometry nor vehicle length data are used.

TABLE OF CONTENTS

LIST OF FIGURES

LIST OF TABLES

ACKNOWLEDGEMENTS

I would like to express my sincere appreciation and gratitude to my advisors, Professor Xiao Qin and Professor Alan J. Horowitz. I cannot complete this dissertation without their invaluable guidance and encouragement. I would also like to express my appreciation to the members of my committee, Professor Yue Liu, Professor Jie Yu and Professor Jun Zhang.

I would like to thank my family. I cannot complete my Ph.D. study without their support.

1 INTRODUCTION

Time used to travel from origin to destination is very valuable information collected by Advanced Transportation Management Systems (ATMS). Currently, travel time information is mostly provided on limited access roadways such as freeways. Traffic flow on limited access roadways is not interrupted periodically by traffic signals and can generally be considered as spatially homogeneous within a roadway segment, where flow rate, density and speed are generally consistent when vehicles travel along the roadway segment. Average spot speeds, link travel speeds and travel times can be converted between one another without introducing significant conversion error. One single average spot speed can be used to indicate travel time for a very long roadway segment with consistent geometry, homogeneous vehicle mix and stationary traffic. Traffic detectors collecting point measurements of performance like loop detectors are typically installed with a half-mile spacing and can perform well enough to provide travel times on limited access roadways.

With the development of detection technologies, many new methods to collect travel times have appeared, such as vehicle re-identification, vehicle signature matching, Bluetooth MAC address matching, license plate matching, toll tag matching, global positioning system devices, and cellular phones.

1.1 Measure Travel Time on Signalized Urban Arterials

On signalized urban arterials, sparse detection used on limited access roadways cannot provide accurate travel times. This is because traffic flow is periodically interrupted by traffic signals

and vehicles constantly go through deceleration, stop and acceleration. One signalized arterial link can be divided into a free flow section, a deceleration section, a queueing section, and an acceleration section (1). Traffic flow can no longer be considered as spatially homogeneous along a roadway segment with signals. In order to provide accurate travel times, measurements of performance from multiple points on a signalized link are needed, which requires much higher costs compared to sparse detection used on limited access roadways.

The new travel time collection technologies that have recently appeared are promising, but it is challenging to deploy them on signalized urban arterials in real-time. A signalized link often includes multiple nodes including signals, entrance points and exit points. If the travel time data collection points are selected and detection equipment is installed based on locations of these nodes, there will be too much equipment installed and it is a waste of resources. If the data collection points are selected far away from each other to collect route travel times, then spatial homogeneity may be inappropriately assumed again on signalized links. Additional errors are introduced when decomposing route travel times to individual segment travel times of roadway segments composing the route.

Generally, directly measuring travel times between two points along a signalized urban arterial through detection technologies is associated with many challenges including high implementation costs and fixed infrastructure constraints.

1.2 Estimate Travel Time through Modeling

A different approach to estimate signalized link measurements of performance appeared long before the new detection technologies came into play. Researchers have been studying various theories to model queueing at signalized intersections, such as input-output models, shock wave models, signal processing models, and probabilistic models. The extra delay time induced by queueing has also been continuously researched and various delay models have been developed including deterministic queueing models, shock wave models, steady-state stochastic models, and time-dependent models.

However, most of these queueing and delay models are very complex and were developed for planning and signal design purposes. With long data collection and analysis periods, like 15 minutes, these models tend to smooth the traffic flow dynamics and are not suitable for real time operations. In addition, most of these models were developed based on simulation studies. Traffic flow is impacted by many known and unknown factors. It is very challenging to analyze the traffic flow uncertainties using traffic simulations to model known factors. It was found in the literature review process that carefully performed empirical studies and models suitable for real-time operation purposes are very rare.

1.3 Research Objectives

Given the limitations of existing methods and studies in estimating queue and delays on arterials, the goal of this dissertation is to propose a methodology that addresses this issue from two aspects.

1. Capable of providing real-time estimation of travel times on short signalized urban arterial segments for operational purposes that can produce quick and reliable results, while capturing the traffic flow dynamics on signalized arterials;
2. Employs simple and direct approaches that are practical for daily operations, which should minimize modeling assumptions for implementation without compromising estimation accuracy, and be able to utilize detector data that are commonly available like volume, speed and occupancy.

The outcome of this research would be a queueing model and an arterial traffic flow model that can be used in real-time to estimate queue lengths and traffic flow dynamics at signalized intersections and travel time on signalized arterial streets. More specifically, the model shall be able to estimate the vehicle queue length or traffic flow dynamics in real-time with volume, speed and occupancy as inputs from just one or two spots in a signalized link. Outputs from the model will be compared with field travel time data to verify the model performance.

1.4 Research Design

Figure 1 presents the key research components of this dissertation and the process of the research design. The relationships among detector volume, speed and time occupancy along signalized arterials will be analyzed theoretically and experientially. The detector volume, speed and time occupancy will be compared with the generalized flow rate, space mean speed and density to answer the following questions.

- Are detector volume counts divided by the data collection time interval equivalent to the generalized flow rates?
- Which measurement of performance more accurately describes the vehicle arrivals and departures, detector volume counts or the generalized flow rates?
- Is detector time occupancy correlated to the generalized density?
- Is detector time occupancy equivalent to space occupancy?
- Can detector time occupancy be used as inputs to improve the queue estimation model?

Generally, input-output techniques for queue estimation are facing two challenges, how to handle long queues extending beyond the input detector and how to remove accumulated errors over time. Based on analyses of the theoretical and field cumulative input-output diagrams, improvements will be proposed to improve the performance of the input-output technique. The improved model will be tested and compared using field detector and queue data.

A simple approach to estimate travel time along a signalized arterial link suitable for real-time traffic operations will be developed. The estimation inputs will only require widely available detector volume, speed and time occupancy data. The developed model will be tested and compared using field travel time data.

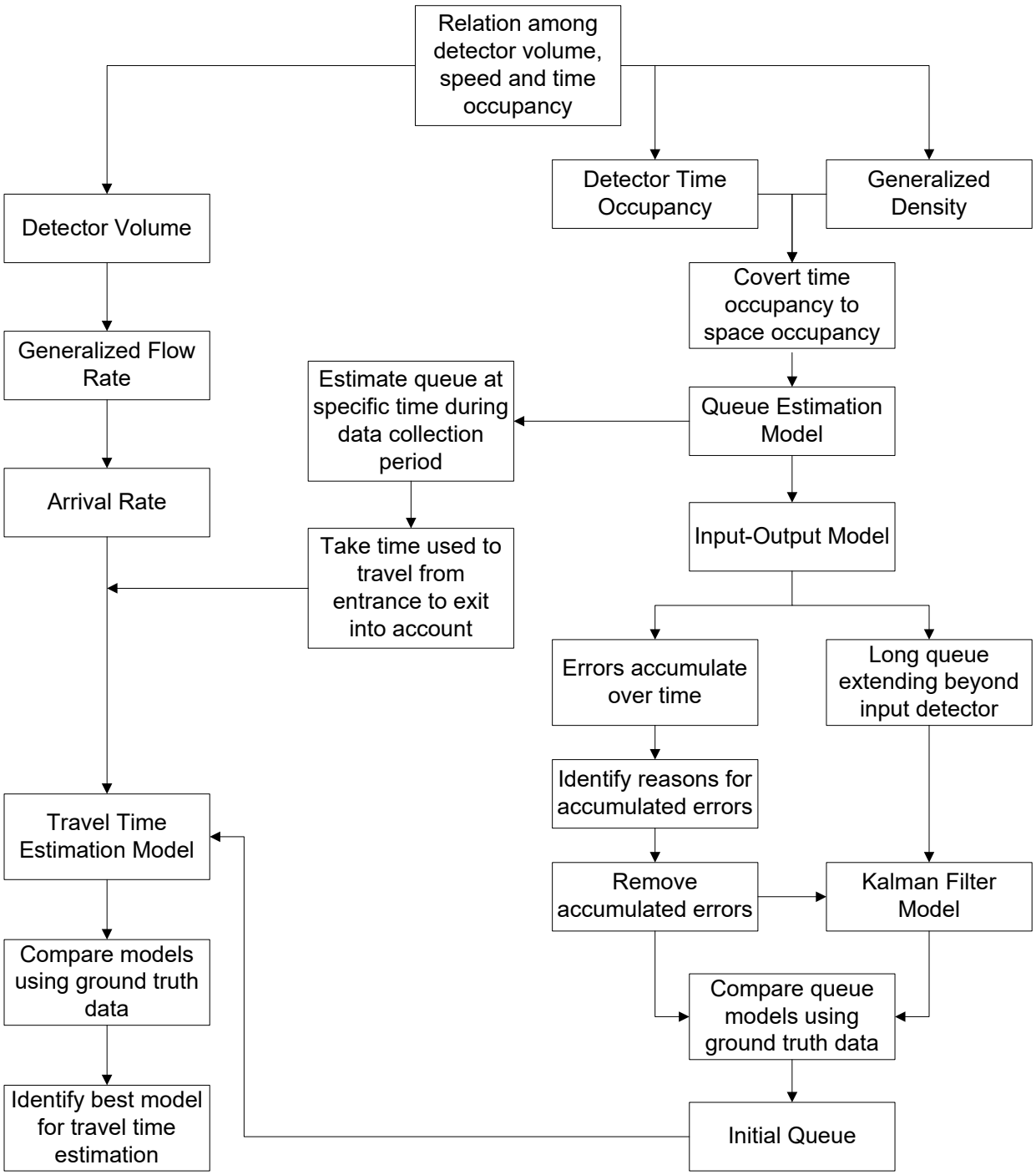

Figure 1 Key Research Components

1.5 Challenges Faced and Research Contributions

Traffic flow theories define flow rate, density and space mean speed very specifically and strictly. In practice, the most widely used data are detector vehicle count, time occupancy and speed data, which are often used interchangeably as flow rate, density and space mean speed, respectively. A knowledge gap exists that these two sets of variables can only be used interchangeably with specific conditions. If comparisons of these two sets of variables are done not in the same time-space region, then the results will be dependent on traffic conditions of the specific project location analyzed and not transferable to other project locations with different traffic conditions.

Most current queue and travel time estimation models are very complex and very challenging for implementation in practice. More complex models often require more assumptions. Complexities of the models do not guarantee accurate estimation results. Practitioners prefer to use simpler methods with minimum assumptions, even if this means the sacrifice of accuracy.

This research will connect traffic flow theories with real world traffic operations and narrow the knowledge gap in studying the characteristics of interrupted flows through field detector data with very short-time intervals, like 10 seconds. Short intervals can help to understand the signalized arterial traffic flow dynamics. The queueing model can estimate the vehicle queue length at traffic signals and on-ramps so that when the queue length exceeds a certain threshold, the vehicle queues can be flushed. The signalized arterial traffic flow model to be developed can provide real-time measurements of performance at any location along a signalized arterial link,

which are essential inputs for real-time applications and operations like connected vehicles, adaptive traffic signal control, traffic management, traveler information, and incident management. The model relies on traditional point measurements of performance so that existing detection infrastructures can be utilized to prevent introducing high costs.

In addition, the Federal Highway Administration Office of Operations is leading numerous activities to advance the implementation and practice of operations performance measurement at the Federal, State, and local levels (2). The results from this dissertation will allow various agencies to measure progress toward meeting their objectives of arterial transportation system management and operations.

1.6 Organization of Dissertation

The rest of the dissertation is organized as followed. The next section presents a summary of the literature review on existing studies in traffic flow characteristics, and queuing and delay estimation models. Then, Chapter 3 and Chapter 4 present the methodology and data used for this study, respectively. Chapter 5 summarizes preliminary analysis results of the relationships among flow rate, speed, density, and time and space occupancy. Chapter 6 presents the findings on arterial traffic flow characteristics and describes the proposed model. Finally, Chapter 7 presents the conclusions of this research.

2 LITERATURE REVIEW

In order to collect arterial link travel time information useful for traffic management centers and road users, traffic professionals have been researching and implementing two major categories of methods, directly measuring travel times between two points along an arterial street through detection technologies or estimating average travel speeds through various models based on detector data.

This literature review section starts with a review of the available detection technologies capable to collect measurements of performance at point and link levels, followed by a review of queue estimation models and delay estimation models.

2.1 Detection Technology

2.1.1 Point Measurement of Performance

Volume, speed and occupancy are usually the three basic types of information collected by traffic detectors to describe traffic conditions at any point of a roadway. There are a variety of commercially available traffic detection technologies in practice, including inductive loops, magnetic sensors, video image detectors, microwave radar sensors, infrared sensors, laser radar sensors, ultrasonic sensors, and acoustic sensors.

The inductive loop detector is the most widely used technology of traffic detection. As shown in Figure 2 (4), a loop detector system consists of three parts, a detector oscillator, a lead-in cable, and a loop embedded in the pavement consisting of one or more turns of wire. The oscillator

serves as source of energy for the loop. When a vehicle passes over the loop or is stopped within the loop area, it reduces the loop inductance, causing an increase in the oscillator frequency. The change in inductance or frequency activates a relay or circuit which sends an electrical output to the controller signifying that it has detected the presence of a vehicle. Single loop detectors can directly measure traffic counts and time occupancies, while direct measurements of speeds require a dual loop or speed trap setup.

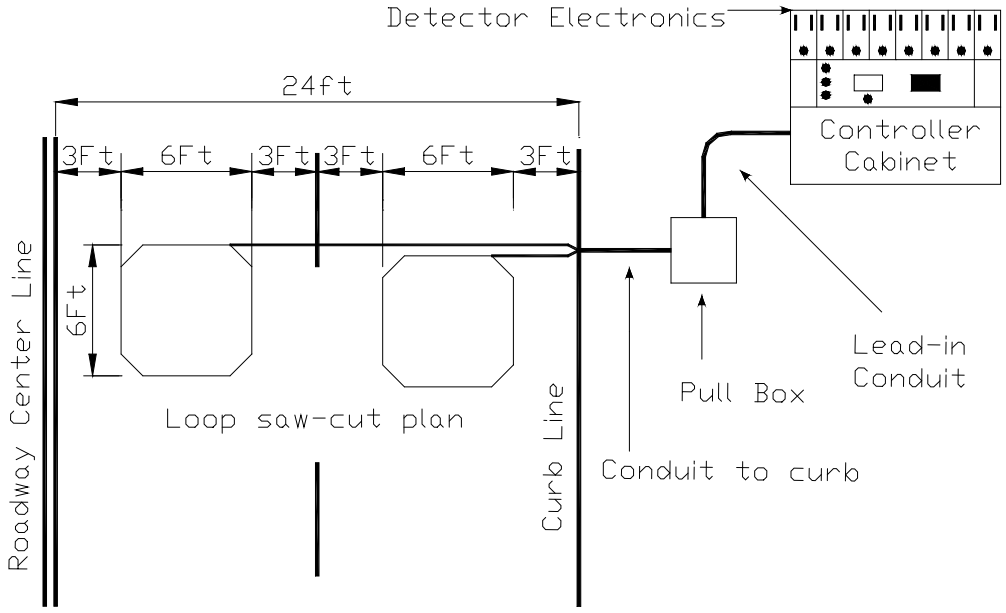

Figure 2 Inductive Loop Detector System
(Cited from Traffic Detector Handbook 2nd Edition (4))

2.1.1.1 Volume

Volume is measured as the number of vehicles passing the detector location or a point on a roadway during a data collection time interval. The equivalent hourly volume is often referred to as the flow rate.

2.1.1.2 Speed

The average travel speed along an arterial street link is defined as the length of the link divided by the travel time of vehicles traversing the link, including all stopped delay times. It is also known as the "space mean speed". The speed data collected by a detector are the arithmetic average of speeds of vehicles observed passing a point on a roadway, which is also referred to as the "time mean speed" or the average spot speed. The space mean speed is more important and often used as the performance measurement of signalized urban arterials. Figure 3 shows an example of the 10-second average spot speed data collected by a microwave sensor mounted at a midblock location.

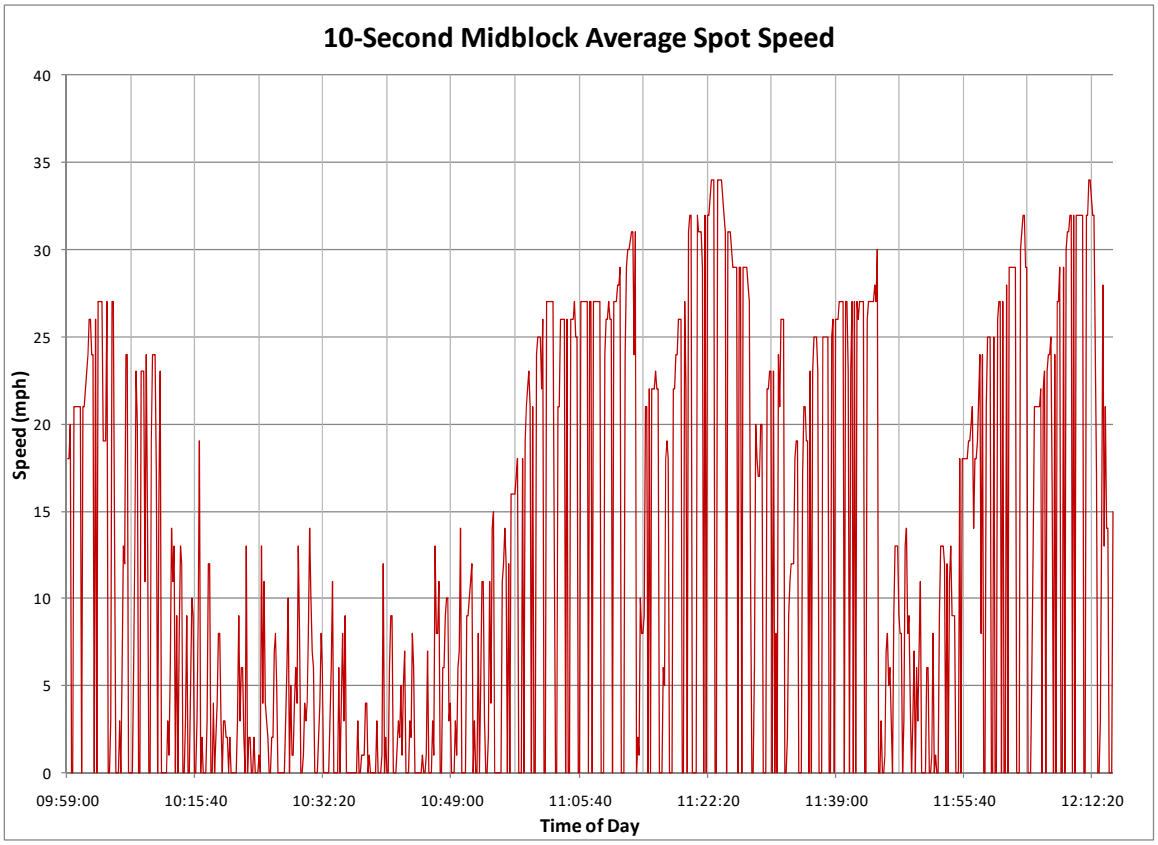

Figure 3 10-Second Midblock Average Spot Speed

Figure 4 (5) shows a comparison between the average spot speed data collected by a microwave sensor at a midblock location and the space mean speed data converted from the travel time data collected by the "floating car" technique. There were 40 floating car runs shown in Figure 4 and the arterial link included a signalized intersection. The floating car technique, also referred to as the test vehicle technique, is one of the most common travel time collection methods. The driver of the test vehicle controls the speed of the vehicle in a manner that the number of vehicles passed by the test vehicle and the number of vehicles passing the test vehicle remain as close as possible (6).

Figure 4 indicates that average spot speeds cannot accurately represent link space mean speeds.

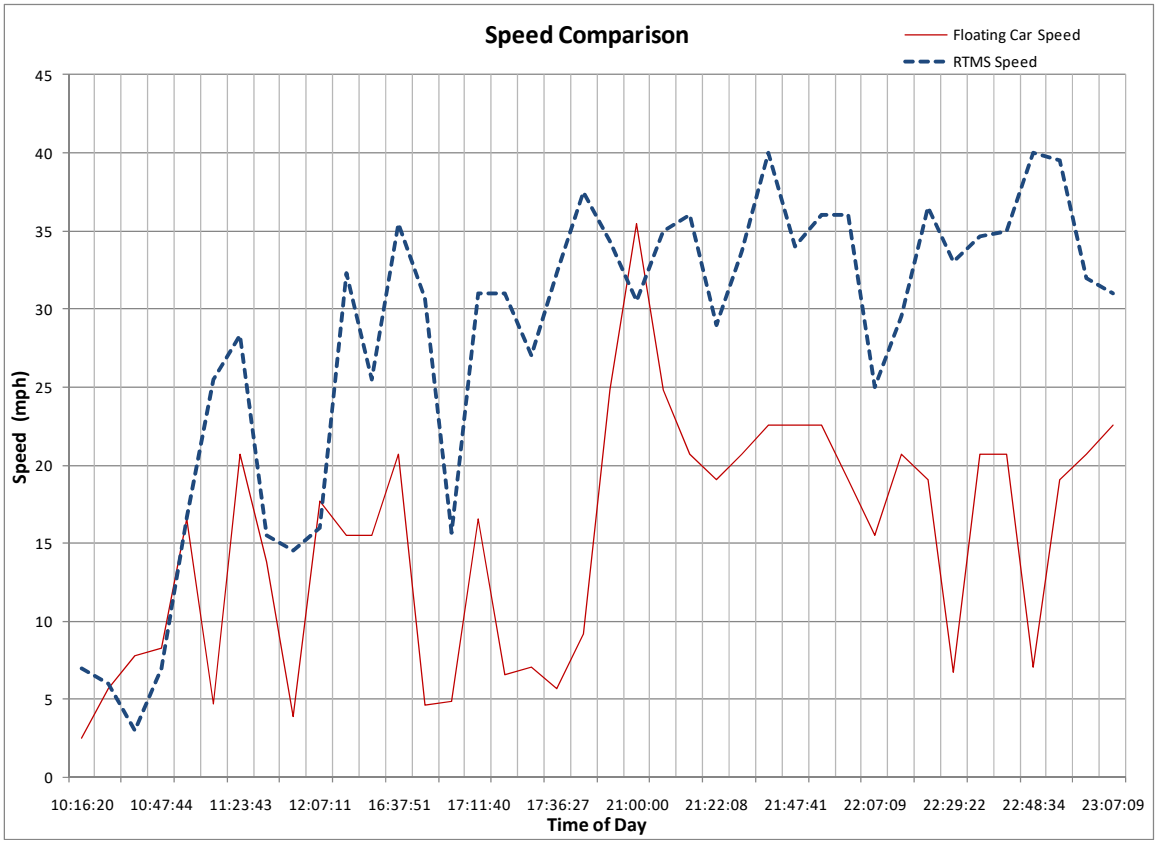

Figure 4 Comparison between Detector Spot Speed and Floating Car Speed (Cited from Riggio and Wu (5))

2.1.1.3 Occupancy

Occupancy collected by a detector is actually time occupancy, which is defined as the percentage of time the detection zone is occupied by a vehicle. The detector speed can then be calculated as shown below (Equation 1 and Figure 5). If the detector speed is available, time occupancy can be calculated similarly. Note the detector speed is actually measured as the space mean speed of vehicles crossing the detection zone.

$$S_A = \frac{L}{t} = \frac{L_v + L_d}{\frac{T \times O}{N}} = \frac{(L_v + L_d) \times N}{T \times O}$$ **Equation 1**

where

S_A = speed collected by a detector (ft/s),
L = detector effective detection length (ft),
t = time a detector is occupied by a vehicle (second),
L_v = average physical vehicle length (ft),
L_d = detector detection zone length (ft),
T = time interval for calculation (second),
O = time occupancy collected by a detector, and
N = the number of vehicles passed a detector during the calculation time interval (veh).

Note if $O = 0$, then S_A is set to free flow speed, which means no vehicles passing the detection zone or vehicles stopping outside of the detection zone during the time interval.

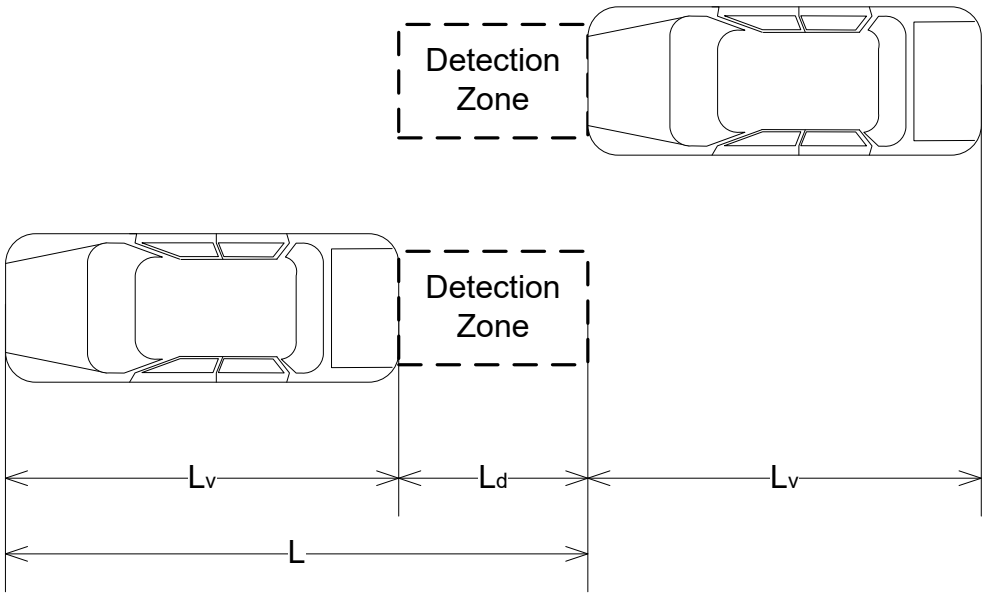

Figure 5 Detection Zone Occupied by a Vehicle

2.1.2 Link Measurement of Performance

As indicated by Figure 4, measurements of performance at a single point cannot represent the performance of the whole signalized arterial link. Collecting data at multiple points may provide

improvements, but this approach will dramatically increase the design, installation, operations, and maintenance costs.

Two common types of link measurements of performance are space mean speed and travel time, which cannot be directly collected by traditional point measurement of performance detection technologies. Other measurements at the link level include density, vehicle queue length and space occupancy. Density is the number of vehicles per mile per lane at a given time. Queue length can be described by two ways, the number of vehicles in the queue or the length in feet. Converting between the number of vehicles and the length in feet requires assuming average physical vehicle length and average space headway between vehicles. Space occupancy is defined as the proportion of space of a roadway that is covered by vehicles. Video image detectors are the only detectors currently available that can directly collect space occupancy data. However, this technology has various disadvantages including "what you see is what you get". If vehicles cannot be seen (for example, during bad weather), then they cannot be detected.

It is difficult to directly measure the link space mean speed. According to the Highway Capacity Manual (HCM) 2000 Equation 15-6 (1), the space mean speed on a link can be computed as Equation 2. The running time can be easily calculated using the free flow speed or midblock average spot speeds. The delay time can be obtained from various queueing and delay models, which often use point measurements of performance as inputs.

$$S_A = \frac{3600L}{T_R + d} \qquad \textbf{Equation 2}$$

where

S_A = space mean speed of through vehicles on the link (mi/h),
L = link length (mi),
T_R = total of running time on all segments in the defined link (s), and
d = control delay for through movements at the signalized intersections (s).

Based on Equation 1, Click and Boden (7) performed a simulation study to measure time occupancy at multiple points on a signalized link and translate the time occupancy into delay. The theoretical free flow occupancy of a given detector was first calculated. The occupancy reported by the detector minus the theoretical free flow occupancy of this detector was then computed and considered as the occupancy associated with delay for this specific detector. The simulation study found that cycle length and approach speed did not have significant impacts on the results. In addition, one stop bar detector plus one upstream detector was sufficient to produce reasonable estimation.

Click and Boden presented two very interesting occupancy vs. distance-from-stop-bar curves as shown in Figure 6 (7) and Figure 7 (8), respectively. The occupancy values shown in the figures are average values over a 15-minute period. Generally, the occupancy values are higher near the stop bar and decrease while moving away from the stop bar. Figure 6 shows the simulation occupancy curve plotted using data generated by VISSIM, a commercial traffic microsimulation package. The occupancy dip near the stop bar stems from cases when the 6-foot stop bar loop may not be occupied by vehicles. Figure 7 shows the field occupancy curve plotted using the morning peak period field data. The lower occupancy values at the stop bar are because some vehicles did not stop close enough to the stop bar and were not detected.

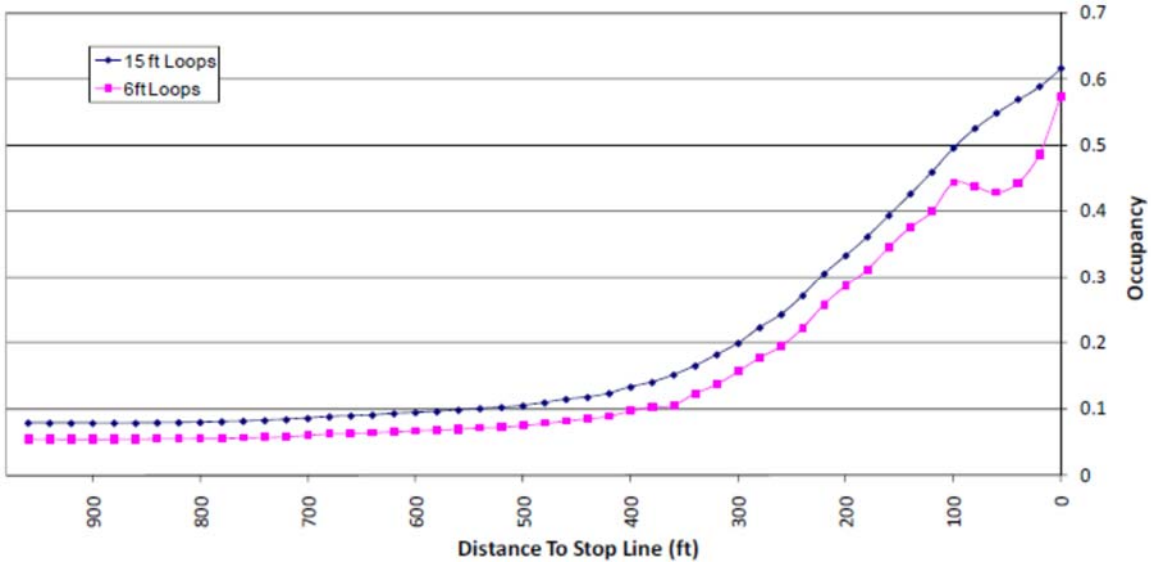

Figure 6 Simulation Occupancy Curve for Steady-State Queueing (Citied from Click and Boden (7))

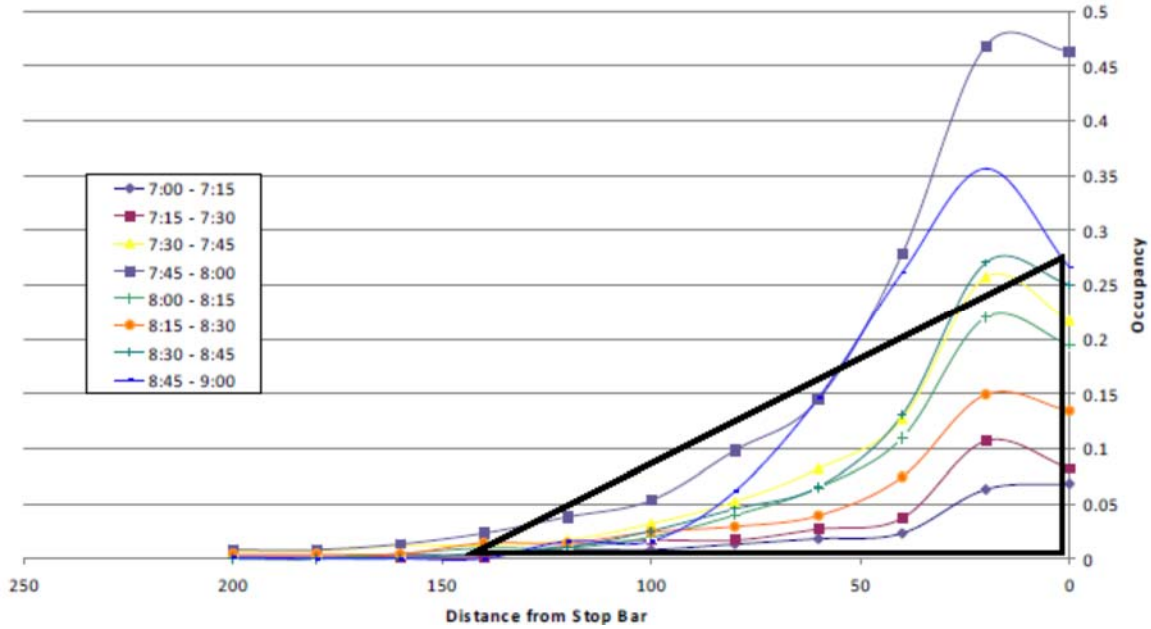

Figure 7 Field Occupancy Curve for Morning Peak Period (Cited from Boden and Click (8))

Geroliminis and Skabardonis (9) reformatted Equation 1 and added the red time cycle split to estimate the upstream detector "blocking occupancy" when queue has reached to the detector location and the detector is occupied by a stopped vehicle. Note this condition is sometimes referred to as the queue over detector effect. Wu et al. (10) studied the arterial fundamental diagram using high-resolution event-based signal phasing and loop detector data. The study demonstrated that after removing the queue over detector effect, the flow occupancy diagram did not show random fluctuations and was independent of detector locations.

$$O = \frac{(L_v + L_d) \times N}{T \times S_f} + \frac{r}{c} \qquad \textbf{Equation 3}$$

where

O = upstream detector "blocking occupancy" when queue has reached to the detector location,
S_f = vehicle free flow speed (ft/s),
r = red phase time (second), and
c = cycle length (second).

Zhang (11) developed a simple model to estimate space mean speeds on an arterial link. The model consists of two components, the critical volume to capacity ratio and volume and occupancy measured by loop detectors. The model assumes time occupancy measured as space occupancy and converts space occupancy to density as shown below.

$$D = \frac{O \times 5280}{L_v + L_d} \qquad \textbf{Equation 4}$$

where

D = density (veh/mile/lane)
O = time occupancy collected by a detector,
L_v = average physical vehicle length (ft), and
L_d = detector detection zone length (ft).

Minnesota Department of Transportation (Mn/DOT) evaluated four alternative detection methods to determine queue lengths at metered freeway on-ramps (12). The magnetic sensor queue length array method provided the best result, which had six magnetic sensors installed every 50 feet in alternating lanes along the on-ramp with the first sensor starting at 50 feet upstream of the ramp meter stop line. If the time occupancy of a sensor is higher than a pre-determined threshold, then it is determined that the queue has reached the sensor location. The queue length is estimated as the distance from the sensor location to the ramp meter stop line plus half of the distance between two sensors. This method introduces higher costs associated with the number of sensors needed. In addition, a reliable method is needed to determine the time occupancy threshold value, which does not exist currently.

2.1.3 Travel Time Measurement

It has always been challenging to measure space mean speeds or travel time on signalized urban arterials. This is because a section of urban street often includes multiple signalized intersections, which interrupt traffic flow and cause delay consisting of deceleration delay, queue move-up time, stopped delay, acceleration delay, and random effects (1). It should be noted that average travel speeds are often the direct outputs of modeling and travel times are often the direct outputs of detection technologies.

Practitioners and researchers have been researching and implementing a variety of methods to physically directly measure travel times between two points along urban streets through detection technologies. These detection technologies include at least the following.

- Vehicle re-identification or vehicle signature matching
- Media Access Control (MAC) address matching
- Vehicle license plate matching
- Vehicle toll tag matching
- Floating car technique
- Global Positioning System (GPS) devices
- Cellular phones
- Radio communication systems
- Transit vehicles equipped with automatic vehicle locators
- Aerial photographs
- Mechanical devices attached to odometers
- Pickup-delivery trucks

If data for all vehicles travelling in the roadway network cannot be collected, probe-based monitoring techniques are often resorted to for tracking only a subset of all vehicles. The population measurements of performance are then estimated based on data collected from the samples. Sample sizes or probing rates play a very important role in the performance measurement estimation results. Generally, a probing rate of 5% is necessary to prevent biased estimation (13) and a higher percentage is usually needed for oversaturated traffic conditions.

Another factor affecting the estimation is the outlier identification and filtering process used to reduce biases.

Hellinga and Fu (14) developed a stratified sampling method to improve the population mean delay estimation based on probing sample mean delay values. This method stratified the population by arrival time to create sub-intervals within each study period.

Although the travel time data collected by probing techniques are generally considered accurate, probing techniques are facing at least the following challenges.

- Privacy issues
- Minimum sample size or probing rates required
- Biased results because of differences between the population and the samples
- High implementation costs
- Fixed infrastructure constraints
- Multiple routes between data collection points
- No point measurements of performance and queue length data directly available
- Cannot be used for signal actuation (that is, dynamically changing signal timing in response to traffic conditions)

2.1.3.1 Vehicle Re-identification

Kwong et al. (15) described a system to estimate arterial travel time using the individual vehicle re-identification technique based on matching vehicle signatures from magnetic sensors (16). The matching procedure was based on a statistical model of signature distance.

Sun et al. (17) developed a method to derive travel time and travel time distributions using a platoon re-identification algorithm based on matching extracted vehicle color signatures from video image detectors. The platoon re-identification algorithm performed better than the individual vehicle re-identification algorithm in the re-identification accuracy including the mean percent error for travel time and the variance of the percentage of error. However, the length of the arterial test segment was short and the test segment did not include a traffic signal.

Abdulhai and Tabib (18) attempted to improve the accuracy of vehicle inductance signature pattern recognition using distance measures such as statistical measures, neural network based measures and warping insensitive measures. Tests based on freeway loop detector data indicated a considerable improvement in distance measures performance. The distance here refers to the statistical distance, which quantifies the closeness between two samples, two random variables, or two probability distributions. Distance measures evaluate the closeness of two vehicle signature waveforms.

2.1.3.2 Media Access Control Address Matching

The MAC address of an electronic device, such as a cell phone, a laptop, a Bluetooth headset, or a GPS device, is unique. Once a MAC address is assigned to a device, that device can be uniquely identified among all other network devices.

One study (19) attempted to use MAC addresses from various electronic devices to estimate travel time along a 5.8-mile section of freeway and an 8.5-mile section of an urban arterial. In

this study, a whip antenna was mounted adjacent to the roadway to detect MAC addresses from visible devices. MAC address matches were obtained for about 1% of the traffic between the entry and the exit points, though the percentage could be further improved in future deployments. Besides the relatively low probe sample size, the challenge is that various devices have various communication ranges, such as an 802.11g device has a 300-foot outdoor range and a Class 2 Bluetooth headset has a 33-foot range.

Other researchers explored the potential issues of MAC address matching like clock synchronization between detection stations, detection latency and multiple transportation modes present (20). Three unavoidable challenges are pointed out. First, because different devices have different communication ranges, some devices can be detected multiple times by one detection station, while other devices cannot be detected at all. The researchers proposed multiple readers at a single detection station to resolve this issue. Second, it is recognized that travel times vary between different days and between different time periods during the same day. It is important to screen outliers within the data set with the consideration of the travel time varying nature. However, the researchers have yet to identify an effective algorithm, given the fact that different calculation algorithms can produce very different results. Third, MAC addresses cannot be detected if devices are not set to discoverable mode. With users' increased awareness of privacy protection and improved technology (21), fewer devices may be detected. The MAC address matching rate of this study is 1.5% to 4.5%, which is slightly below required probing rates for congested conditions. It is also pointed out that the vehicle trajectories and spot speeds cannot be collected using MAC address matching.

Given that a vehicle could be detected anywhere within a 300-foot radius of the receiver for 802.11g devices, additional data processing measures are needed to prevent introducing a rather substantial error for MAC address matching on a short urban arterial segment. For example, an 802.11g device can be detected multiple times by a receiver within the effective range and generate multiple matches for the same device. In order to reduce the error, the matching process can always use the first reading of a device by a receiver or the longest travel time among all matches.

2.1.3.3 Vehicle License Plate Matching

The License Plate Recognition (LPR) technology is widely used in Electronic Toll Collection (ETC) systems. It uses optical character recognition software to process vehicle license plate images taken and identifies the vehicle by its license plate. Vehicle license plates can be collected with arrival times at various checkpoints to compute travel times between checkpoints. The license plate recognition and matching process can also be done manually.

Clark et al. (22) evaluated three methods to identify travel time data outliers in a vehicle license plate matching study. They are a percentile test, a mean absolute deviation test and a standardizing statistical test. The standardizing test method was recommended because it was considered to be the most robust to outlier data by the researchers.

2.1.3.4 Vehicle Toll Tag Matching

In electronic toll collection systems, some vehicles are equipped with toll tags to facilitate the payment processing. These toll tags are actually Radio-Frequency Identification (RFID)

transponders (Figure 8) transmitting signals to receivers (Figure 9) via Dedicated Short-Range Communications (DSRC). Each toll tag has a unique identification number and can be uniquely identified by tag readers. Similarly to MAC address matching and license plate matching techniques, the toll tag matching technique can also provide travel times between two tag readers. Read performance varies depending on tag and reader configuration and environment. Using the eGo Plus Windshield Sticker Tag shown in Figure 8 and the Encompass 4 reader shown in Figure 9, the typical read range should be 12 to 17 feet.

Figure 8 An Example of Toll Tag
(Cited from TransCore (23))

Figure 9 An Example of Toll Tag Reader and Antenna (Cited from TransCore (23))

Hellinga (24) examined three tag matching algorithms to calculate the individual vehicle travel time. They are maintaining the origin list in chronological order and applying a sequential search, maintaining the origin list in chronological order and applying a modified sequential search considering the minimum travel time, and sorting the origin list in non-descending order by tag IDs and applying a binary search. The analytical and simulation results indicated that the third algorithm was the most computationally efficient.

2.1.3.5 Global Positioning System Devices

Generally, Global Positioning System (GPS) devices can collect position and instantaneous velocity information. The Mobile Century field experiment (25) included about 100 vehicles each carrying a GPS-enabled Nokia N95 cell phone driving around on a 10-mile freeway segment. Time-stamped latitudes, longitudes and altitudes of each vehicle were collected every 3 seconds, along with the vehicle instantaneous velocity. The data were then processed and

published on the Internet to demonstrate the feasibility of the proposed system for real-time traffic monitoring. The probing rate of this experiment was 2-3%.

2.1.3.6 Cellular Phones

Similar to GPS devices, cellular phones can be tracked and provide travel time information between two cellular phone towers. A route connecting two cellular phone towers consists of multiple roadway segments. Hellinga et al. (26) presented an algorithm to decompose the route travel time to individual segment travel times of roadway segments composing the route. The route travel time was collected using cellular phone based traffic monitoring systems. Inferring travel times from cellular phone position data requires five steps, which include map matching, path identification, probe filtering, travel time allocation, and travel time aggregation.

2.2 Queue Estimation Models

Traffic flow consists of both deterministic components and stochastic components. Deterministic components can be described by a mathematical expression and stochastic components can only be analyzed through probability or statistics because knowledge about them is incomplete. Steady state models assume specific statistical distributions of the arrival and departure processes, and typically include a deterministic component to account for the red time and a stochastic component to account for delays caused by queueing. Steady-state models break down in oversaturated conditions (27, 28).

A review of literature reveals that models utilizing detector data to estimate vehicle queues within signalized links in real time are very rare. Four major types of queue estimation models have been studied by researchers.

2.2.1 Simple Input-Output Model

The input-output technique was first proposed by Webster (29) and later on improved by many researchers. This technique calculates the difference between the number of vehicles exiting a signalized link and the number of vehicles entering the link during a certain time interval. The calculated difference is considered as the number of vehicles within the signalized link or the vehicle queue length.

Sharma et al. (30) evaluated two input-output algorithms for vehicle delay and queue length measurements. The difference between these two algorithms is that the first algorithm uses the saturation headway data to estimate the number of departures from the stop bar and the second algorithm uses the stop bar detector to measure the actual departures. Two assumptions were made, vehicles do not change lanes after crossing the advance detectors and the first-in-first-out principle applies. It was found that both algorithms could produce satisfactory estimates of the maximum queue length. The total delay for vehicles in the queue in this study was estimated as the total area below the queue polygon. It is interesting to note that the second algorithm did not perform consistently better than the first algorithm in spite of more input information. The start-up lost time used was 4 seconds and the saturation headway used was 2 seconds.

Input-output techniques are often used in research and practice because of their simplicity to implement and providing reasonable queue length estimates with balanced volumes. However, the performance of the input-output technique estimation is not always satisfactory. In addition, generally, input-output techniques are facing two challenges, how to handle long queues extending beyond the input detector and how to remove accumulated errors over time.

Alternative techniques were analyzed by the same researchers (31) and the input-output technique was the method recommended for real-time operations. The input-output technique can be used for real-time operations like signal control and it is feasible to rely on the existing detection infrastructure. It was also pointed out that more than one video image detectors might be necessary to measure queues longer than 250 feet.

2.2.2 Kalman Filter Model

2.2.2.1 Kalman Filter Model

Vigos et al. (32) developed an input-output technique based model to estimate the number of queued vehicles within signalized links. This model employs a Kalman filter and uses data from multiple detectors as inputs, which is presented below as Equation 5 and Equation 6. Time occupancy data collected by detectors are translated into space occupancy data and used as one of the inputs. The other inputs include vehicle counts entering and exiting the signal link. Equation 5 consists of two major components, the time update component and the measurement update component. The time update is responsible for projecting forward the current state and error covariance estimates to obtain the estimate for the next time step. The measurement update is responsible for the feedback, incorporating a new measurement into the estimate to obtain an

improved estimate. Wu et al. (33) tested this Kalman filter model using manually collected field queue data and demonstrated that this algorithm could produce reasonable estimates at metered freeway on-ramps.

$$Q_n = Q_{n-1} + T(V_{in} - V_{out}) + K(q_{n-1} - Q_{n-1}) \quad \textbf{Equation 5}$$

where

Q_n = predicted number of queued vehicles in the next time period (veh),
Q_{n-1} = number of queued vehicles in the current time period (veh),
T = time interval for number of queued vehicles calculation (second),
V_{in} = flow rate entering the signalized link (veh/h),
V_{out} = flow rate exiting the signalized link (veh/h),
K = Kalman filter gain parameter, $0 \leq K \leq 1$, and
q_{n-1} = number of queued vehicles calculated from detector time occupancy data (veh), which is the result from Equation 6.

$$q_{n-1} = \frac{L \times n}{l + D} \times O_{n-1} \quad \textbf{Equation 6}$$

where

q_{n-1} = number of queued vehicles calculated from detector time occupancy data (veh),
L = length of the signalized link available for queue storage (ft),
n = number of lanes,
l = average physical vehicle length (ft),
D = safety distance between vehicles (ft), and
O_{n-1} = time occupancy collected by detectors.

Equation 6 is used to translate time occupancy data to space occupancy data. Vehicle queue length in a signalized link is directly related to space occupancy. Papageorgiou and Vigos explored the relationships between time occupancy and space occupancy (34). It was found that time occupancy was not identical to space occupancy and it was not simply proportional to space

occupancy on signalized links. The relationships were complicated and a set of formulas were proposed to convert measured time occupancy to estimated space occupancy (32). These researchers also concluded that the location of the detector was important to the occupancy conversion. In addition, if the measurement update interval was short, a higher number of detectors could improve the space occupancy or the queue length estimation.

Lee et al. (35) slightly modified the original Kalman Filter model and introduced a single point correction mechanism to eliminate accumulated errors and improve the model performance. When the mid-link detector time occupancy change from last time interval is greater than 35%, the queue length will be set to half of the maximum queue length. This single point correction mechanism is developed based on a simulation analysis indicating that the back of the queue is close to the mid-link detector location, when there is a significant increase or decrease of the mid-block detector time occupancies.

2.2.2.2 Exponential Smoothing Model

Vigos and Papageorgiou (36) developed a simplified exponential smoothing estimator based on the Kalman filter model to estimate queue lengths using one single time-occupancy measurement in a signalized link. The simulation results showed reasonable estimation performance with the advantage of low calibration efforts. Equation 7 is the proposed exponential smoothing formula. If Equation 7 is rearranged to Equation 8, it is identical to Equation 5 with the predictive flow based time update component removed.

$$Q_n = K_{ES} \times q_{n-1} + (1 - K_{ES})Q_{n-1}$$ **Equation 7**

$$Q_n = Q_{n-1} + K_{ES}(q_{n-1} - Q_{n-1})$$ **Equation 8**

where

K_{ES} = exponential smoothing coefficient, $0 \leq K_{ES} \leq 1$.

2.2.2.3 Volume Balancing

When Wu et al. (37) tested the Kalman filter using field manually collected queue data, it was found that measured entering and exiting volumes for the signalized link over a long period of time were considerably and unexpectedly different, leading to the conclusion that some detectors are prone to miscounting. In order to account for this miscounting behavior, an adjustment factor was introduced to balance the volume input and volume output, which created slightly modified version of Equation 5.

$$Q_n = Q_{n-1} + T(CV_{in} - V_{out}) + K(q_{n-1} - Q_{n-1})$$ **Equation 9**

where

C = adjustment factor to account for the miscounting of the detectors.

A simple input-output model to calculate the number of vehicles in a signalized link during the calculation time period was also included for comparison.

$$Q_n = Q_{n-1} + N_{in} - N_{out}$$ **Equation 10**

where

N_{in} = vehicle counts entering the signalized link during a data collection time interval like 10 seconds (veh), and
N_{out} = vehicle counts exiting the signalized link during the same time interval (veh).

A volume balancing ratio was also introduced to Equation 10 to create a slightly modified version.

$$Q_n = Q_{n-1} + CN_{in} - N_{out} \quad \textbf{Equation 11}$$

The analysis shows that the volume balancing ratio improves both models, the Kalman Filter and the simple input-output model. While the simple input-output model may provide more accurate prediction with balanced volumes, the Kalman filter tends to provide better estimation when the volume balancing ratio deviates from 1. Although the Kalman filter provides generally a better prediction, the simple input-output model is simpler to implement.

2.2.3 Shock Wave Model

Lighthill and Whitham (38, 39) and Richards (40) developed the shock wave theory for uninterrupted traffic flow, and later it was applied by Stephanopoulos and Michalopoulos (41, 42) to signalized intersections. Stephanopoulos et al. investigated the queueing and discharging dynamics at isolated signalized intersections by employing the simple continuum model. The difference between the queue size and the queue length was emphasized. The queue size usually refers to the number of vehicles in the queue and assumes compact queues, which tends to miscalculate the queue length by using average space headway for calculation. A shock wave was defined as the propagation of an abrupt discontinuity of flow or density. A model was

developed to estimate queue lengths by tracing the trajectory of shock waves based on the conservation equation. The model successfully described the queueing and discharging processes in both temporal and spatial dimensions. The model inputs require known vehicle arrival information, which are often not available in practice. The conservation equation attempts to describe traffic flows solely based on deterministic components of traffic flows.

2.2.3.1 Break Point Identification

Liu et al. (43) developed a break point identification process to rebuild traffic shock waves using high-resolution event-based loop detector data. A break point is defined as the point in a time-space diagram where a shock wave propagates through the advanced detector location of a signalized intersection. The first precondition of the identification process is that the back of queue must traverse the advance detector location during queueing and discharging processes. The second precondition is that there is a traffic state change before and after the break point. If either of the preconditions does not exist, then the break point cannot be identified. The field evaluation results demonstrated that the break point identification process could estimate long queues extending beyond the advance detector location with satisfactory accuracy. The advanced detectors used in the study were located about 400 feet upstream from the stop bar.

Because of the uniqueness of the high-resolution event-based data or second-by-second data, this model cannot be used with its original form if such data are not available. In addition, it is assumed that advanced detectors are available and signal timing information is known at run time.

In the queue building process, when the queueing shock wave had propagated to the advance detector location, the advanced detector will be occupied by vehicles and the detector time occupancy will increase from the free flow range to the queue over detector range. 3 seconds was used as the occupancy threshold to determine the occurrence of this phenomenon (break point A in Figure 10). In the queue discharging process, 2.5 seconds was used as the time gap threshold to indicate that the queue discharging shock wave had reached the advance detector location (break point C in Figure 10). These two threshold values are experiential numbers selected based on specific field data collected from specific sites so that the same values may not be applicable to other data sets with longer aggregation intervals and other sites with different field conditions. Longer occupancy aggregation intervals tend to smooth the occupancy values.

Figure 10 shows break points A, B and C, which are identified through examining the high-resolution data and then used to rebuild traffic shock waves within a signal cycle. A set of formulas developed to rebuild traffic shock waves are described below. If break point C cannot be identified, then T_C can be assumed to happen at T_r^{n+1} (44). Liu et al. (45) further improved the model by introducing parameters including the vehicle desired travel speed and the vehicle acceleration and deceleration rates.

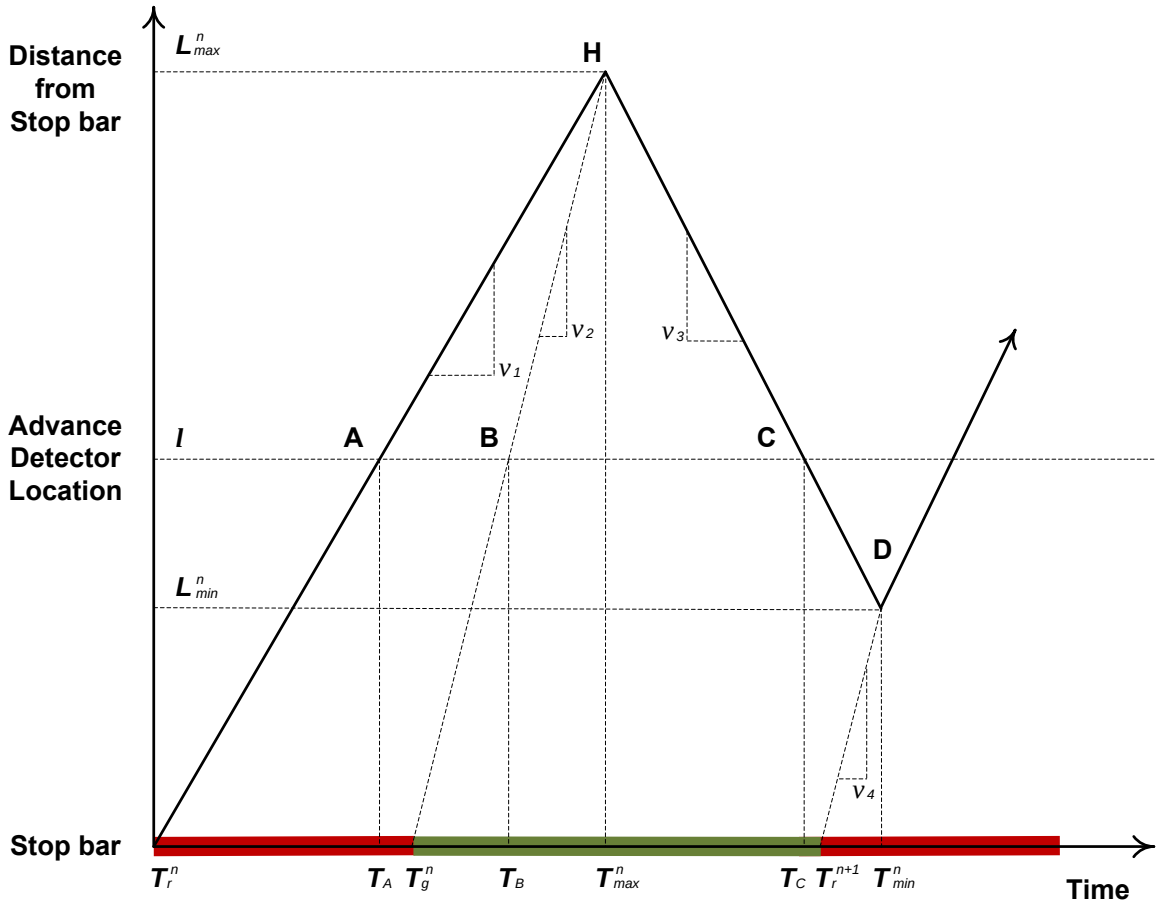

Figure 10 Break Points and Shock Waves

$$L^n_{max} = l + \frac{T_C - T_B}{\frac{1}{v_2} + \frac{1}{v_3}}$$ **Equation 12**

$$T^n_{max} = T_B + \frac{L^n_{max} - l}{v_2} = T^n_g + \frac{L^n_{max}}{v_2}$$ **Equation 13**

$$L^n_{min} = \frac{\frac{L^n_{max}}{v_3} + T^n_{max} - T^{n+1}_r}{\frac{1}{v_3} + \frac{1}{v_4}} = \frac{\frac{l}{v_3} + T_C - T^{n+1}_r}{\frac{1}{v_3} + \frac{1}{v_4}}$$ **Equation 14**

$$T^n_{min} = T^{n+1}_r + \frac{L^n_{min}}{v_4}$$ **Equation 15**

$$v_1 = \frac{L_{max}^n - l}{T_{max}^n - T_A}$$ **Equation 16**

$$v_2 = \frac{l}{T_B - T_g^n}$$ **Equation 17**

where

T_A = timestamp when the rear end of the queue crosses the advance detector location during queueing (second),
T_B = timestamp when the discharge shock wave crosses the advance detector location (second),
T_C = timestamp when the rear end of the discharging queue crosses the advance detector location (second),
v_1 = queueing shock wave velocity (ft/s),
v_2 = queue discharging shock wave velocity (ft/s),
v_3 = departure shock wave velocity (ft/s),
v_4 = queue discharging shock wave velocity in the next cycle (ft/s)
L_{max}^n = maximum queue length (ft),
T_{max}^n = timestamp when the maximum queue length is reached (second),
L_{min}^n = residual or minimum queue length (ft),
T_{min}^n = timestamp when the residual or minimum queue length is reached (second),
l = the distance from the advanced detector location to the stop line (ft), and
T_r^{n+1} = timestamp of the start of the red phase in the next cycle (second).

$$v_3 = \frac{q_m - q_a^n}{k_m - k_a^n}$$ **Equation 18**

where

q_m = saturation flow rate (veh/s),
q_a^n = arrival flow rate during the queue discharging process (veh/s),
k_m = saturation density (veh/ft), and
k_a^n = arrival density during the queue discharging process (veh/ft).

2.2.4 Probabilistic Model

Various probabilistic models have been developed to account for the stochastic components of queueing behaviors at traffic signals.

For example, a Markov model was developed to describe the dynamics of the queue length and the queue length standard deviation evolution over time (46). The dynamics of queueing was modeled with a combination of a linear function and an exponential function. The linear component is applicable if the queue length standard deviation remains small. When the queue length standard deviation reaches the same order of magnitude as the expectation value of the queue length, the queue follows the exponential model component to reach the equilibrium value.

Viti and van Zuylen (47) summarized the disadvantages of generic probabilistic queueing models as evaluating the expectation values or queue lengths for specific time intervals, assuming specific arrival and departure patterns, assuming stationary averages, assuming no initial queue, and ignoring the queue transitioning process. They developed a probabilistic model (Equation 19 and Equation 20) to estimate the probability distribution of queues at fixed time controlled signals for the within-cycle process and demonstrated to calculate the maximum length of the back of the queue using the probabilistic queueing model. This model was further improved to estimate the probability distribution of the overflow queue length at fully actuated traffic signals (48, 49). Unlike generic probabilistic models of queues, this improved model does not assume any specific probability distribution of the arrivals. This model does assume constant vehicle discharge headway in the green phase. The performance of this model is close to results generated by a commercial microsimulation software package.

The probability for the number of vehicles queued during the red phase can be expressed as Equation 19.

$$P_Q(i,t) = \sum_{j=0}^{i} \left[P_Q(j, t-\Delta t) \cdot P_a(i-j, \Delta t) \right] \qquad \textbf{Equation 19}$$

where

$P_Q(i,t)$ = the probability of i vehicles queueing at time t during the red phase,
i = number of queued vehicles at time t (veh),
j = number of queued vehicles at time $t - \Delta t$ (veh), and
$P_a(i-j, \Delta t)$ = the probability of $i - j$ vehicles arriving during the time period Δt.

The probability for the number of vehicles queued during the green phase can be expressed as Equation 20.

$$P_Q(i,t) = \sum_{l=0}^{[i+s\cdot\Delta t]} \left[P_Q(i-l+s\cdot\Delta t, t-\Delta t) \cdot P_a(l, \Delta t) \right] \qquad \text{for } \boldsymbol{i} \in [\mathbf{0}, \boldsymbol{N_{max}}]$$

Equation 20

$$P_Q(i,t) = \sum_{j=0}^{[s\cdot\Delta t - l]} \left[P_Q(j, t-\Delta t) \cdot \sum_{l=0}^{[s\cdot\Delta t]} P_a(l, \Delta t) \right] \qquad \text{Otherwise}$$

where

s = vehicle departure flow rate (veh/s), and
l = number of queued vehicles arriving during the time period Δt (veh).

Zheng and van Zuylen (50) developed a model to describe the delay probability distribution at fixed time controlled signals with initial queues and stochastic arrivals and departures. It is

found that arrival patterns have minimal influence on the delay distribution in undersaturated conditions, but play a significant role in the delay distribution in oversaturated conditions. Delay in undersaturated conditions has relatively more uncertainty than that in oversaturated conditions.

2.2.5 Other Models

Sanchez et al. (51) attempted to analyze four queue estimation methods using wireless magnetic sensors installed on a single lane loop on-ramp. The four methods are time occupancy measurements at ramp entrance, the simple input-output model, speed measurements at ramp entrance, and the vehicle magnetic signature re-identification technique. None of the four methods performed well under saturated on-ramp conditions. The simple input-output model showed the evident cumulative errors over the analysis time period. The speed based method could only indicate either unsaturated or saturated conditions.

In addition to the above queue estimation models discussed, many more methods have been developed by various researchers to estimate queues. Prikryl and Kocijan (52) developed a method based on a Gaussian process model of the occupancy-queue relationship.

Data collected by a variety of probe-based monitoring techniques can also be used to estimate queue length at traffic signals (53, 54, 55, and 56).

Muck (57) introduced two very important definitions relevant to determine the queue length when the vehicle queue has extended beyond the advance detector upstream to the signal. The

first one is the “fill-up time”, which is defined as the time passed from the beginning of the red phase to the moment the detector is constantly occupied by a vehicle. The second one is the time occupancy of a detector during the green phase. Another interesting concept mentioned was to limit the measurement interval to a part of the green phase, when vehicles were certainly moving. Using the proposed linear regression model, the queue length could be estimated up to ten times of the distance from the advance detector to the stop bar. However, the correlation coefficient of the queue length and the smoothed congestion characteristic was 0.64, which indicated that the relationship was far from perfectly linear and there might be other factors involved.

2.3 Delay Estimation Models

Traffic flow along a signalized arterial link is periodically interrupted by traffic signals. Drivers frequently decelerate, stop and accelerate due to signal phasing changes and queueing at the signalized intersection. Any extra travel time in addition to the free flow running time is delay. Four major types of delay models have been developed to estimate delay at signalized intersections.

2.3.1 Deterministic Queueing Model

Deterministic queueing models consider a traffic signal as a service provider that provides a high service rate and periodically stops servicing. The total aggregate delay incurred by all vehicles on a signalized intersection approach is determined as the area between the arrival and departure curves as shown in Figure 11.

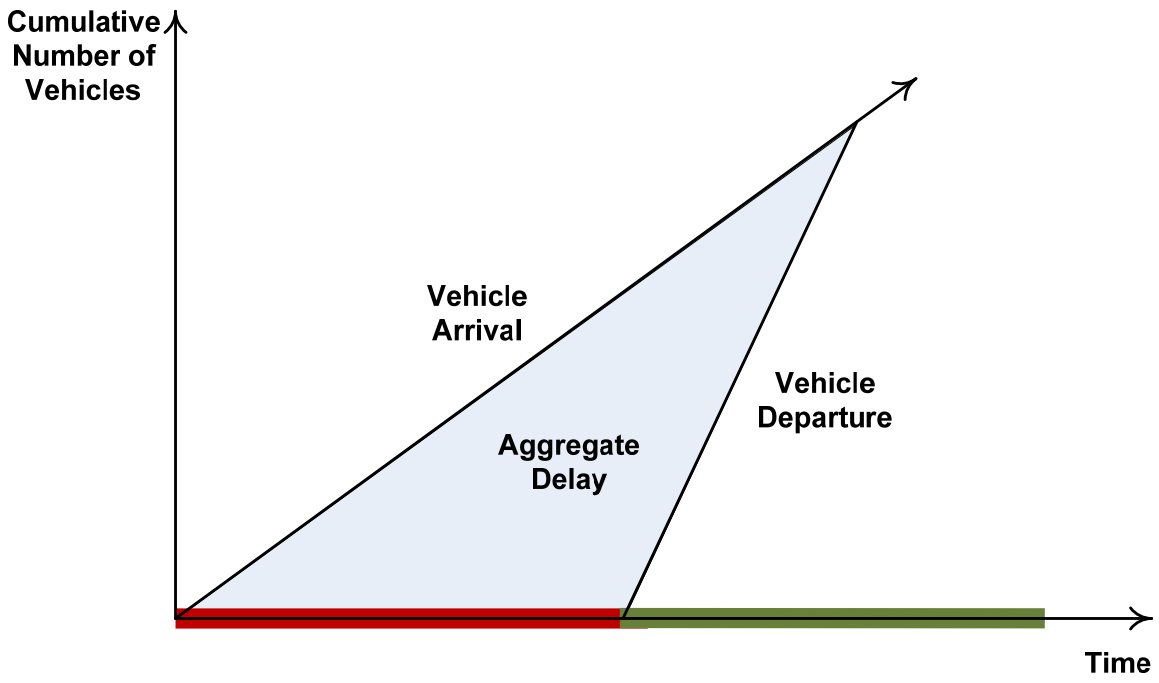

Figure 11 Queue Diagram at Signalized Intersection

Deterministic queueing models assume that vehicles arrive at a uniform and constant rate, vehicles decelerate and accelerate instantaneously, and vehicles queue vertically at the intersection stop line. In vertical queueing models, it is assumed that vehicles do not occupy space and vehicle spatial locations are usually not considered.

2.3.2 Shock Wave Model

Shock wave models assume that vehicles follow a non-random and consistent path with instant deceleration and acceleration. Shock wave models consider that vehicles queue horizontally so that vehicle spatial locations or trajectories can be tracked (Figure 12).

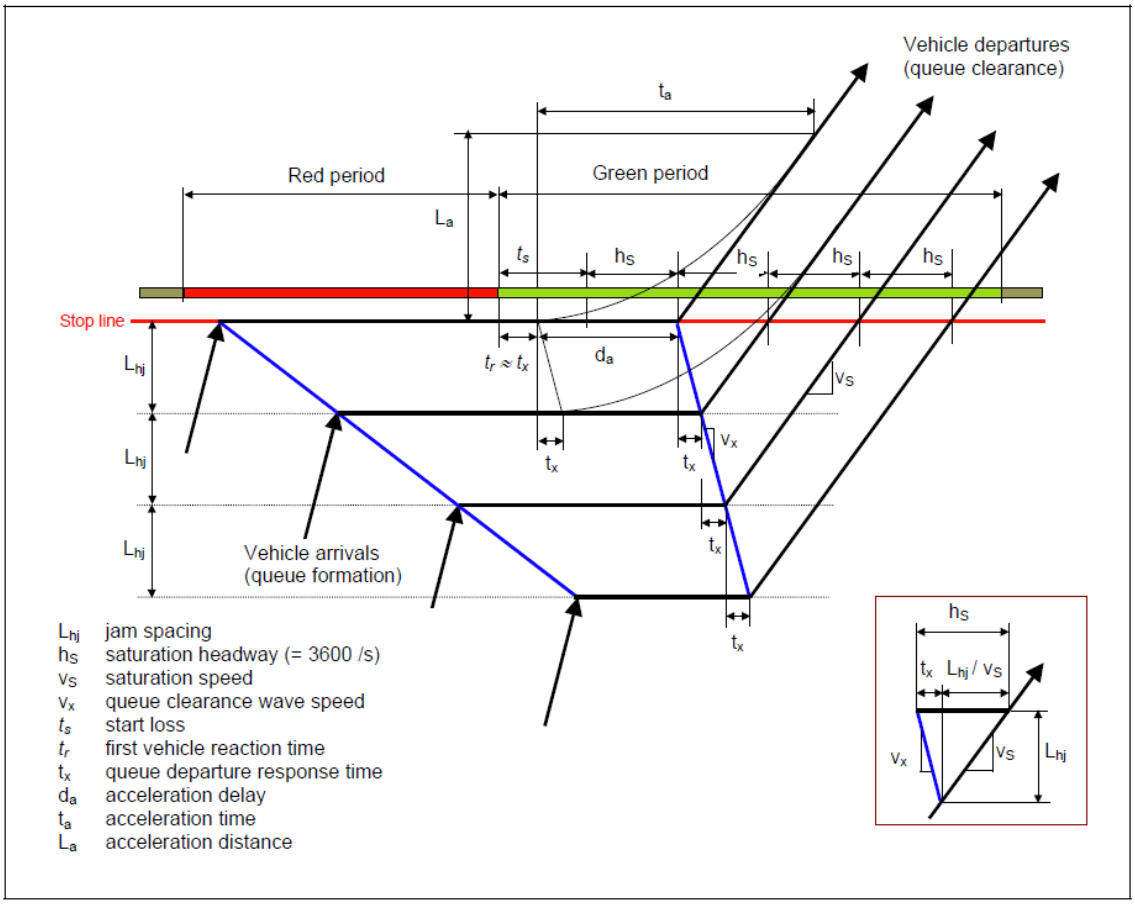

Figure 12 Shock wave Diagram at Signalized Intersection (Cited from Akcelik and Besley (58))

Skabardonis and Geroliminis (59) proposed a model to estimate the travel time on a signalized urban arterial link as the sum of the free follow time and the delay at the traffic signal. The delay at the traffic signal is calculated as the sum of three types of delays as listed below.

- The delay of a single vehicle approaching a signalized intersection without any interaction with other vehicles, including deceleration, acceleration and the stopped time.
- The delay because of the queues formed at the intersection, calculated using the shock wave theory with consideration of offset and platoon dispersion.

- The oversaturation delay caused when the arrival rate is greater than the service rate at the signal.

Skabardonis and Geroliminis (60) further improved the model to account for long queues and queue spillovers later on.

2.3.3 Steady-State Stochastic Model

Steady-state stochastic models assume that vehicle arrivals follow a certain known distribution like a Poisson distribution, vehicles departure with a constant average headway, the system always remains under-saturated with a steady state, and vehicles decelerate and accelerate instantaneously. If arrivals are platooned because of an upstream traffic signal, steady-state stochastic models cannot be applied. The delays estimated by steady-state stochastic models tend to infinity as shown in Figure 13 when volume-to-capacity ratios approach 1.

Heidemann (61) developed one of the many steady-state stochastic delay models. One of the fundamental and most quoted models is the Webster's delay formula (27) as shown in Equation 21. The first term represents the uniform delay, the second term considers the random or stochastic delay, and the third term is an empirical correction term. The third term is usually around 10% of the sum of the first and the second terms.

$$d = \frac{C(1-\frac{g}{C})^2}{2(1-\frac{g}{C}X)} + \frac{X^2}{2v(1-X)} - 0.65\,(\frac{C}{v^2})^{\frac{1}{3}} X^{2+5\frac{g}{C}} \qquad \textbf{Equation 21}$$

where

d = average delay per vehicle for through movements at the signalized intersections (s),
C = cycle length (s),
g = effective green time for lane group (s),
X = v/c ratio or degree of saturation for lane group,
v = lane group arrival flow rate (veh/h), and
c = lane group capacity (veh/h).

2.3.4 Time-Dependent Stochastic Model

Akcelik and Rouphail (62) developed one of the numerous time-dependent stochastic delay models based on the coordinate transformation technique. As shown in Figure 13, delay calculated by steady-state stochastic models becomes infinite when the volume-to-capacity ratio is asymptotic to 1. Kimber and Hollis (63) used the coordinate transformation technique to overcome the weakness of steady-state stochastic models so that delays estimated become asymptotic to the deterministic oversaturation model results. Although there is no rigorous theoretical basis behind them, time-dependent stochastic models can produce reasonable results in practice. This is the reason why time-dependent stochastic models have been incorporated into a number of capacity guides, such as the United States *Highway Capacity Manual*, Canadian *Capacity Guide for Signalized Intersections* and Australian *Traffic Signals Capacity and Timing Analysis*.

2.3.5 Comparison of Delay Models

Dion et al. (64) compared a variety of delay models at a pre-timed signalized intersection with traffic conditions ranging from undersaturated conditions to oversaturated conditions using

microscopic simulation. The models compared included deterministic queueing models, shock wave models, steady-state stochastic models, and time-dependent stochastic models. The results demonstrated that all of the models produced relatively consistent delay estimates while traffic was undersaturated with volume-to-capacity ratios below 0.6. While traffic conditions were becoming oversaturated with volume-to-capacity ratios higher than 0.6, the delay estimate difference between models increased dramatically. The following figure shows the relationships between the average approach delay and volume-to-capacity ratios for various models.

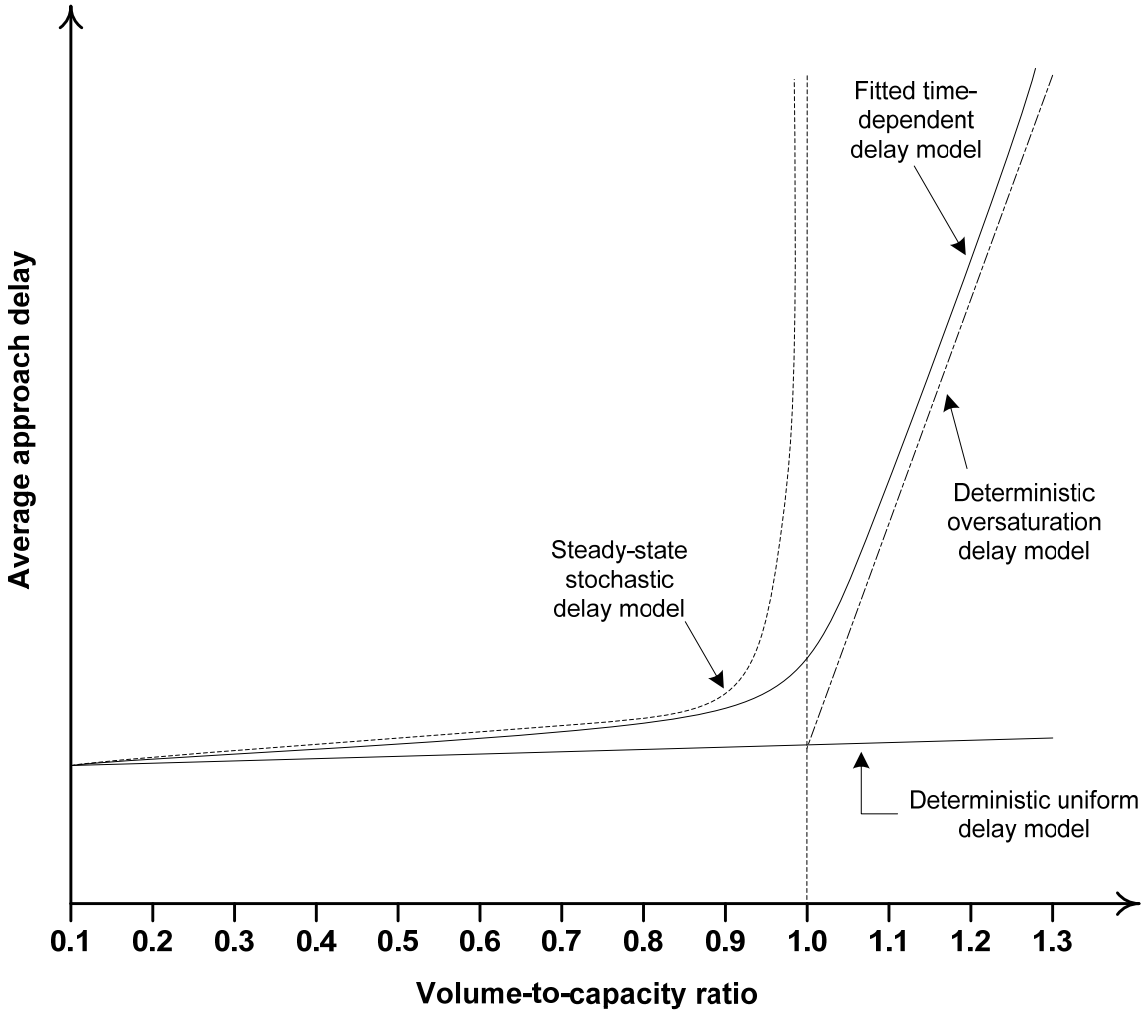

Figure 13 Average Approach Delay and Volume-to-Capacity Ratio Relationships (Cited from Dion et al. (64))

2.3.6 HCM 2000 Model

The HCM 2000 model has been used widely in practice by various agencies in the United States for planning, design and operations involving traffic signals. HCM 2010 was recently published and includes a slightly modified version of the HCM 2000 model. Generally, there are two principal components of the total time that a vehicle spends on a segment of an urban street, which consists of running time and control delay at signalized intersections.

2.3.6.1 Determining Running Time

To compute the running time for a segment, the time mean speed data collected at midblock locations can be used as a space mean speed.

$$T_R = \frac{L}{S_{sensor}}$$ **Equation 22**

where

S_{sensor} = speed data collected at midblock locations (mi/h).

2.3.6.2 Determining Control Delay

Control delay is the total delay attributed to traffic signal operation at signalized intersections. Control delay defined by HCM 2000 includes initial deceleration delay, queue move-up time, stopped delay, and final acceleration delay. The following formulas are HCM 2000 Equations 16-9, 16-11, 16-12, and F16-1, respectively (1).

$$d = d_1(PF) + d_2 + d_3$$ **Equation 23**

$$d_1 = \frac{0.5C(1-\frac{g}{C})^2}{1-[\min(1,X)\frac{g}{C}]}$$ **Equation 24**

$$d_2 = 900T\left[(X-1) + \sqrt{(X-1)^2 + \frac{8kIX}{cT}}\right]$$ **Equation 25**

$$d_3 = \frac{1800Q_b(1+u)t}{cT}$$ **Equation 26**

where

d = control delay for through movements at the signalized intersections (s),
d_1 = uniform control delay assuming uniform arrivals (s),
d_2 = incremental delay to account for effect of random and oversaturation queues, adjusted for duration of analysis period and type of signal control (s), this delay component assumes that there is no initial queue for lane group at start of analysis period,
d_3 = initial queue delay to account of effect of an initial queue to occur at the start of the analysis period (s),
PF = progression adjustment factor,
C = cycle length (s), cycle length used in pretimed signal control, or average cycle length for actuated control,
g = effective green time for lane group (s); green time used in pretimed signal control, or average lane group effective green time for actuated control,
X = v/c ratio or degree of saturation for lane group,
T = duration of analysis period (h),
k = incremental delay factor that is dependent on controller settings,
I = upstream filtering/metering adjustment factor,
c = lane group capacity (veh/h),
Q_b = initial queue at the start of the analysis period (veh),
t = duration of unmet demand the analysis period (h),
u = delay parameter.

2.3.6.3 Improvements to HCM 2000 Model

Extensive efforts have been done to improve the HCM 2000 model. Wang and Hobeika (65) developed an intersection control delay estimation algorithm based on the HCM 2000 model. The algorithm performed slightly better than the HCM 2000 model according to the field test at a single intersection. The calculation interval was one cycle, though the cycle length was not mentioned. This calculation interval may be too long for congested short urban arterial segments between signals. The algorithm computed the intersection control delay using the queue vs. time curve at the signal based on three simplified vehicle arrival cases. The algorithm can become very complex and not feasible if every single arrival case is considered.

Noroozi and Hellinga (66) developed a method to improve the HCM 2000 point delay estimates by calculating the distribution of average lane group delay with varying peak hour volumes.

Li et al. (67) developed an analytical overflow delay model to incorporate the upstream signal filtering or metering effect. Isolated intersection delay models usually assume random arrivals. However, with the upstream signal filtering or metering effect, closely spaced signals along a signalized arterial link cannot be assumed to have random arrivals.

2.3.7 Route Travel Time

Zheng and van Zuylen (68) developed a delay distribution model for an urban trip over a route with two consecutive fixed-time controlled signalized intersections. The proposed model assumes uniformly distributed arrivals and departures at the first intersection. Delay

distributions are analyzed for different signal coordination scenarios and under different degrees of saturation. The estimated delay distributions are evaluated using microsimulation.

Lei et al. (69) developed a method for estimating travel time distributions along corridors containing multiple bottlenecks. The model calculates the number of queued vehicles ahead of a probe vehicle, along with the prevailing congestion level, queue discharge rates at the bottlenecks, and flow rates associated with merges and diverges. The lane-by-lane delay at each bottleneck along the corridor is estimated to produce a route-level travel time distribution. The model uses inputs including the entering and exiting flow rates and a sense of the lane-by-lane distribution of traffic at each bottleneck. The model is evaluated using the NGSIM project data.

2.3.8 Other Delay Models

Daganzo (70, 71) developed the Cell Transmission Model (CTM) to describe various traffic conditions. A section of a roadway is divided into a series of cells with equal lengths, which are equal to the distance vehicles travel in one time interval with the free flow speed. Under free flow conditions, it is assumed that all vehicles in a cell can advance to the next cell within one time interval.

$$n_i(t+1) = n_i(t) + y_i(t) - y_{i+1}(t) \quad \textbf{Equation 27}$$

$$y_i(t) = min\{n_{i-1}(t), Q_i(t), N_i(t) - n_i(t)\} \quad \textbf{Equation 28}$$

where

$n_i(t+1)$ = the number of vehicles in cell i at time $t+1$,
$n_i(t)$ = the number of vehicles in cell i at time t,

$y_i(t)$ = the number of vehicles entering cell i between time t and $t+1$,
$y_{i+1}(t)$ = the number of vehicles entering cell $i+1$ between time t and $t+1$,
$n_{i-1}(t)$ = the number of vehicles in cell $i-1$ at time t,
$Q_i(t)$ = the capacity flow into cell i between time t and $t+1$, and
$N_i(t)$ = the maximum number of vehicles can be present in cell i at time t.

If $n_i(t) > y_{i+1}(t)$, then some vehicles in cell i cannot advance to the next cell within one time interval. The average delay for vehicles left in the cell is one time interval. Various researchers have attempted to improve the CTM, such as using cell densities instead of cell occupancies to allow the CTM to include uneven cell lengths (72).

Colyar and Rouphail (73) developed an experiential method (Equation 29) to estimate intersection control delay from second-by-second speed data collected by portable onboard emissions and engine diagnostics measurement devices.

$$Control\ Delay = 0.3 \times Total\ Delay + 0.7 \times Stopped\ Delay \quad \textbf{Equation 29}$$

Akcelik et al. (74) developed an exponential queue discharge model to describe the queue discharge flow rate at traffic signals (Equation 30).

$$q_s = q_n\left[1 - e^{-m_q(t-t_r)}\right] \quad \textbf{Equation 30}$$

where
q_s = queue discharge flow rate at time t (veh/h),
q_n = maximum queue discharge flow rate (veh/h),
m_q = queue discharge model coefficient,
t = time since the start of the green phase (s), and

t_r = response time needed for the first vehicle to start moving since the start of the green phase (s).

Fu and Hellinga (75) demonstrated an analytical model to fit delay under highly undersaturated and highly oversaturated conditions into a single curve.

Liu et al. (76, 77) developed a State-Space Neural Network (SSNN) model to predict arterial travel time. Trained by using the extended Kalman Filter approach, this model could produce reasonable short-term travel time predictions. Generally, neural network based models require off-line training with extensive input and output data sets, which makes these models difficult to accommodate input data changes, output data changes or input-output mapping changes. Models developed for one specific site cannot be implemented to different sites without completely retraining.

3 METHODOLOGY

This research aims to explore the traffic flow characteristics on signalized arterials, identify practical methods to describe signalized arterial traffic flow status, and estimate queue lengths and travel time based on real-time short interval detector data.

3.1 Major Hypothesis

This study is mainly motivated by the following three major hypotheses:

- Due to the dynamic nature of traffic flows on signalized arterials, detector volume, speed and time occupancy data do not necessarily form clear relationships as shown on freeways, but may still be correlated and can be used to describe traffic flow characteristics.
- There is a simple and direct approach to estimate the vehicle queue length along a signalized arterial segment, which should be practical for daily operations without compromising estimation accuracy, and be able to utilize detector data that are widely available like volume, speed and occupancy.
- There is a practical approach to estimate travel time with reasonable level of accuracy and reliability using volume, speed and time occupancy data collected by detectors. This approach can provide travel time estimation close to travel time directly measured using detection technologies, but overcome the limitation and incompetency of these technologies.

Detailed discussions of the hypotheses are described in the following sections.

3.1.1 Relationship between Volume, Speed and Occupancy

Most traffic flow theories agree that for homogeneous and steady state traffic flows, a basic relationship exists between flow rate v, density d and space mean speed s, as shown by Equation 31. Note that knowing any two variables would allow the third variable to be calculated.

$$v = ds \qquad \textbf{Equation 31}$$

where

v = flow rate (veh/hour),
d = density (veh/mile/lane), and
s = space mean speed (miles/hour).

In this research, this basic relationship will be explored first at the detector level and then at the link level between two detectors.

In research and practice, time occupancy and space occupancy have been used interchangeably or their relationship has been treated as linear. Various researchers have developed linear relationships between time occupancy and space occupancy and between time occupancy and density as shown by the following equations discussed in the literature review chapter.

$$S_A = \frac{(L_v + L_d) \times N}{T \times O} \qquad \textbf{Equation 1}$$

$$D = \frac{O \times 5280}{L_v + L_d} \qquad \textbf{Equation 4}$$

$$q_{n-1} = \frac{L \times n}{l + D} \times O_{n-1} \qquad \textbf{Equation 6}$$

Other researchers (35 and 78) also developed similar linear relationships between time occupancy and space occupancy. In addition, more studies (79 and 80) have been performed to investigate the relationship between time occupancy and density using limited access roadway detector data. It was concluded that the relationship would be close to linear if the heavy vehicle percentage is low because the average physical vehicle length could have a significant impact on the relationship.

However, the traffic condition on signalized urban arterials is more complex than that on freeways. Traffic flow is periodically interrupted by traffic signals and vehicles go through deceleration, stop and acceleration constantly. Traffic flow can no longer be considered as spatially homogeneous along a roadway segment with signals.

By utilizing field data, this study will investigate whether the close to linear relationship between time occupancy and density remains for signalized arterials. This analysis is critical as it is closely related to the final goal of estimating travel time.

3.1.2 Vehicle Queue Length Estimation

As presented in Section 2.2, four major types of queue estimation models have been studied by researchers, the simple input-output model, the Kalman filter model, the break point identification process, and probabilistic models. Probabilistic models are not in the research scope of this dissertation because ATMS real time operations in practice are not ready to handle the probability distribution of queues as inputs.

The Kalman filter model provides better estimation than the simple input-output model, but the Kalman filter coefficient has different values for different intersections or different values for different time periods at the same intersection (3). The simple input-output model is simple to implement in practice, but it cannot handle long queues exceeding beyond the input detector and tends to accumulate errors over time. The break point identification process can estimate long queues extending beyond the input detector location with satisfactory accuracy, but it requires high-resolution event-based data or second-by-second data.

A simple and direct approach to estimate the vehicle queue length should be as simple as the input-output model, but provide similar performance as the Kalman filter model. In this research, improvements to the simple input-output model will be attempted and the improved model will be compared with the Kalman filter model to evaluate the model performance.

3.1.3 Travel Time Estimation

As summarized in Section 2.3, four major types of delay models have been developed to estimate delay at signalized intersections. They are deterministic queueing models, shock wave models, steady-state stochastic models, and time-dependent stochastic models. Although there is no rigorous theoretical basis behind them, time-dependent stochastic models can produce the most reasonable results among all models in practice. This is the reason why time-dependent stochastic models have been widely used and incorporated into a number of national capacity guides. However, time-dependent stochastic models are not intended for real-time operation purposes.

This research will develop a practical approach to estimate travel time using widely available volume, speed and time occupancy data collected by detectors. The estimated travel time will be compared with the field travel time data to evaluate the level of estimation accuracy and reliability.

3.2 Data Needs

Field data are needed given the purposes of this study, from several perspectives.

- Detector volume, speed and occupancy data are necessary. Flow rate, density and space mean speed data along signalized arterial links are also necessary.
- Short-time interval detector and queue data (e.g. 10 seconds) are needed to make the models useful in a real-time context.
- To be able to study the dynamics of traffic flow under the influence of signals, distance to the signal would be a critical factor to be investigated. In practice, detectors are usually placed at midblock and stop-bar. In order to minimize the inputs to the models and maintain the model simplicity, signal timing data will not be used for the model development.
- Field data could reflect the influence of average physical vehicle length and heavy vehicles on the correlation among different measurements of performance, which could help better identify the relationships and dynamics if any. The vehicle length data are necessary.

3.3 Analysis Approach

Given the research goals and the underlying hypotheses, it is very critical to clearly define all measurements of performance at the detector and link levels studied in this dissertation.

3.3.1 Definition of Detector Volume, Speed and Occupancy

Detector volume $V_{detector}$ is the number of vehicles passing the detection zone during a data collection time interval.

Depending on detection technologies, the speed data collected by a detector may be directly measured using the Doppler Effect. The arithmetic average of directly measured speeds of vehicles passing the detection zone is referred to as the time mean speed or the average spot speed. The speed data collected by a detector can also be the space mean speed of vehicles traversing the detection zone, which is an average of vehicle speeds over a short roadway segment rather than a point during a data collection time period.

There are several ways to collect the detector space mean speed (81). This research uses the widely adopted method, known as the harmonic mean speed, as shown by Equation 32. With per vehicle length and time data directly measured by a detector, Equation 32 provides the space mean speed as the harmonic mean of speeds of vehicles passing the detection zone.

$$S_{detector} = \frac{N}{\sum_{i=1}^{N} \left(\frac{1}{\frac{L_i + L_d}{t_i}} \right)}$$ **Equation 32**

Where

$S_{detector}$ = vehicle speed collected by a detector (ft/s),
L_i = physical vehicle length of vehicle i (ft), and
t_i = time the detector is occupied by vehicle i (second).

The average travel speed along an arterial street link is defined as the length of the link divided by the travel time of vehicles traversing the link, including all stopped delay times. The link average travel speed is a space mean speed, which is often used as the link level performance measurement of signalized urban arterials.

Occupancy collected by a detector is actually time occupancy O_{time}, which is defined as the percentage of time the detection zone is occupied by a vehicle. Depending on detection technologies, the time occupancy data collected by different technologies may be different. Time occupancy can be collected by summing the durations of all vehicles traversing the detection zone in the data collection time period and dividing the total duration by the time period, which is the method used in this research. Time occupancy can also be calculated by using Equation 33, which estimates time occupancy based on directly measured per vehicle length and speed data (82).

$$O_{time} = \frac{\sum_{i=1}^{N} \left(\frac{L_i + L_d}{S_i}\right)}{T}$$ **Equation 33**

where

S_i = detector directly measured speed of vehicle i (ft/s).

Theoretically, there are generalized definitions of flow rate, density and space mean speed developed by Edie (83 and 84) and Daganzo (85) that apply to all types of traffic conditions and all shapes of time-space regions. Before describing the generalized definitions, it is necessary to start with vehicle trajectories and time-space diagrams, because the generalized flow rate, density and space mean speed are defined within a time-space region, where vehicle trajectories along both the time axis and the space axis are analyzed.

3.3.2 Vehicle Trajectory

When a vehicle travels along a roadway, the position of the vehicle can be expressed as a coordinate in time and space. Spatial values usually indicate the distance from a specific point of the vehicle (like the front center of the vehicle) to an arbitrary selected roadway location. Temporal values usually present time of day or time that has passed from a selected time reference point, like the start of a green phase of a traffic signal.

Figure 14 shows an example of a trajectory of a single vehicle. The location of the front center of the vehicle is recorded at a time interval of Δt. The x axis shows timestamps when the vehicle location data are collected and the y axis shows the longitudinal positions of the vehicle

along the roadway. The vehicle length is shown in Figure 14. If a vehicle is presented as a single point, then the trajectory of the vehicle becomes a curve like shown in Figure 15, which displays the field recorded trajectories of two vehicles passing through three traffic signals along a signalized arterial.

In Figure 15, the vehicle trajectory can be represented mathematically with the vehicle spatial positions as a function of time (85). At each specific point in time and space, a set of measurements can be studied, including vehicle speed, acceleration, space gap, time headway, etc. It should be noted that vehicle trajectory models are deterministic models.

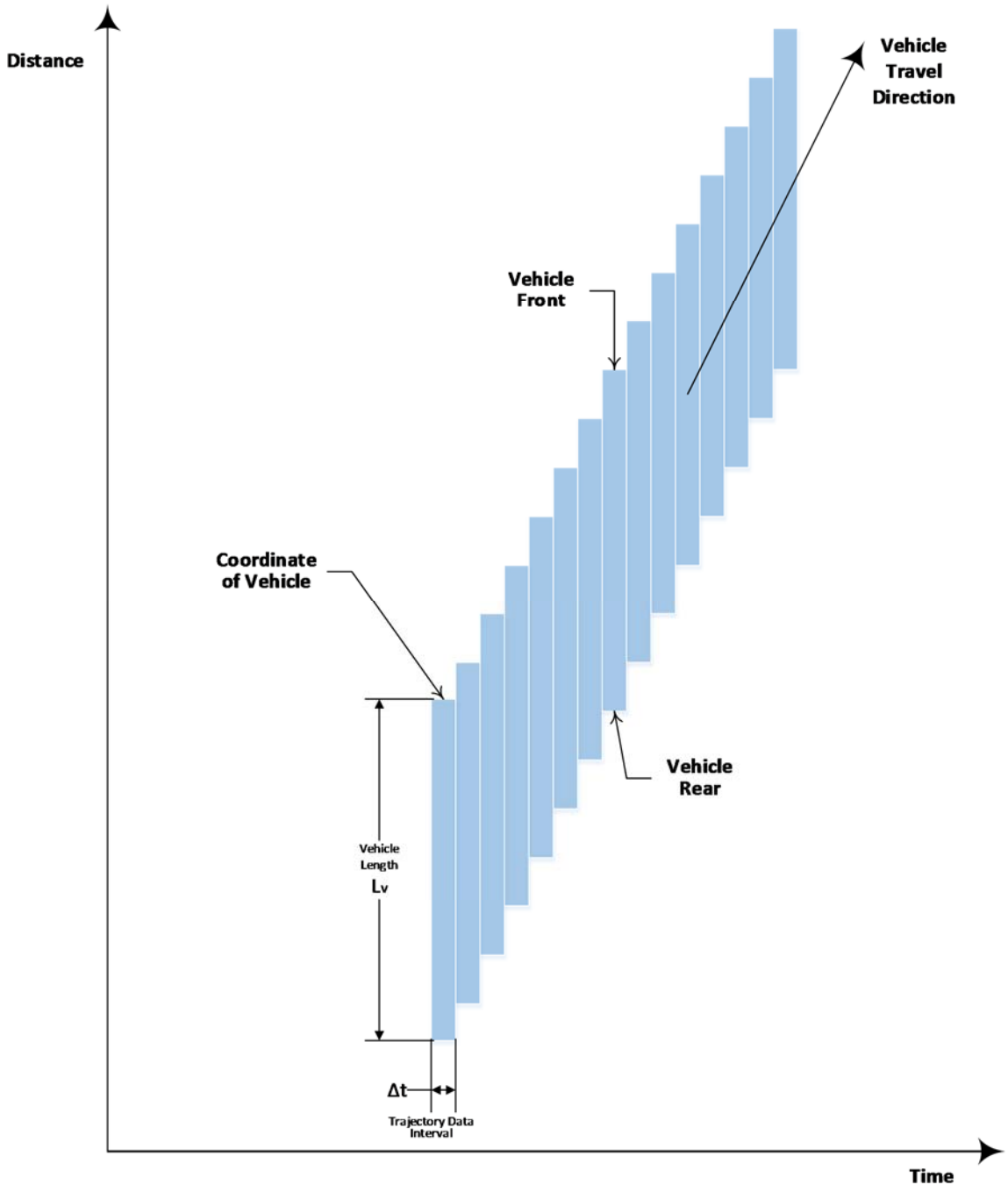

Figure 14 Trajectory of One Vehicle

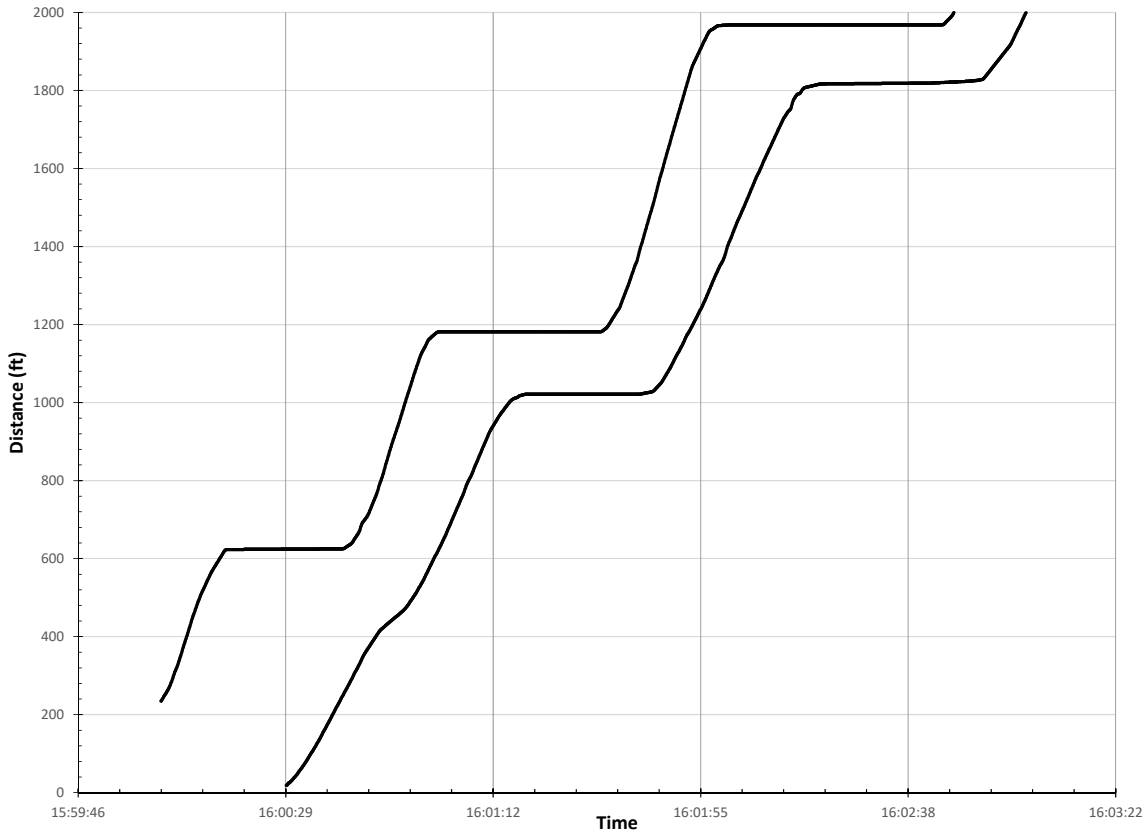

Figure 15 Field Recorded Trajectories of Two Vehicles

3.3.3 Time-Space Diagram

Diagrams like Figure 14 and Figure 15 are called time-space diagrams, which is a common way to visualize, present, and analyze vehicle trajectories. In time-space diagrams, direction has both time and space concepts. Utilizing time-space diagrams, many studies have been performed to describe various point and link measurements of performance, including flow rate, speed, density, occupancy, queue length, delay, etc.

3.3.4 Generalized Definition of Flow, Density and Speed

Edie (83 and 84) and Daganzo (85) developed a set of generalized definitions of flow rate, density and space mean speed within a finite time-space region. In Figure 16, n vehicles traverse a time-space region. The time-space region can be any shape. A rectangular region is used to simply the formulas, which represents vehicles travel over a roadway section of a length Y during a time interval T. Within this time-space region, each vehicle i travels distance y_i during time t_i. Within this time-space region, the flow rate v equals to the total distance traveled in the roadway section by all vehicles divided by the area of the region, as shown by Equation 34. The density d equals to the total time spent by all vehicles in the roadway section divided by the area of the region, as shown by Equation 35. The space mean speed s is the total distance traveled by all vehicles in the roadway section divided by the total time spent by all vehicles in the roadway section, as shown by Equation 36.

In addition, within this time-space region, the basic relationship between flow rate, density and space mean speed remains valid, as shown by Equation 31.

Flow Rate $v = \frac{\sum_{i=1}^{n} y_i}{Y \times T}$ **Equation 34**

Density $d = \frac{\sum_{i=1}^{n} t_i}{Y \times T}$ **Equation 35**

Space Mean Speed $s = \frac{\sum_{i=1}^{n} y_i}{\sum_{i=1}^{n} t_i}$ **Equation 36**

$v = ds$ **Equation 31**

where

v = flow rate within the time-space region,
d = density within the time-space region,
s = space mean speed within the time-space region,
y_i = distance traveled by vehicle i,
t_i = time spent by vehicle i within the time-space region,
Y = length of a roadway section, and
T = observation time interval.

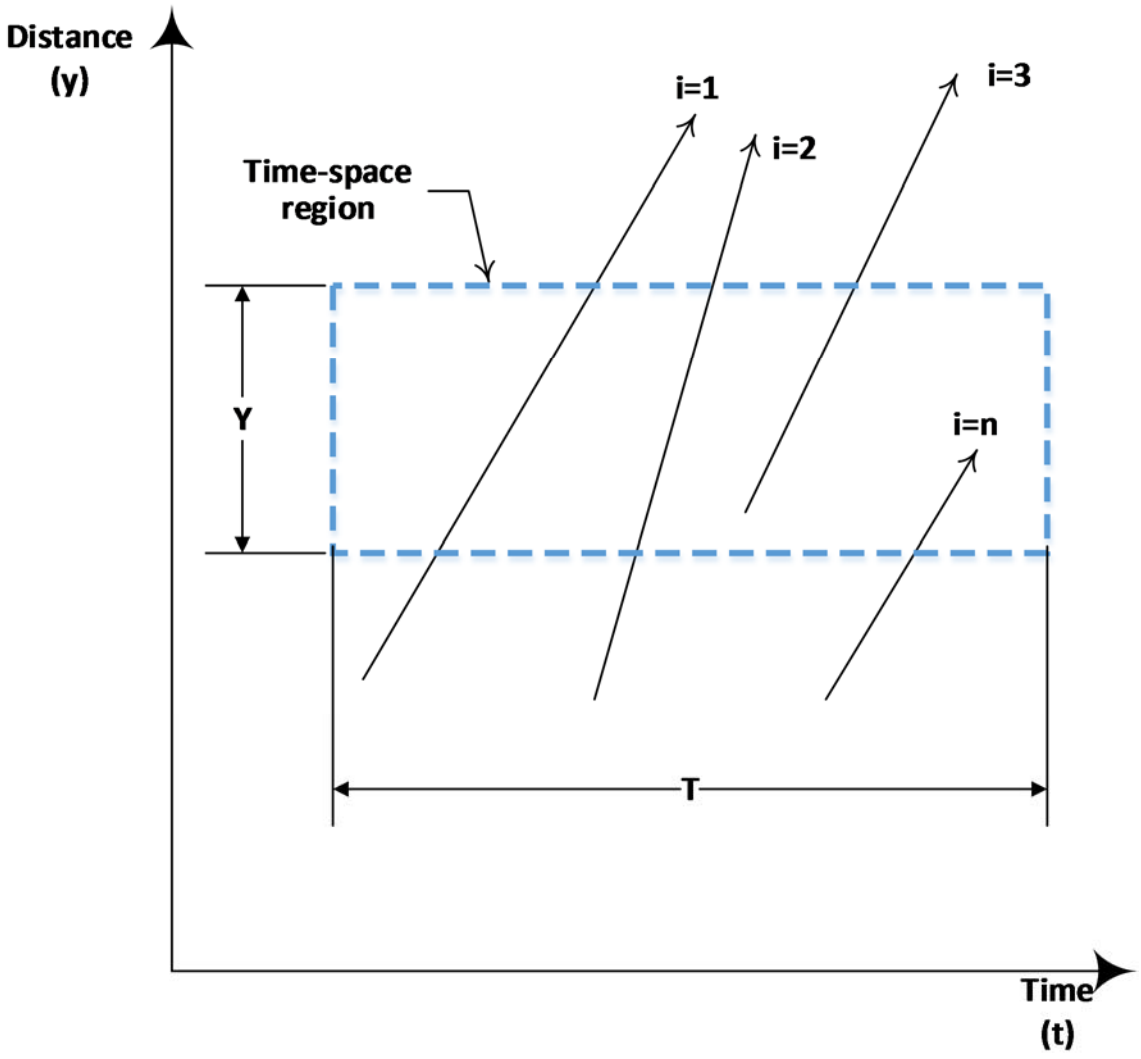

Figure 16 A Time-Space Region with n Vehicle Trajectories

Different approaches used by different detection technologies will produce different results for the same performance measurement. Furthermore, it is extremely critical to analyze the measurements within the same time-space region. Many studies have been done to evaluate the fundamental relationship shown by Equation 31 with flow rate, space mean speed and density all defined in different time-space regions, and the analyses may or may not show the fundamental relationship exists, depending on the regions selected and the traffic conditions.

Even within the same defined time-space region, different methods of data aggregation can result in very different conclusions. The generalized definitions provide the best way to aggregate flow rate, space mean speed and density within a time-space region. Theoretically, the generalized definitions are generalized so that they apply to all types of traffic conditions and all shapes of time-space regions.

However, it is very difficult to collect the generalized flow rate, space mean speed and density data in the field. Cassidy and Coifman (79) analyzed the generalized definitions using freeway detector data collected by dual loop detectors. The study didn't use a fixed data collection time period, instead the time period was selected to allow each defined rectangular time-space region to hold the trajectories of 25 vehicles approximately. Kim and Hall (80) further investigated the generalized definitions using the detector data aggregated into groups of about 20 vehicles.

From here on, all reference to flow rate, space mean speed and density will use the generalized definitions, unless otherwise noted.

4 DATA FOR ANALYSIS

Data used in this dissertation include field data collected at three different project sites.

4.1 NGSIM Peachtree Street Data

4.1.1 Field Data

As a part of the Federal Highway Administration Next Generation Simulation (NGSIM) program (86 and 87), vehicle trajectories on a segment of Peachtree Street in Atlanta, GA were collected between 4:00 PM and 4:15 PM on November 8, 2006. Peachtree Street is an arterial running primarily north-south in Atlanta, GA. The speed limit on Peachtree Street is 35 MPH. The data were collected using video cameras mounted on a 30-story building, which is located at 1100 Peachtree Street NE, Atlanta, GA.

Figure 17 shows the project site where the vehicle trajectory data were collected. The site is approximately 2,100 feet long, with four signalized intersections, one unsignalized intersection, and two to three arterial through lanes in each direction through the project area. Video data were collected using eight video cameras over an approximate 6.5-hour period from 9:30 AM to 1:30 PM and from 4:00 PM to 6:30 PM on November 8, 2006, and 4-hour period from 8:00 AM to 12:00 PM on November 9, 2006. Complete vehicle trajectories were transcribed for two 15 minute periods, one from 12:45 PM to 1:00 PM and the other from 4:00 PM to 4:15 PM, for a total of 30 minutes at a resolution of 10 frames per second. The data used in this dissertation are the 4:00 PM to 4:15 PM dataset.

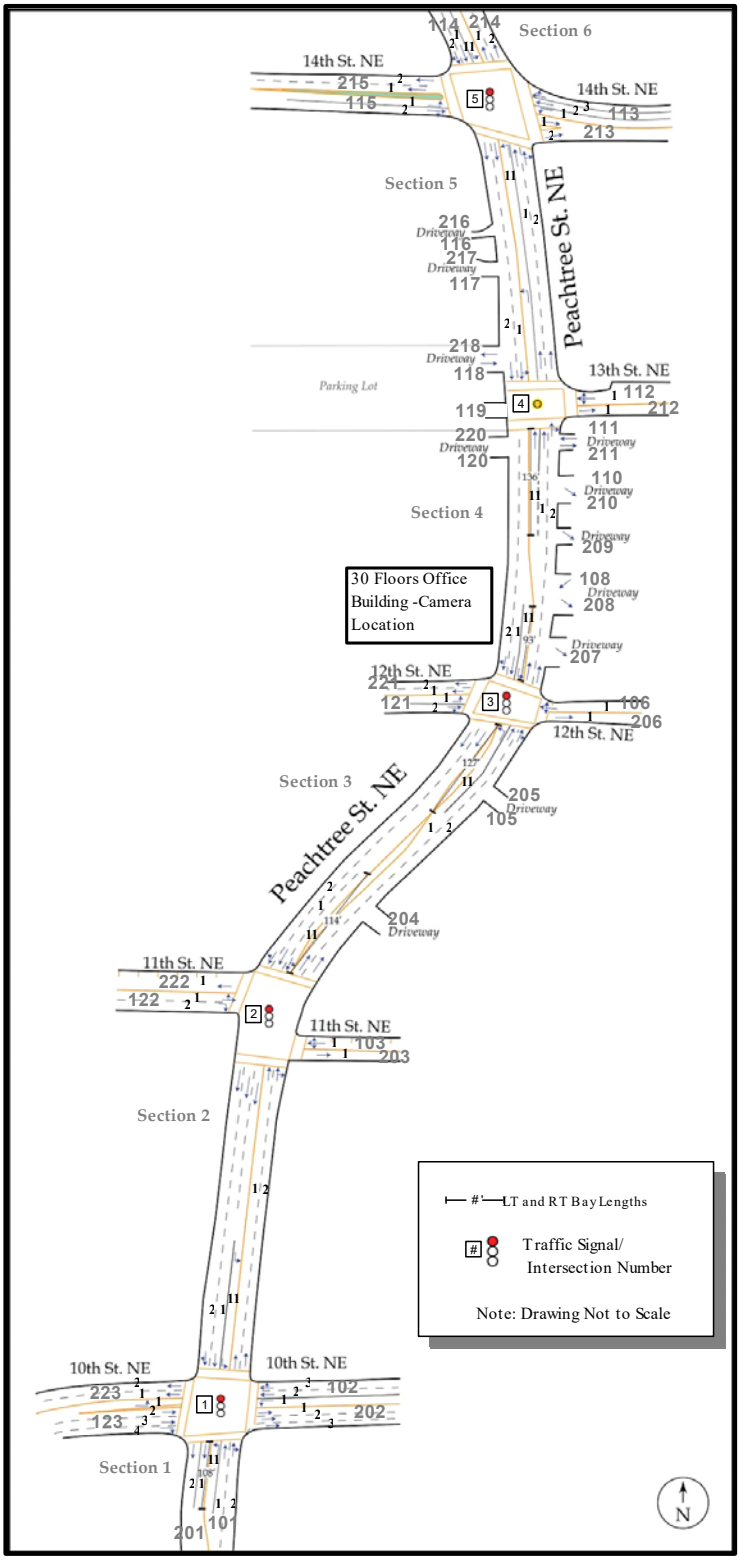

Figure 17 NGSIM Peachtree Street Project Area
(Cited from Home of the Next Generation Simulation Community (87))

Vehicle tracking was performed for the data from 4:00 PM to 4:15 PM. Immediately after 4:15 PM, new vehicle detection was stopped. To account for full vehicle trajectories, tracking continued to allow the vehicles which were already detected to be tracked completely to the end of the study area. The actual tracking time is from 4:00:00 PM to 4:17:13 PM.

Every tenth of a second, a single data point for a vehicle is recorded and the record is specified by a unique number assigned to each vehicle . Each record has twenty-four data fields, including vehicle, time, location, and movement information. Table 1 shows the data fields used in this dissertation and the data description as explained in the vehicle trajectory data dictionary (87). Table 2 shows data record samples of a vehicle with Vehicle ID equal to 11. Figure 18 shows the vehicle trajectories for all vehicles traveling southbound along Peachtree Street in the afternoon dataset, which includes 253,994 data records of 433 vehicles.

Table 1 NGSIM Data Structure

Data Field	Unit	Data Description
Vehicle ID	Number	Vehicle identification number (ascending by time of entry into section)
Global Time	Millisecond	Elapsed time since Jan 1, 1970 (midnight UTC/GMT)
Local Y	Feet	Longitudinal (Y) coordinate of the front center of the vehicle along the median of Peachtree Street. The start point is at the southern boundary of the study area.
Vehicle Length	Feet	Length of vehicle
Lane ID	Number	Current lane position of vehicle. Lane numbering is incremented from the left-most lane, except for locations where left-turn or right-turn bays exist. Left-turn bays are numbered starting from 11 and are incremented from the left-most left-turn bay.
Direction	Number	Moving direction of the vehicle. 1 - east-bound (EB), 2 - north-bound (NB), 3 - west-bound (WB), 4 - south-bound (SB).

Table 2 NGSIM Data Record Sample

Vehicle ID	Time	Local Y	Vehicle Length	Vehicle Speed	Lane ID
11	16:01:04.7	253.080	15.0	9.54	2
11	16:01:04.8	252.126	15.0	9.54	2
11	16:01:04.9	251.171	15.0	9.54	2
11	16:01:05.0	250.217	15.0	9.54	2
11	16:01:05.1	249.263	15.0	9.54	2
11	16:01:05.2	248.309	15.0	9.54	2
11	16:01:05.3	247.355	15.0	9.54	2
11	16:01:05.4	246.401	15.0	9.54	2
11	16:01:05.5	245.447	15.0	9.54	2
11	16:01:05.6	244.496	15.0	9.57	2
11	16:01:05.7	243.530	15.0	9.56	2
11	16:01:05.8	242.545	15.0	9.23	2
11	16:01:05.9	241.616	15.0	8.33	2
11	16:01:06.0	240.875	15.0	6.80	2
11	16:01:06.1	240.300	15.0	4.79	2
11	16:01:06.2	239.916	15.0	2.79	2
11	16:01:06.3	239.698	15.0	1.26	2
11	16:01:06.4	239.669	15.0	0.36	2
11	16:01:06.5	239.694	15.0	0.06	2
11	16:01:06.6	239.699	15.0	0.05	2
11	16:01:06.7	239.690	15.0	0.08	2
11	16:01:06.8	239.684	15.0	0.08	2
11	16:01:06.9	239.679	15.0	0.08	2
11	16:01:07.0	239.673	15.0	0.08	2

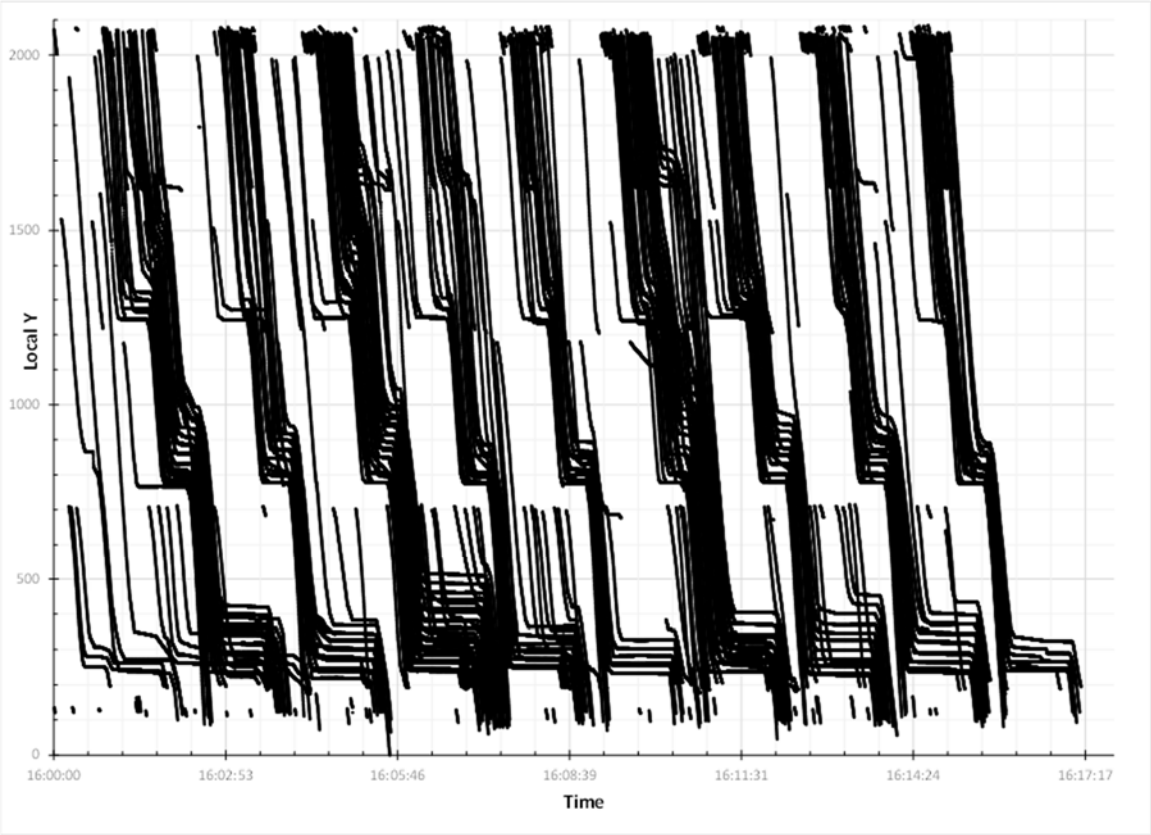

Figure 18 NGSIM Peachtree Street Afternoon Dataset
Southbound Traffic Vehicle Trajectories

4.1.2 Detector and Link Placement

The NGSIM Peachtree Street dataset does not include any short interval field detector data. For the research goals of this paper, detector data with short data collection intervals are necessary. Thirty-three sets of virtual detectors are placed as shown in Figure 19 and Table 3. Each set of detectors include a detector for each lane, even though only one detector is shown. Six sets of virtual detectors are selected for analysis. Detector Set #401 is 12-foot long located 6 feet from the stop bar, to present the common stop bar detection used in practice. All other detectors are 6-foot long. Detector Set #407 is located at about 75% link length from the stop bar, to present the advanced detector commonly installed by signal operation agencies at mid-block locations.

Detector Set #411 is placed at 40 feet from the stop bar to compare with the stop bar Detector Set #401, and analyze the difference between traffic conditions at the stop bar and traffic conditions immediately upstream to the stop bar. Detector Set #418 is placed very close to the upstream signal and used to analyze the potential dynamics caused by the upstream signal. To compare the impacts between signalized intersections and unsignalized intersections, Detector Set #422 is placed at the center of the link upstream of a signalized intersection and Detector Set #430 is placed at the center of the link upstream of an unsignalized intersection.

In the real world, traffic detectors are facing many challenges that can affect the detector data accuracy. These challenges include roadway geometries like significant roadway vertical profile changes, roadway horizontal curves, or roadway uneven terrains. Vehicles traveling on lane lines or changing lanes also cause detectors to double counts or miss counts. Detectors can have sensitivity issues such that detectors may be activated even if vehicles are not inside the detection zone. In addition, detector data are often processed by the detector internal software to achieve smoothed data. All of these factors introduce additional errors to the analysis. The virtual detector approach can prevent these additional errors being introduced so that the analysis can focus on the targeted problems.

A link is defined in this study as the roadway segment between two virtual detectors, from downstream detector downstream edge to the upstream detector upstream edge. Note the intersection stop bar locations used are not the original stop bar locations indicated in the NGSIM Peachtree Street dataset, but the improved and corrected locations by other researchers (88). Table 4 shows the links selected for further analysis.

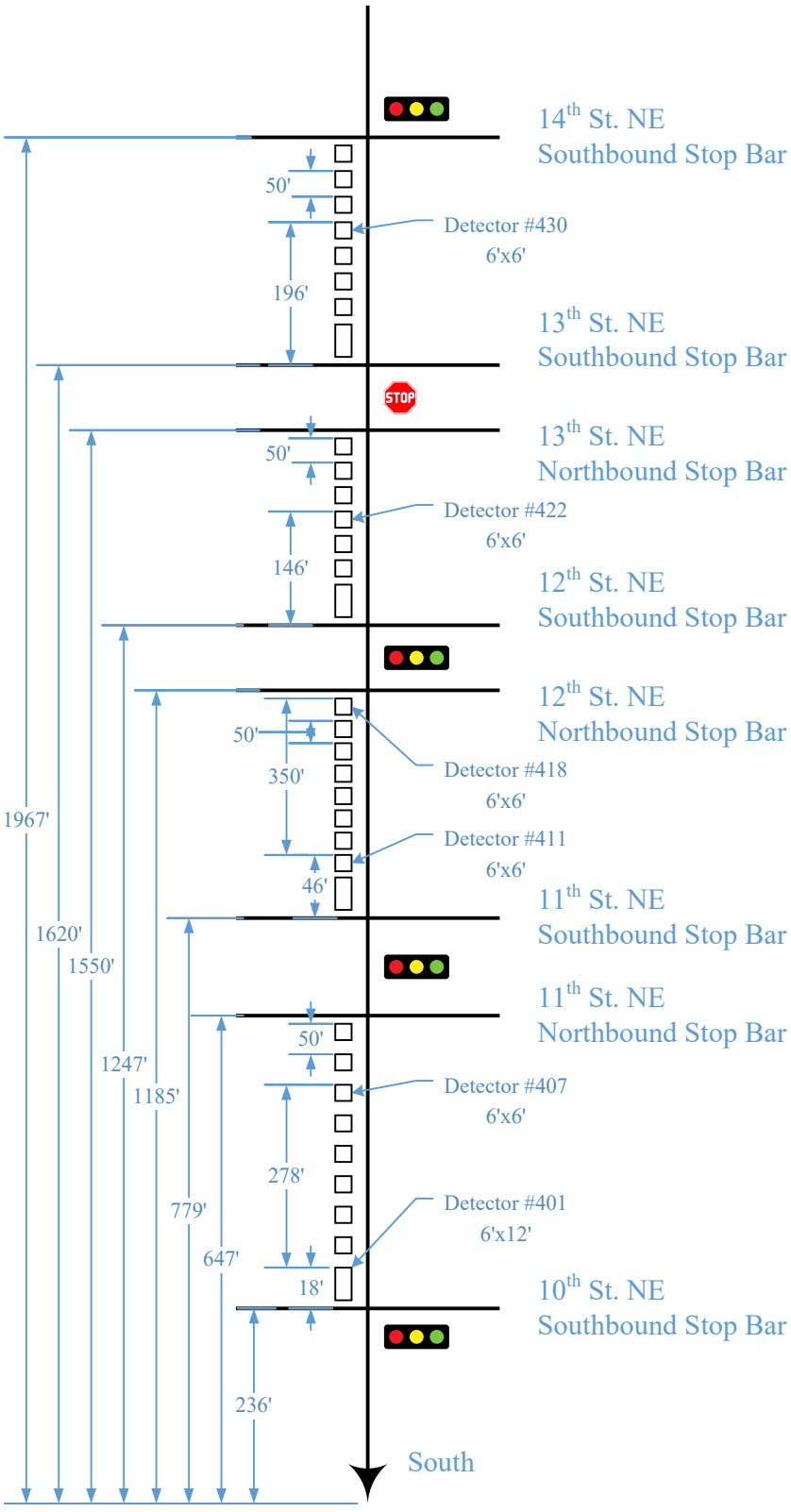
14th St. NE
Southbound Stop Bar
50'
Detector #430
6'x6'
196'
13th St. NE
Southbound Stop Bar
STOP
13th St. NE
Northbound Stop Bar
50'
Detector #422
6'x6'
146'
12th St. NE
Southbound Stop Bar
12th St. NE
Northbound Stop Bar
50'
350'
Detector #418
6'x6'
Detector #411
6'x6'
46'
11th St. NE
Southbound Stop Bar
11th St. NE
Northbound Stop Bar
50'
Detector #407
6'x6'
278'
Detector #401
6'x12'
18'
10th St. NE
Southbound Stop Bar
1967'
1620'
1550'
1247'
1185'
779'
647'
236'
South

Figure 19 Detector Placement

Table 3 Detector Positions

Detector ID	Stop Bar	Detector Center	Detector Length (ft)	Detector Downstream Edge	Detector Upstream Edge
401	236	248	12	242	254
402	236	279	6	276	282
403	236	329	6	326	332
404	236	379	6	376	382
405	236	429	6	426	432
406	236	479	6	476	482
407	236	529	6	526	532
408	236	579	6	576	582
409	236	629	6	626	632
410	779	791	12	785	797
411	779	822	6	819	825
412	779	872	6	869	875
413	779	922	6	919	925
414	779	972	6	969	975
415	779	1022	6	1019	1025
416	779	1072	6	1069	1075
417	779	1122	6	1119	1125
418	779	1172	6	1169	1175
419	1247	1259	12	1253	1265
420	1247	1290	6	1287	1293
421	1247	1340	6	1337	1343
422	1247	1390	6	1387	1393
423	1247	1440	6	1437	1443
424	1247	1490	6	1487	1493
425	1247	1540	6	1537	1543
426	1620	1632	12	1626	1638
427	1620	1663	6	1660	1666
428	1620	1713	6	1710	1716
429	1620	1763	6	1760	1766
430	1620	1813	6	1810	1816
431	1620	1863	6	1860	1866
432	1620	1913	6	1910	1916
433	1620	1952	6	1949	1955

Table 4 Link Positions

Detector Set ID	Stop Bar	Detector Center	Detector Length (ft)	Detector Downstream Edge	Detector Upstream Edge	Link ID	Link Length (ft)
401	236	248	12	242	254	401-407	290
407	236	529	6	526	532		
411	779	822	6	819	825	411-418	356
418	779	1172	6	1169	1175		
422	1247	1390	6	1387	1393	422-430	429
430	1620	1813	6	1810	1816		

4.1.3 Detector and Link Data Processing

When a vehicle's front falls inside a detector, the defined detector will be activated, until the vehicle's rear leaves the detector. The vehicle front position is directly available from the dataset defined as Local Y. The vehicle rear position equals to the vehicle front positon plus the vehicle length. To simply the data processing, vehicle lateral coordinates (Local X) are not considered. As long as the vehicle front or rear Local Y falls between the detector upstream and downstream edge Y coordinates, it is assumed the detector is activated by the vehicle. This assumption produces the detector data that are more accurate than the real world detector data. This is because given detectors are 6-foot wide and travel lanes are 12-foot wide, the real world detector tends to miscount when a vehicle travels on top of the lane line so that detectors on both lanes may fail to detect the vehicle.

The detector data collection time interval uses 10 seconds to simulate the worst case scenario that a single heavy vehicle can significantly change the detector measurements. In addition, the short time internal can keep the traffic flow randomness and dynamics from being smoothed by a

longer time interval. As a result, the analysis time interval used this study is a fixed time interval, which is 10 seconds.

The detector volume, speed, and time occupancy are generated every 10 seconds. The detector volume is the number of vehicles crossed the detection zone in the data collection time interval. The detector speed is the harmonic mean speed. The detector time occupancy is estimated as the total duration of all vehicles traversing the detection zone in the interval divided by the data collection time interval. It should be noted that the NGSIM dataset includes the vehicle spot speed every tenth of a second. But the spot speed data from the dataset are not used in this study, as pointed out by other researchers (89) that values in the velocity and acceleration fields of NGSIM datasets should be handled carefully, and it is suggested to directly estimate speeds from Local Y values whenever possible.

The link volume, speed, and time occupancy are generated using the same method as the detector data, except the time occupancy can be over 100%, given there can be multiple vehicles traveling along the link during a data collection time interval. For example, two vehicles traveled along the link during the 10-second data collection time interval. If each vehicle spent 6 seconds traveling along the link, the link time occupancy of the time interval would be 120%.

Figure 20 shows an example of the process to generate detector data from the vehicle trajectory data records during one data collection time period.

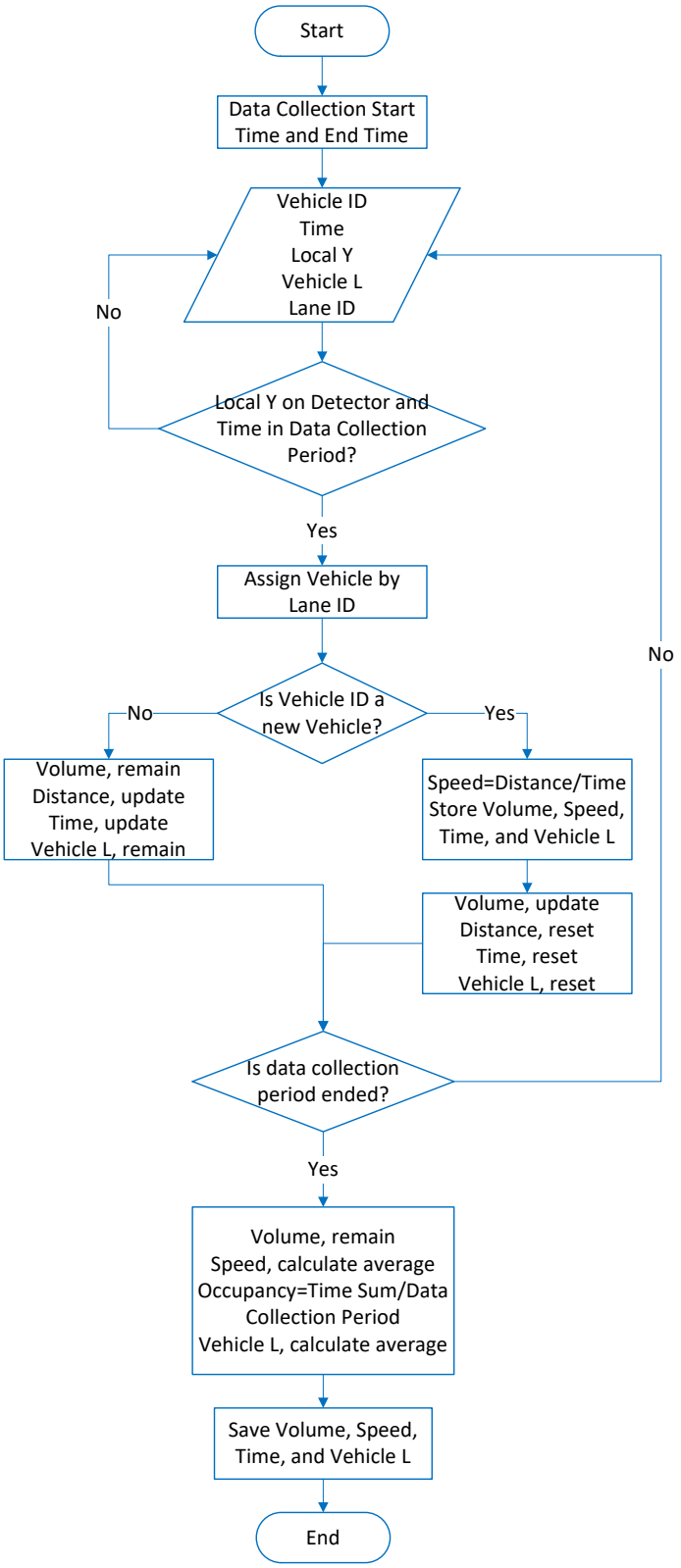

Figure 20 Detector Data Processing During a Data Collection Period

In addition, the generalized flow rate, speed and density data are also generated by using Equation 34, Equation 35 and Equation 36 in specifically defined time-space regions. The generalized flow rate, speed and density data are difficult to collect in practice. The NGSIM dataset provides the position of each vehicle every tenth of a second so that it is possible to measure the distance traveled by each vehicle and the time spent by each vehicle in a defined time-space region, with the accuracy of one tenth of a second. The time-space region for each vehicle can be defined as where and when the vehicle front enters the detection zone and the vehicle rear leaves the detection zone. The generalized flow rate, speed and density data are calculated every 10 seconds and used as the ground truth baseline for comparison.

4.2 Field Data Collected in New York City

Another set of field data used in this dissertation were collected as a part of the Beta Test for a large project to deploy microwave sensors and video image detectors along arterial streets (Figure 21) in Lower Manhattan by New York City Department of Transportation (NYCDOT). The data from these detectors are being provided to servers running TransSuite application software installed at the NYCDOT Transportation Management Center (TMC). The data are processed and converted to average travel speed information for display on the NYCDOT developed “flow map”. This “flow map” provides real time traffic condition information to New York City public agency staff to meet their operational needs and provide traveler information to the public via the World Wide Web.

Detector volume entering, speed and occupancy data were collected by microwave sensors installed at mid-block locations with a side-fire configuration. Detector volume entering, speed and occupancy data were raw detector data recorded every 10 seconds. Queue length data used were collected at two signalized intersections, Canal Street at Lafayette Street and Canal Street at Mercer Street. At each intersection, a video image detector was installed on a pole downstream to the stop bar to cover the eastbound travel lanes. The two video image detectors recorded and stored the video and detector volume exiting throughout the data collection time period. An observer then reviewed the recorded video, and manually counted the total number of queued vehicles and recorded the number in spreadsheets every 10 seconds. Because the available queue storage space is short for both intersections' eastbound approaches, about 350 feet for Lafayette and 200 feet for Mercer, the collected ground truth queue data is reasonably reliable. Canal Street has two travel lanes and three travel lanes in the eastbound direction at Lafayette and Mercer, respectively. Volume exiting data were also raw detector data recorded every 10 seconds.

All detector volume, speed, occupancy and queue length data sets were carefully synchronized. Data for one 24-hour period at each intersection are used for the analysis in this dissertation.

Figure 21 Detector Locations along Canal Street

4.3 Metered On-ramp Data

In addition to the NGSIM and New York City datasets, to further verify the analysis results this study also utilized field manually collected queue length data as a part of a larger project to evaluate ramp metering on Wisconsin freeways (90). The purpose of this larger study was to determine the benefits of ramp meters in the Milwaukee area freeway system, to determine underlying relationships that permit evaluation of new ramp meters or ramp meter systems elsewhere, and to develop a coherent framework for performing evaluation of ramp meter effectiveness on a whole system. Data collected included floating car runs, queue length counts, tube counts, origin-destination studies, questionnaires and archiving of a variety of loop detector

data (volumes, speeds and occupancies). Queue length data were collected at four locations, US 45 southbound on-ramps at Capitol Drive, Burleigh Street, North Avenue, and Wisconsin Avenue. There was an observer physically presented at each location. The observer manually counted the total number of on-ramp queue vehicles and recorded the number on a data collection sheet every 20 seconds, throughout the 1.5 hour morning and afternoon peak periods. Because the geometry is relatively simple and the ramp length is short at these four on-ramps, the field queue data is reasonably reliable. Detector volume and occupancy data collected were raw loop detector data recorded every 20 seconds. All data sets were carefully synchronized.

4.4 Sample Size

With a 5% margin of sampling error and a 95% confidence level, the sample size needed to develop a model for one detector or one link is calculated as shown in Equation 37. According to the calculation, at least 385 10-second detector data records are needed to develop the model at one detector or one link. Between 4:00:00 PM and 4:17:00 PM, there are 102 10-second time periods. Each virtual detector of the NGSIM dataset has 102 10-second data records. So data from a minimum of four detectors are needed for the analysis.

$$n_0 = \frac{Z^2 p(1-p)}{e^2} = \frac{1.96^2 \times 0.5 \times (1-0.5)}{0.05^2} = 384.2 \qquad \textbf{Equation 37}$$

where

n_0 = sample size without considering the finite population correction factor,
Z = value based on confidence level, 1.96 for 95% confidence,
p = estimated variance in population, 50% is used for the worst scenario, and
e = margin of sampling error, 5% is used.

5 ANALYSIS OF FLOW, DENSITY, SPEED, AND OCCUPANCY

This chapter starts with an analysis to examine the relationships among the detector volume, speed and time occupancy data, followed by the analysis to correlate the detector volume, speed and time occupancy to the generalized flow rate, density and space mean speed in a commonly used time-space region. Within this time-space region, the analyses show that the generalized density has a strong correlation with the detector time occupancy. However, using the equivalent hourly volume of the detector vehicle counts as the flow rate may introduce estimation errors during real-time traffic operations. A new performance measurement defined as the *traffic flow intensity* is introduced to represent the traffic flow conditions for real-time traffic operation purposes. All analyses will be done in specifically defined time-space regions. Field data will be utilized to confirm the findings.

5.1 Detector Volume, Speed and Time Occupancy

Figure 22 shows the relationship between time occupancy and the ratio of flow to time mean speed for freeway traffic flow. Cassidy and Coifman (79) demonstrated that harmonic mean speed was the ratio of flow to density and this relation held as an identity when the generalized definitions were followed. There was also a close to linear relationship between detector time occupancy and the ratio of flow to time mean speed, if the vehicle lengths did not change much during the observation periods. Freeway detector data collected by dual loop detectors were used for the analysis. The study didn't use a fixed data collection time period, instead the time period was selected to allow each defined rectangular time-space region to hold the trajectories

of 25 vehicles approximately. The study also demonstrated that the identity relation might not hold if traffic variables were not defined by following the generalized definitions.

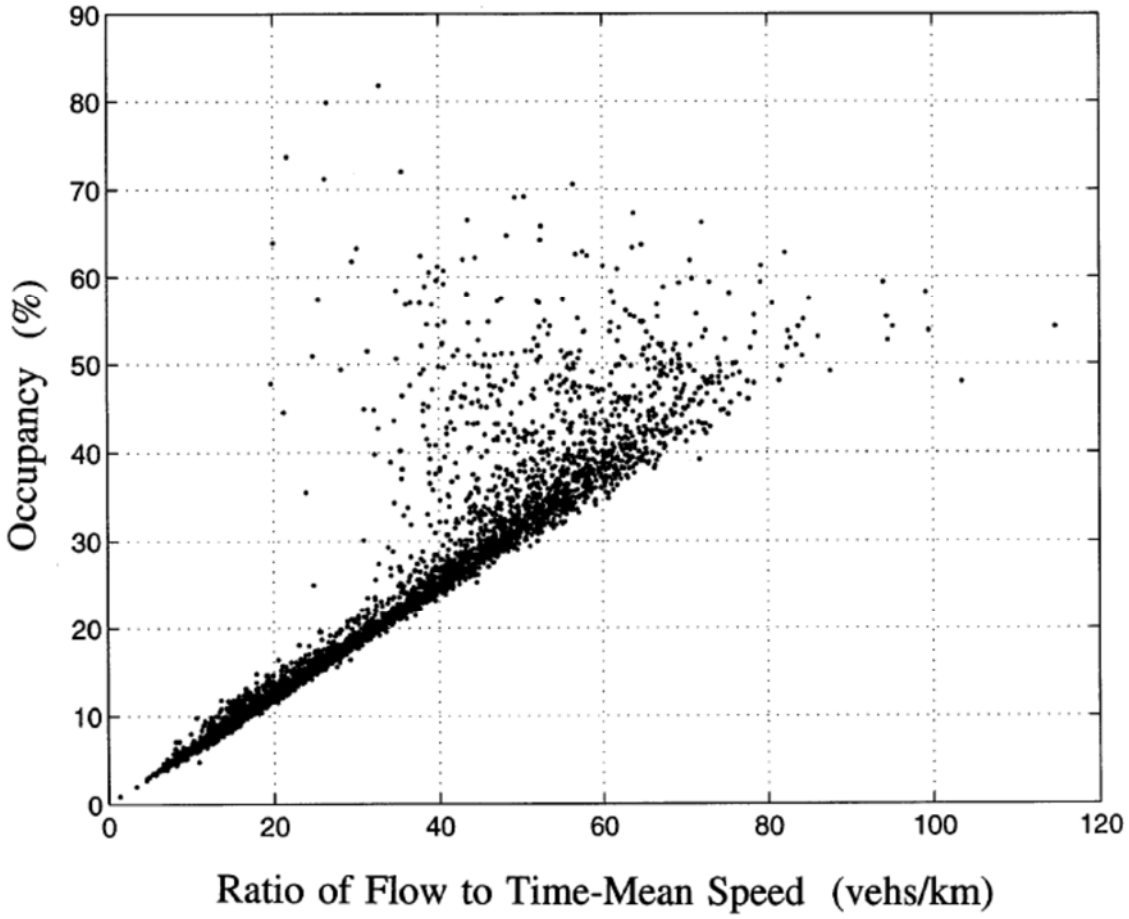

Figure 22 Ratio of Flow to Time Mean Speed vs. Time Occupancy with 30-second Time Intervals
(Cited from Cassidy and Coifman (79))

For comparison, Figure 23 shows the relationship between detector time occupancy and the ratio of detector volume to detector speed at the midblock location. Figure 24 shows the relationship between detector space occupancy and the ratio of detector volume to detector speed at the stop bar location. Both figures are plotted using the New York City dataset.

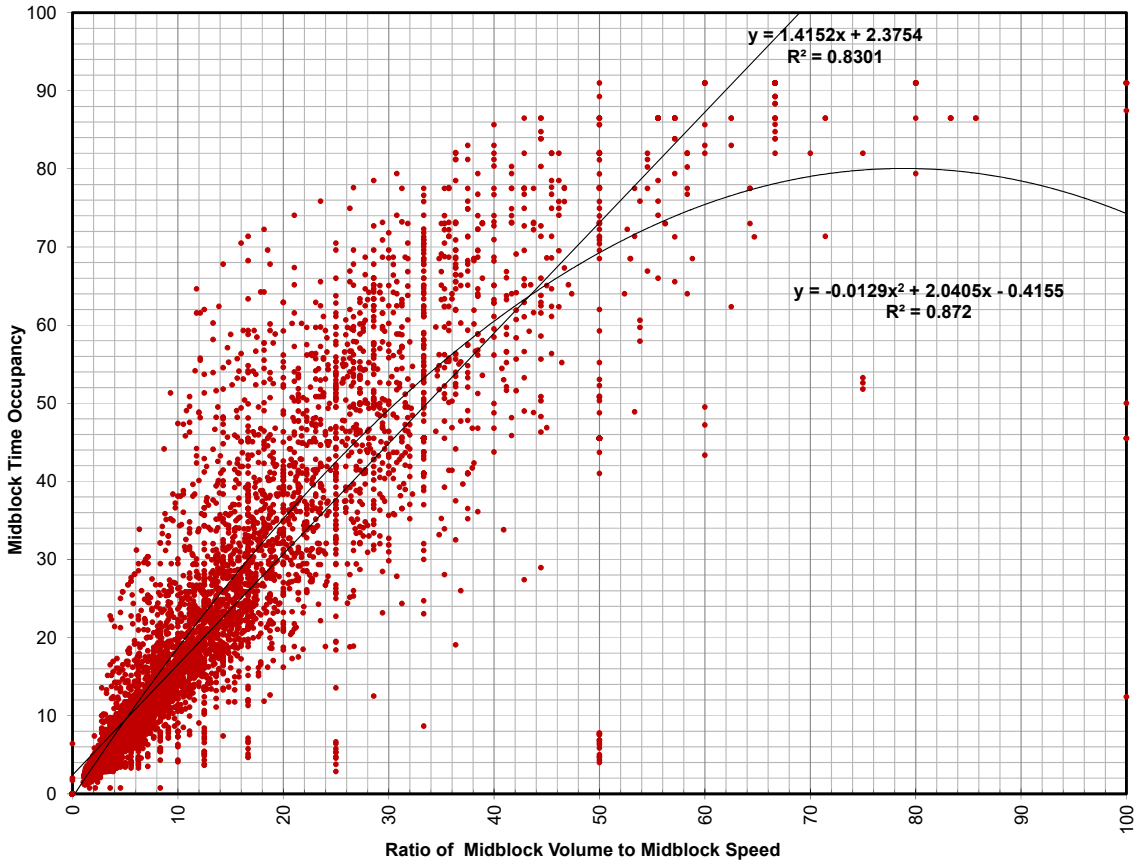

Figure 23 Ratio of Detector Midblock Volume to Speed vs. Time Occupancy (Plotted using New York City midblock detector data)

For the New York City field data, only time occupancy is collected at midblock and only space occupancy is collected at stop bar. This is because of the configurations of the video image detectors installed at stop bar, which cannot accurately collect and process time occupancy and space occupancy simultaneously in real time. In addition, the video image detectors at stop bar were configured to collect both vehicle queue length and space occupancy data. However, only queue length data were collected during red phases and only space occupancy data were

collected during green phases. This is because video images detectors can only pick up queues when vehicles are not moving.

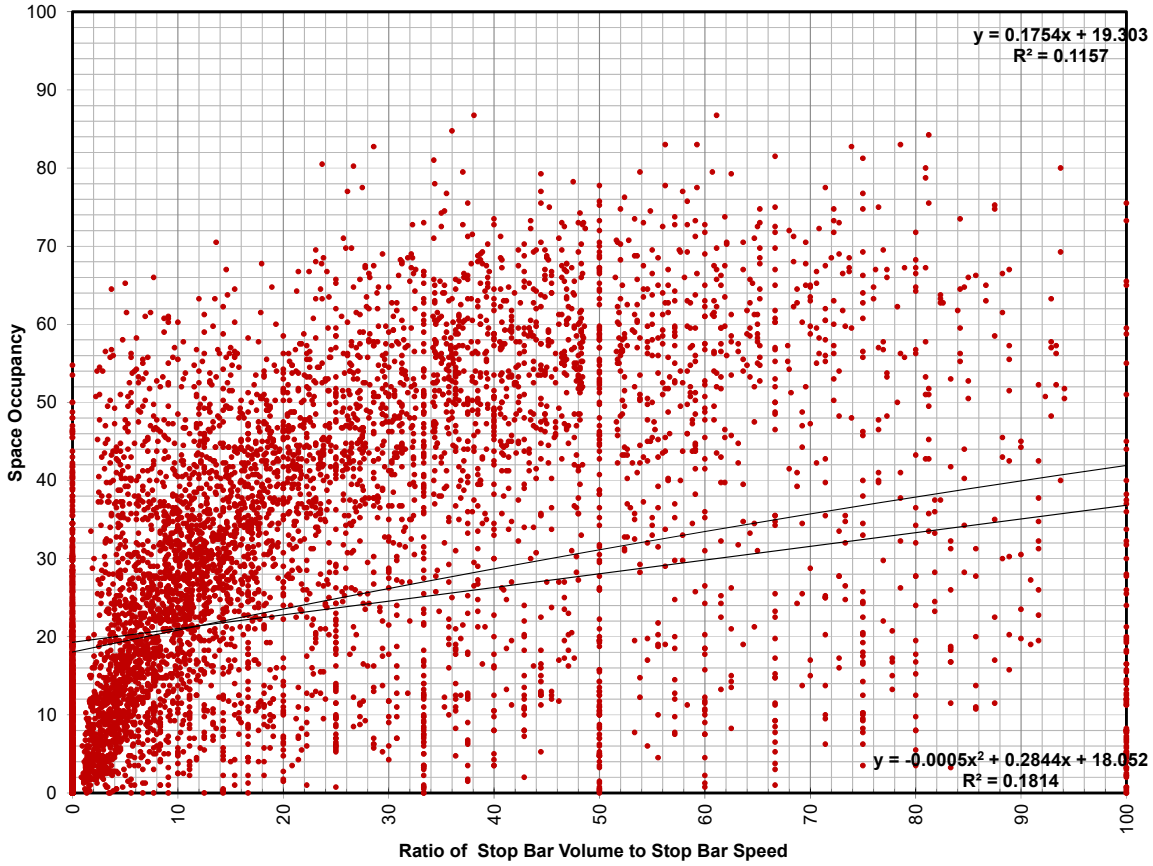

Figure 24 Ratio of Detector Stop Bar Volume to Speed vs. Space Occupancy (Plotted using New York City stop bar detector data)

Based on field observations, the traffic is constantly moving at the midblock location during off-peak hours. During peak hours, vehicle queues normally pass beyond the midblock microwave sensor location. Figure 23 and Figure 24 present a certain clustering of data, which indicates a possible non-liner relationship exists between the two sets of variables. Because of the different

traffic flow conditions, the diagram at midblock is much less scattered and better shaped than the diagram at stop bar. However, the arterial diagrams are very different from the freeway diagram.

In research and practice, this difference is often explained as traffic flow on signalized urban arterials is very different from that on freeways. Traffic flow on signalized urban arterials is periodically interrupted by traffic signals and vehicles go through deceleration, stop and acceleration constantly. Traffic flow can no longer be considered as spatially homogeneous along a roadway segment with signals. The oversaturated traffic condition along signalized arterials is considered as another major factor.

In addition, the ratio of detector volume to detector speed is usually used as density. Space occupancy and density are considered as identical, which is the proportion of space of a roadway segment that is covered by vehicles. Converting between time occupancy, space occupancy and density requires assuming average physical vehicle length and average space headway between vehicles. Generally, time occupancy and space occupancy have been used interchangeably or their relationship has been treated as linear for both uninterrupted and interrupted traffic flow. Several articles in the literature do point out that the average physical vehicle length could play a critical role in the relationship of time occupancy and space occupancy.

According to the generalized definitions of flow rate, density and space mean speed, the fundamental relationship, $v = ds$, exists within a finite time-space region, which applies to all types of traffic conditions and all shapes of time-space regions, including signalized arterials. This means Figure 23 and Figure 24 should present a close to linear relationship, if the detector

volume, speed and time occupancy data follow the generalized definitions of flow rate, density and space mean speed within a defined time-space region. The following section will examine the difference between the generalized definitions and the detector data.

5.2 Vehicles Crossing a Detector

Traffic detectors are placed at stop bars and midblock locations along signalized arterials. Detector volume, speed and occupancy data are measured with a very short detector length like 6 feet over a very short detector data collection time interval like 10 seconds. Detector volume is measured by counting the number of vehicles crossing the detection zone and detector speed is the harmonic mean speeds of all vehicles crossing the detection zone. Density at the detector location cannot be directly measured by detectors, instead time occupancy is measured as the proportion of time when the detection zone is occupied by vehicles. Figure 25 shows a detector in a time-space diagram during one 10-second data collection time period. Figure 26 shows a close look when vehicles completely crosses a detector with a constant speed in a time-space diagram during one detector data collection time period.

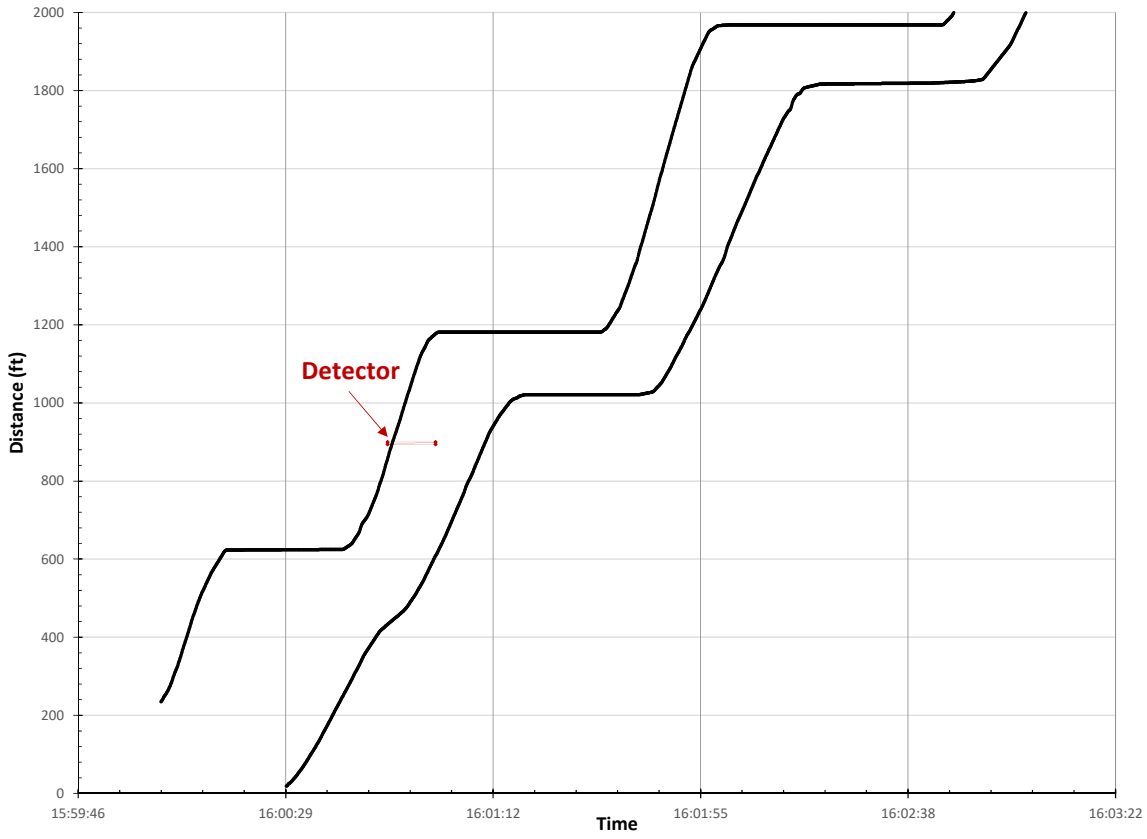

Figure 25 Detector in Time-Space Diagram

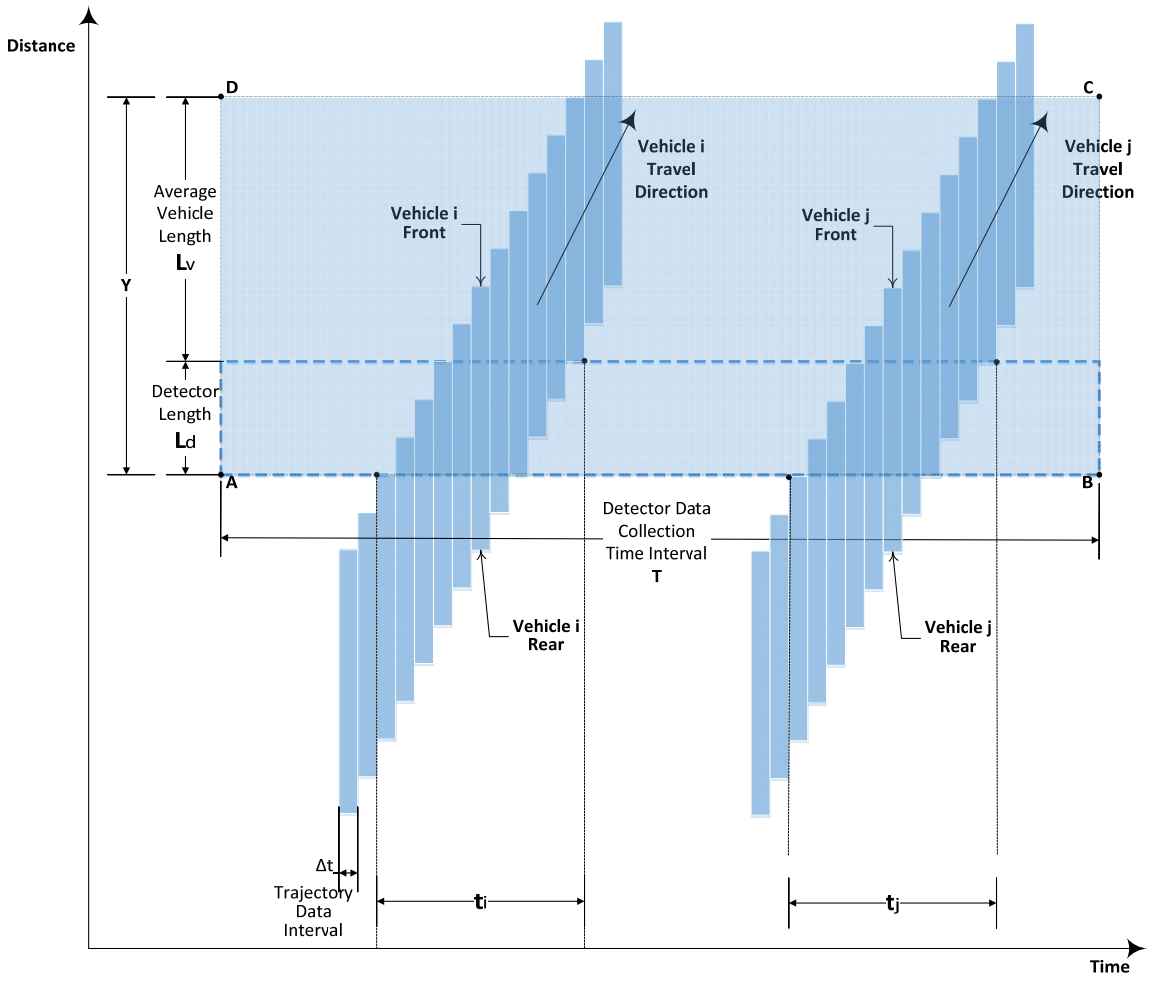

Figure 26 Close Look at Vehicles Crossing a Detector

In this case, the detector volume count $V_{detector}$ is N as shown by Equation 38 and the detector time occupancy is O_{time} as shown by Equation 39. The speed $S_{detector}$ collected by the detector is harmonic mean speed as shown by Equation 32 described in Section 3.1.1.

$$V_{detector} = N \qquad \textbf{Equation 38}$$

$$O_{time} = \frac{\sum_{i=1}^{N} t_i}{T} \times 100\% \qquad \textbf{Equation 39}$$

$$S_{detector} = \frac{N}{\sum_{i=1}^{N} \left(\frac{1}{\frac{L_i + L_d}{t_i}} \right)}$$ **Equation 32**

where

$V_{detector}$ = vehicle counts collected by a detector,
O_{time} = time occupancy collected by a detector (%),
t_i = time spent by vehicle i occupying the detection zone,
T = time interval of detector data collection (second),
L_i = physical vehicle length of vehicle i (ft), and
L_d = detector detection zone length (ft).

The rectangular $Region\ ABCD$ in Figure 26 is the region where and when vehicles' fronts enter the detection zone and vehicles' rears leave the detection zone. The rectangular time-space $Region\ ABCD$ is defined in such a way that the time length T equals to one data collection time interval and the space length Y is the average vehicle length plus the detector length, $L_v + L_d$. According to the generalized definitions, within the rectangular time-space $Region\ ABCD$, for all vehicles,

Total distance traveled is

$$\sum_{i=1}^{n} y_i = \sum_{i=1}^{n} (L_v + L_d) = (L_v + L_d) \times n$$ **Equation 40**

Total time spent is

$$\sum_{i=1}^{n} t_i = O_{time} \times T$$ **Equation 41**

Area of time-space region is **Equation 42**

$$Y \times T = (L_v + L_d) \times T$$

Flow Rate is

$$v = \frac{\sum_{i=1}^{n} y_i}{Y \times T} = \frac{\sum_{i=1}^{n} y_i}{(L_v + L_d) \times T} = \frac{n}{T} \quad \textbf{Equation 43}$$

Density is

$$d = \frac{\sum_{i=1}^{n} t_i}{Y \times T} = \frac{O_{time} \times T}{(L_v + L_d) \times T} = \frac{O_{time}}{L_v + L_d} \quad \textbf{Equation 44}$$

Space Mean Speed is

$$s = \frac{\sum_{i=1}^{n} y_i}{\sum_{i=1}^{n} t_i} = \frac{(L_v + L_d) \times n}{O_{time} \times T} \quad \textbf{Equation 45}$$

where

y_i = distance vehicle i traveled in the time-space region (ft),
n = number of vehicles,
L_v = average physical vehicle length (ft),
L_d = detector detection zone length (ft),
t_i = time vehicle i spent in the time-space region (second),
T = time interval of detector data collection (second),
O_{time} = total percentage of the data collection time interval when the detection zone is occupied by vehicles (%), and
Y = space length of the time-space region defined.

Equation 43, Equation 44 and Equation 45 are the most common methods used in research and practice, which provide a way to correlate the detector volume, speed and time occupancy to the generalized flow rate, density and space mean speed within the rectangular $Region\ ABCD$ as shown in Figure 26. As a result, three sets of data become available for analysis as listed below. Analysis of these three sets of data will be conducted in the following sections.

- The generalized flow rate, density and space mean speed data, generated by using Equation 34, Equation 35 and Equation 36 based on the NGSIM dataset.

- The detector volume, speed and time occupancy data, generated by using the NGSIM dataset as described in Section 4.1.3.
- The estimated generalized flow rate, density and space mean speed data, calculated by using Equation 43, Equation 44 and Equation 45 with the detector volume, speed and time occupancy data.

Figure 27 demonstrates that the fundamental relationship as described by Equation 31 holds valid at the stop bar location, when the generalized definitions are followed.

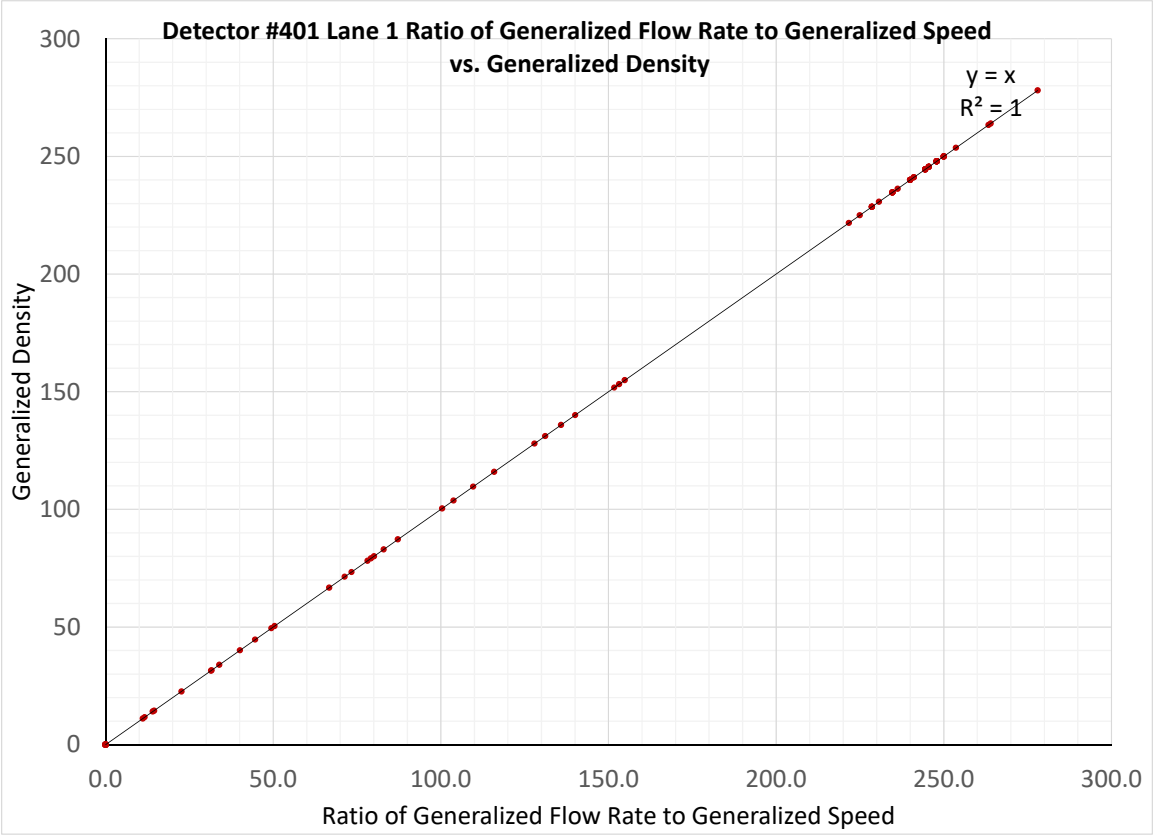

Figure 27 Detector Set #401 Lane 1 Ratio of Generalized Flow Rate to Generalized Speed vs. Generalized Density
(Plotted using NGSIM virtual detector data at stop bar)

5.2.1 Speed

Figure 28 and Figure 29 show the relationships between the generalized speed and the detector speed at both stop bar and midblock locations. Note the generalized space mean speed is defined within the rectangular $Region\ ABCD$ as shown in Figure 26. As shown in Figure 19, Detector Set #401 is located at the stop bar and Detector Set #407 is located at midblock close to the upstream traffic signal. With queueing caused by the traffic signal operation, the stop bar data present more scattering than the midblock data, with the R^2 values of 0.9434 and 0.9977 at stop bar and midblock, respectively.

It is expected for the detector speed data to be close to the generalized space mean speed data, because the detector speed data used in this study is the harmonic mean speeds.

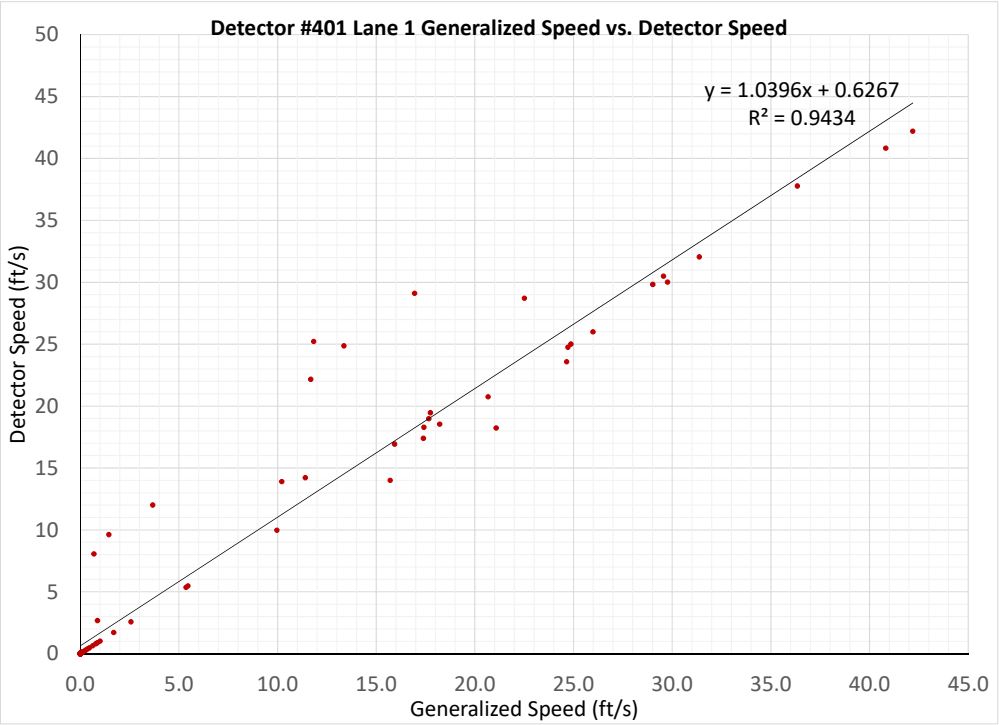

Figure 28 Detector Set #401 Lane 1 Generalized Speed vs. Detector Speed (Plotted using NGSIM data at stop bar)

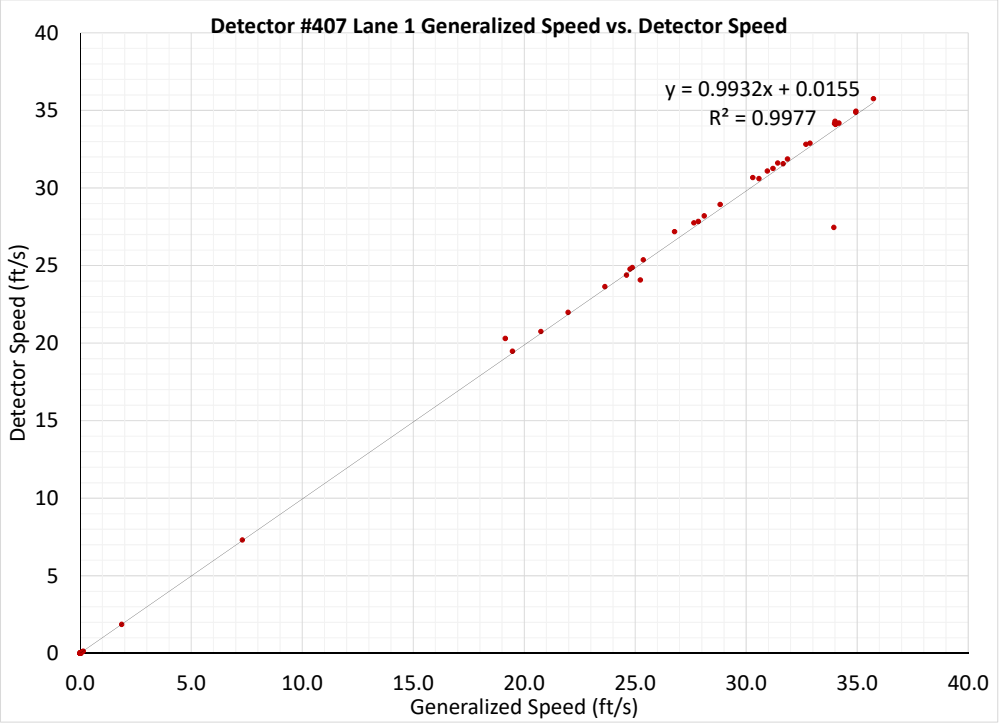

Figure 29 Detector Set #407 Lane 1 Generalized Speed vs. Detector Speed (Plotted using NGSIM data at midblock)

5.2.2 Density

Figure 30 and Figure 31 demonstrate the relationships between the generalized density and the ratio of detector volume to detector speed at stop bar and midblock, respectively. The time-space region used for the generalized density is the rectangular $Region\ ABCD$ as shown in Figure 26. The R^2 values are 0.027 and 0.5888 at stop bar and midblock, respectively.

In Figure 30 and Figure 31, all data points are used to plot the diagrams, which present no correlation between the generalized density and the ratio of detector volume to detector speed. If the outliers are removed from the analysis, the diagrams will be slightly better shaped, but still doesn't present any apparent correlation. Considering the detector speed data are very close to the generalized space mean speed data, it is almost certain that the detector volume is not equivalent to the generalized flow rate. Further analysis is needed to examine the relationship between the detector volume and the generalized flow rate.

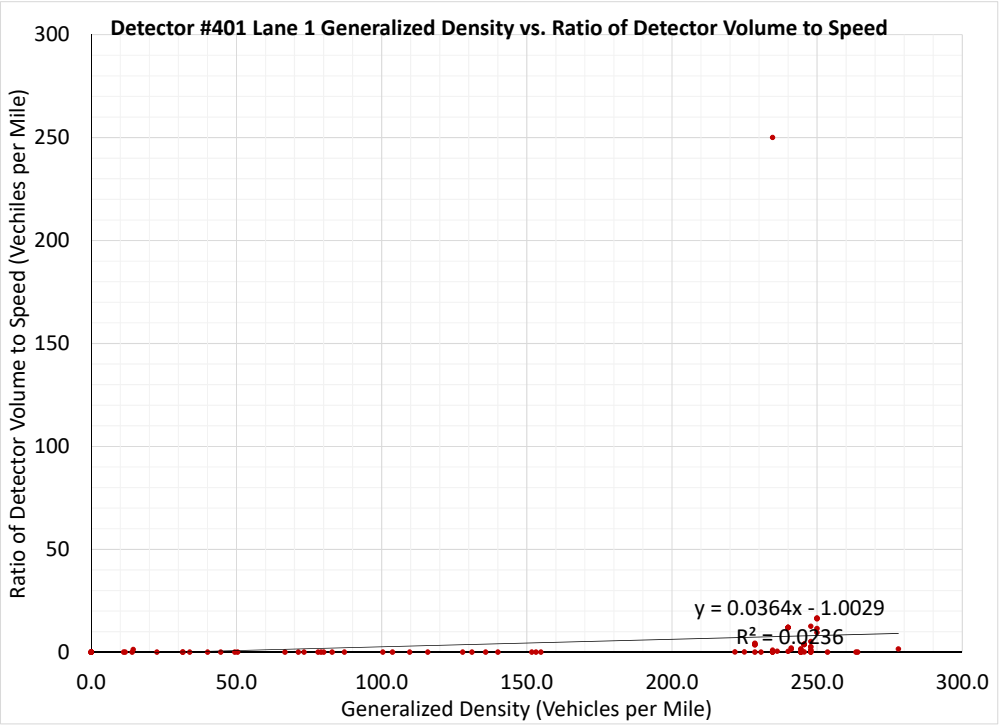

Figure 30 Detector Set #401 Lane 1 Generalized Density vs. Ratio of Detector Volume to Speed
(Plotted using NGSIM data at stop bar)

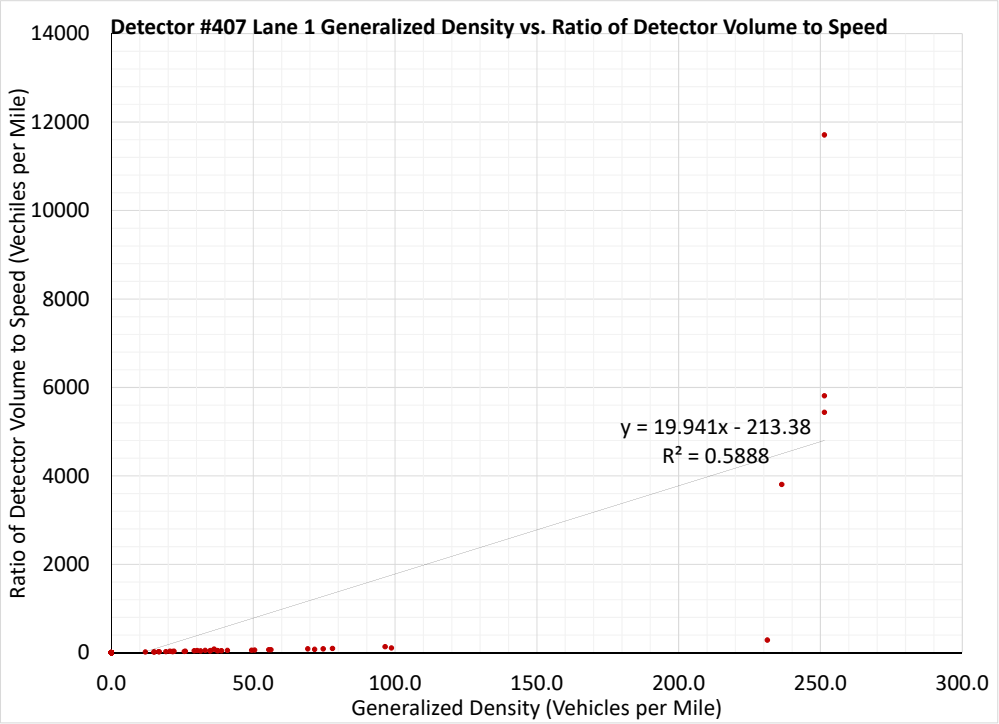

Figure 31 Detector Set #407 Lane 1 Generalized Density vs. Ratio of Detector Volume to Speed
(Plotted using NGSIM data at midblock)

According to Equation 44, the generalized density and the detector time occupancy has a perfect linear relationship if the average physical vehicle length remains constant. This means if the percentage of heavy vehicles is very low like along the NGSIM project corridor, the scatter diagram of the generalized density and the detector time occupancy will present a strong linear correlation. Figure 32 and Figure 33 prove this. The reason that the perfect linear correlation is seldom seen in most previous studies is because most studies don't have the generalized density data available and usually use the ratio of detector volume to detector speed as the estimated detector density.

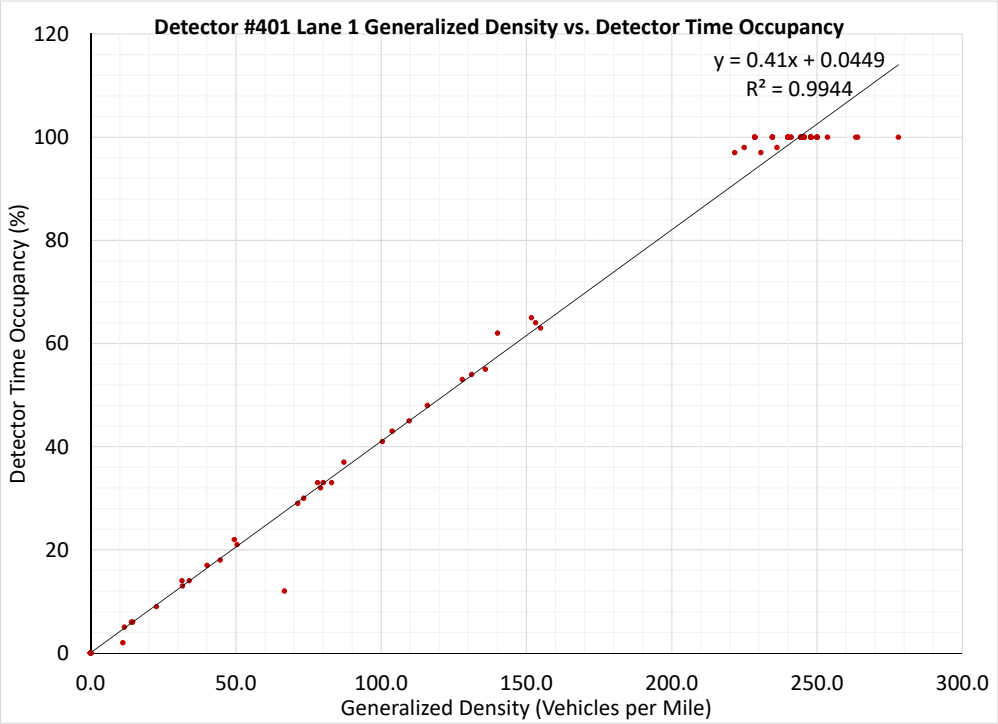

Figure 32 Detector Set #401 Lane 1 Generalized Density vs. Detector Time Occupancy
(Plotted using NGSIM data at stop bar)

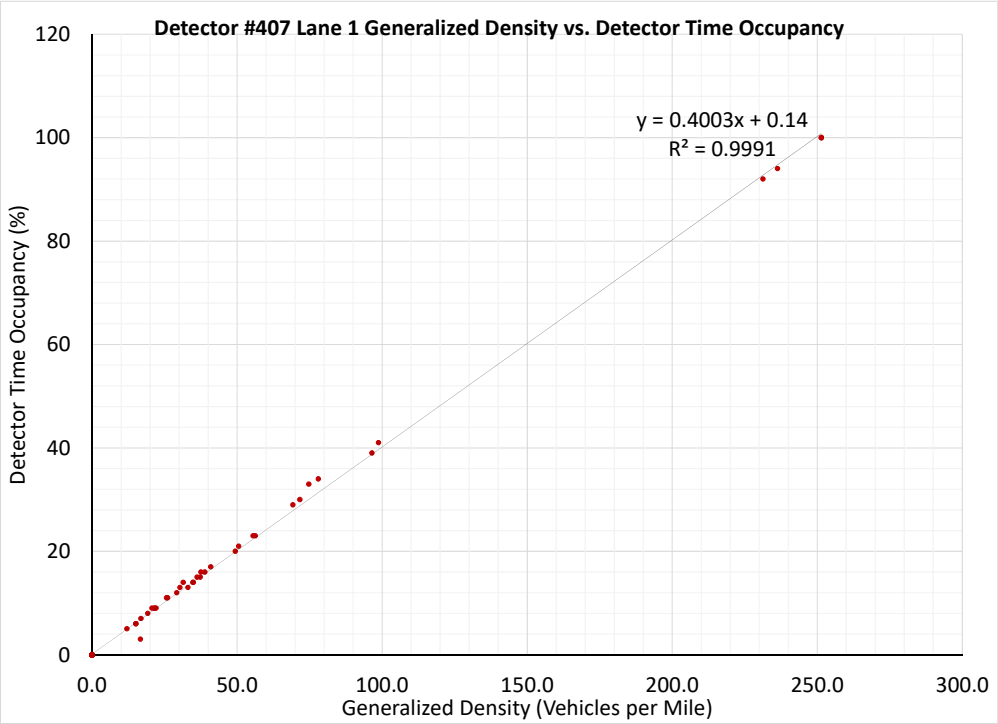

Figure 33 Detector Set #407 Lane 1 Generalized Density vs. Detector Time Occupancy (Plotted using NGSIM data at midblock)

5.2.3 Flow Rate

Equation 43 presents the most common method to convert detector volume to the flow rate at the detector location. The equivalent hourly volume of the detector vehicle counts during the data collection time period is often treated as the flow rate. With non-stationary traffic flow, simply converting detector volume counts to the flow rate may introduce estimation errors, given the volume counts collected by detectors can change dramatically between different data collection time periods. In practice, flow rates are often collected by counting vehicles in a sub-hourly period, like 15 minutes, and converted to an equivalent hourly rate. A peak hour factor is used to describe the flow rate variations in an hour, with lower peak hour factor values indicating greater variability of flow and higher values signifying less variations (91).

Figure 34 and Figure 35 show the relationships between the generalized flow rate and the detector volume at both stop bar and midblock locations. With queueing caused by the traffic signal operation, the stop bar data present more scattering than the midblock data. The R^2 values are 0.8514 and 0.9693 at stop bar and midblock, respectively.

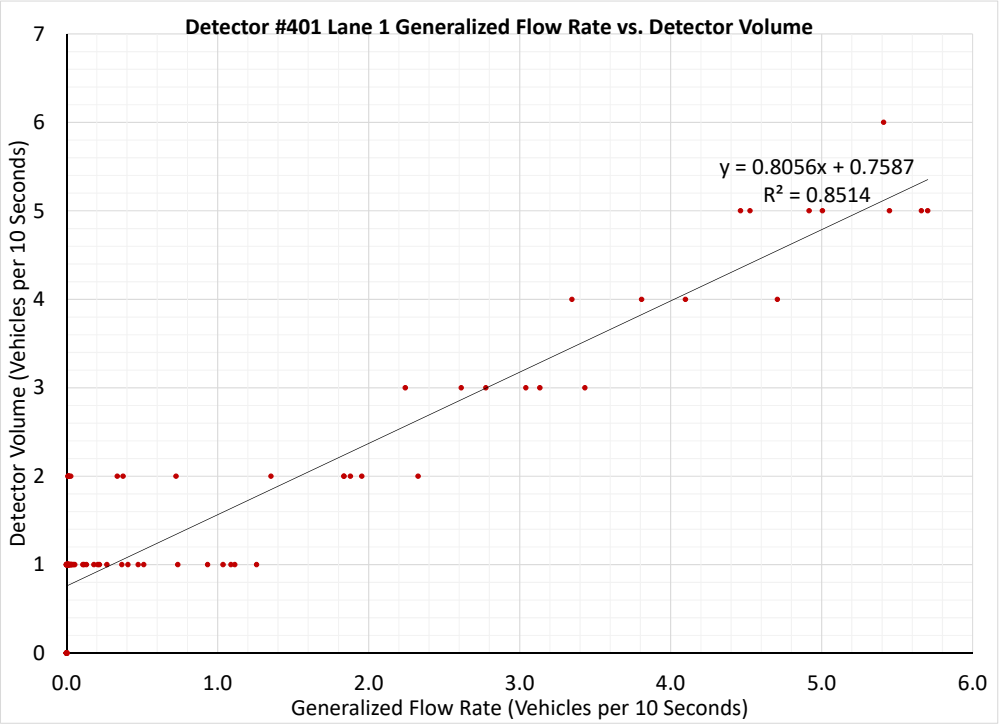

Figure 34 Detector Set #401 Lane 1 Generalized Flow Rate vs. Detector Volume (Plotted using NGSIM data at stop bar)

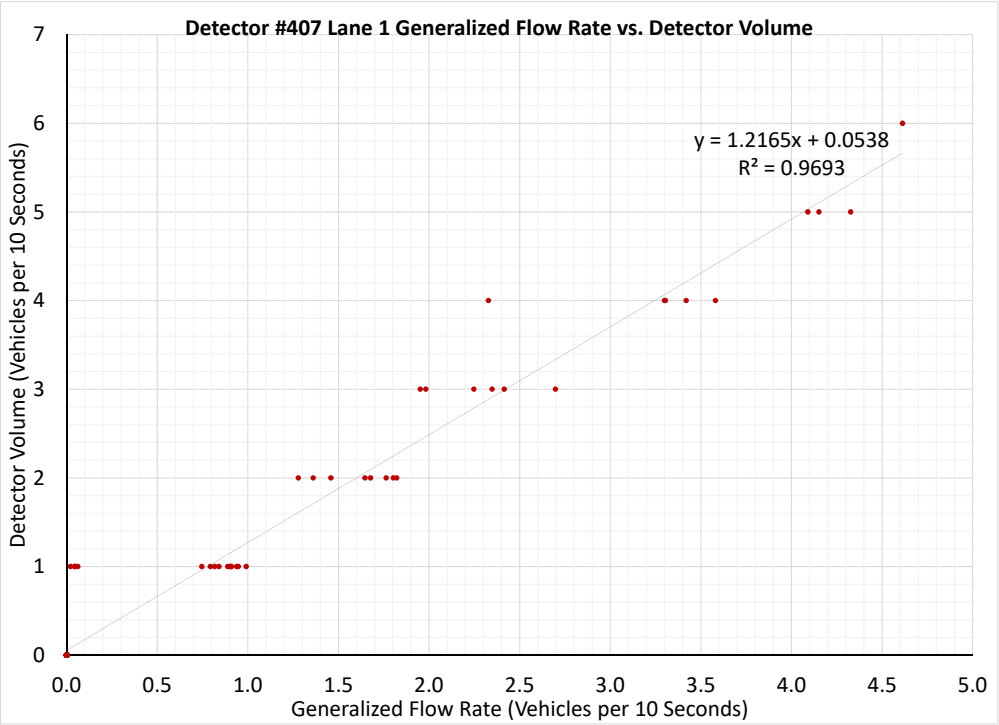

Figure 35 Detector Set #407 Lane 1 Generalized Flow Rate vs. Detector Volume (Plotted using NGSIM data at midblock)

In Figure 34 and Figure 35, the detector volume data are not continuous values, one detector volume value may correspond to many generalized flow rate values, which means various traffic conditions with different generalized flow rates may have the same detector volume. For example, there is only one vehicle crossing the detection zone within the data collection time period. The flow rate of one vehicle spending 2 seconds crossing the detection zone should be different from the flow rate of one vehicle spending 4 seconds crossing the detection zone. However, with Equation 43, these two conditions will have the same flow rate. In addition, as shown by Equation 46, the flow rate is the reciprocal of the average time headway. It always assumes that vehicles would evenly spread across the data collection time period when crossing the detection zone.

$$h_t = \frac{1}{\frac{T}{n}}$$ **Equation 46**

where

h_t = average time headway between vehicles (second).

There are two assumptions made when Equation 43 is developed. One is that vehicles cross the detector with a constant speed. The other is that the distance traveled by vehicles while crossing the detector equals to the detection zone length L_d plus the average physical vehicle length L_v. Under the signalized arterial environment, these two conditions cannot always be met.

In Equation 43, if vehicles don't completely cross the detector during the data collection time period, the total distance traveled by all vehicles divided by the detection zone length L_d plus the average physical vehicle length L_v, $\frac{\sum_{i=1}^{n} y_i}{(L_v+L_d)}$, will not equal to the number of vehicles n. In this case, the generalized flow rate will not be $\frac{n}{T}$.

As a result, simply converting detector volume counts within one data collection time period to use as the generalized flow rate will introduce estimation errors. The significance of the error is impacted by the traffic flow condition. Especially with short data collection time intervals used for real-time operation purposes along signalized arterials, the equivalent hourly volume of the detector vehicle counts during the data collection time period should not be treated as the generalized flow rate. To further analyze these situations, individual time-space regions will be defined for individual vehicles.

5.3 Time-Space Regions for Individual Vehicles

The rectangular *Region EFGH* in Figure 36 is the region where and when vehicle i front enters the detection zone and vehicle i rear leaves the detection zone. The rectangular time-space *Region EFGH* is defined in such a way that the time spent by the vehicle in the time-space region, t_i, equals to the time spent by the vehicle occupying the detection zone. The space length of the time-space region, y_i, is the distance the vehicle traveled during time t_i. For each vehicle, a time-space region like *Region EFGH* in Figure 36 can be defined.

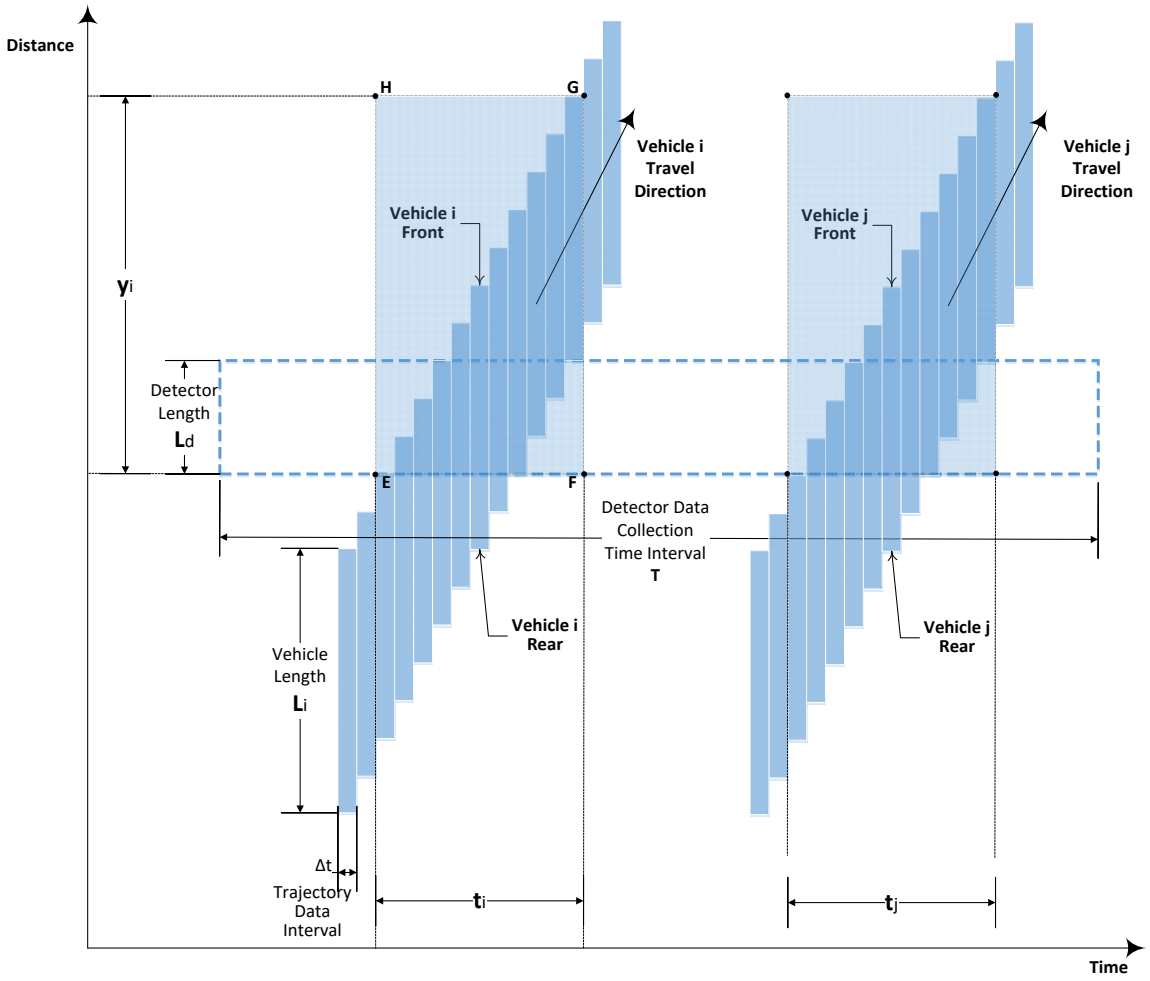

Figure 36 Time-Space Regions for Vehicles Crossing a Detector

According to the generalized definitions, assuming vehicles completely cross the detector during one data collection time interval, within all time-space regions in Figure 36 combined, for all vehicles,

Total distance traveled is

$$\sum_{i=1}^{n} y_i = \sum_{i=1}^{n} (L_i + L_d) = \frac{\sum_{i=1}^{n} (L_i + L_d)}{n} \times n = (L_v + L_d) \times n \quad \textbf{Equation 47}$$

Total time spent is

$$\sum_{i=1}^{n} t_i = O_{time} \times T \quad \textbf{Equation 48}$$

Area of all time-space regions combined is

$$\sum_{i=1}^{n} (y_i \times t_i) = \sum_{i=1}^{n} [(L_i + L_d) \times t_i]$$

$$= \sum_{i=1}^{n} (L_i \times t_i) \quad \textbf{Equation 49}$$

$$+ \sum_{i=1}^{n} (L_d \times t_i) = \sum_{i=1}^{n} (L_i \times t_i) + L_d \times \sum_{i=1}^{n} t_i$$

$$= L_t \times O_{time} \times T + L_d \times O_{time} \times T = (L_t + L_d)$$

$$\times O_{time} \times T$$

Flow rate is **Equation 50**

$$v = \frac{\sum_{i=1}^{n} y_i}{\sum_{i=1}^{n}(y_i \times t_i)} = \frac{(L_v + L_d) \times n}{(L_t + L_d) \times O_{time} \times T}$$

Density is

$$d = \frac{\sum_{i=1}^{n} t_i}{\sum_{i=1}^{n}(y_i \times t_i)} = \frac{O_{time} \times T}{(L_t + L_d) \times O_{time} \times T} = \frac{1}{L_t + L_d} \quad \textbf{Equation 51}$$

Space mean speed is

$$s = \frac{\sum_{i=1}^{n} y_i}{\sum_{i=1}^{n} t_i} = \frac{(L_v + L_d) \times n}{O_{time} \times T} \quad \textbf{Equation 52}$$

Average physical vehicle length is

$$L_v = \frac{\sum_{i=1}^{n} L_i}{n} \quad \textbf{Equation 53}$$

Average vehicle length weighted by time is

$$L_t = \frac{\sum_{i=1}^{n}(L_i \times t_i)}{\sum_{i=1}^{n} t_i} = \frac{\sum_{i=1}^{n}(L_i \times t_i)}{O_{time} \times T} \quad \textbf{Equation 54}$$

where

n = number of vehicles,
L_i = physical vehicle length of vehicle i (ft),
L_d = detector detection zone length (ft),
t_i = time length of the time-space region defined for vehicle i,
T = time interval of detector data collection (second).
y_i = space length of the time-space region defined for vehicle i,
L_v = average physical vehicle length (ft), and
L_t = average vehicle length weighted by the time vehicle spent crossing the detection zone (ft).

Equation 47 calculates the total distance traveled by all vehicles in the combined time-space regions. Equation 48 is the total time spent by all vehicles in the combined time-space regions. Equation 49 is the total area of all time-space regions during the time period combined. The generalized flow rate, density and speed can be estimated using the detector volume, time

occupancy and vehicle lengths, as shown by Equation 50, Equation 51 and Equation 52, respectively.

Equation 53 is the arithmetic average of all vehicle lengths. A special type of average vehicle length is introduced as shown by Equation 54. The time weighted average vehicle length L_t is calculated by considering the time each vehicle spends crossing the defined time-space region. The time weighted average vehicle length L_t is equal to the total area of all time-space regions combined divided by the total time the detection zone is occupied by vehicles during the data collection time period. The time weighted average vehicle length gives bigger weights in the average to cases such that heavy vehicles with longer vehicle lengths spend more time crossing the detection zone.

One assumption made is that vehicles completely cross the detector. The average distance traveled by vehicles while crossing the detector equals to the detection zone length L_d plus the time weighted average vehicle length L_t. During a data collection time period, all vehicles except one or two vehicles can completely cross the detector. Considering the effective detector length is very short, if a vehicle doesn't completely cross the detector, then the speed is very low and the vehicle is most likely in a stop condition. With carefully selected detector speed or time occupancy thresholds, the stop condition can be very easily identified and filtered in the analysis, which will be further analyzed in Chapter 6. Therefore, this assumption should not introduce significant estimation errors.

The generalized flow rate and density cannot be easily measured in the field. Within time-space regions as defined in Figure 36, Equation 50, Equation 51 and Equation 52 provide a way to estimate the generalized flow rate, space mean speed and density using the detector volume count, harmonic mean speed and time occupancy data, along with the average physical vehicle length and the time weighted average vehicle length data. The following sections will compare the generalized flow rate, space mean speed and density with the values estimated by using Equation 50, Equation 51 and Equation 52.

5.3.1 Flow Rate

Figure 37 and Figure 38 present the relationships between the generalized flow and the flow estimated using the detector data for two detectors, one at stop bar and the other at midblock. Although the stop bar data present some scattering, the R^2 values are very close to 1. Within time-space regions defined in Figure 36, the flow estimated using the detector data with Equation 50 is very close to the generalized flow generated by using Equation 34 based on the NGSIM dataset.

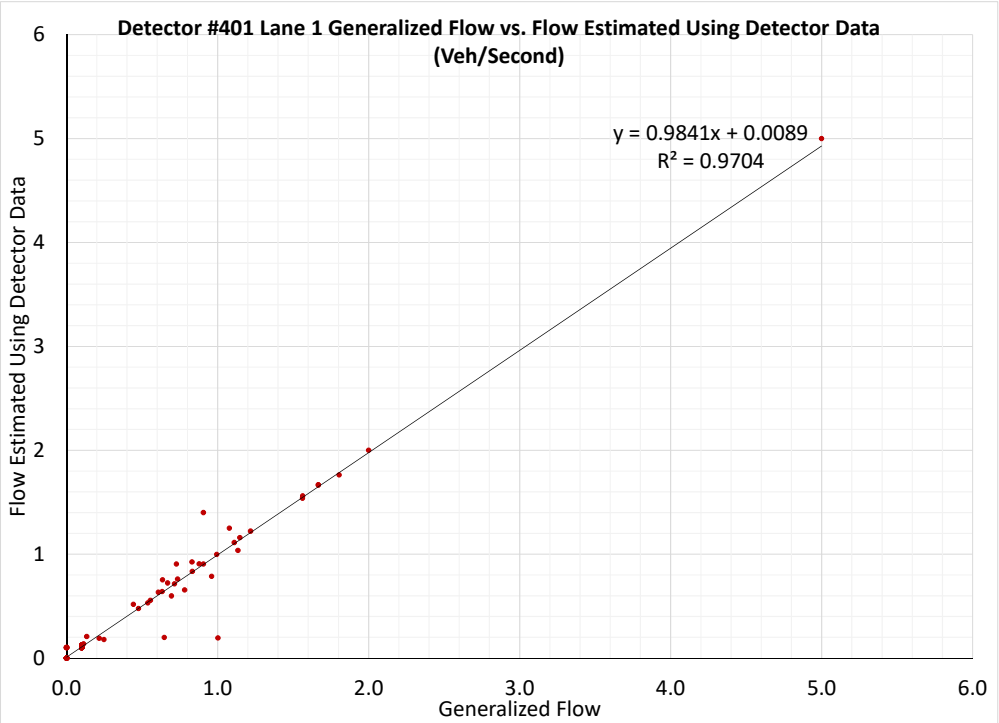

Figure 37 Detector Set #401 Lane 1 Generalized Flow vs. Flow Estimated Using Detector Data
(Plotted using NGSIM data at stop bar)

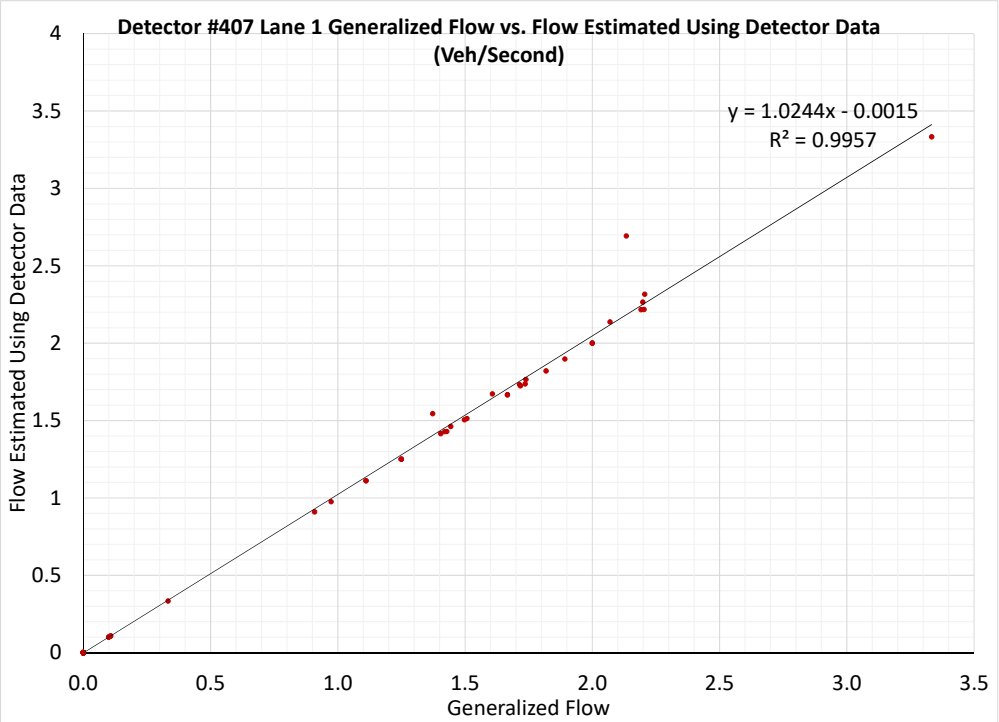

Figure 38 Detector Set #407 Lane 1 Generalized Flow vs. Flow Estimated Using Detector Data
(Plotted using NGSIM data at stop bar)

For this NGSIM dataset, the average physical vehicle length is approximately 16 feet, with very low volume of heavy vehicles and motorcycles. As a result, the average physical vehicle length and the time weighted average vehicle length have very close values and $\frac{L_v+L_d}{L_t+L_d}$ is approximately equal to 1. Equation 50 can be simplified to Equation 55. The estimated results by Equation 55 are shown in Figure 39 and Figure 40.

Equation 55 produces almost the same results as Equation 50 using the vehicle length data. Considering the vehicle length data are not always available in the real world traffic operations, Equation 55 provides a very good and very easy approach to the generalized flow rate estimation in the time-space regions as defined in Figure 36. The estimation is much better than directly using the detector volume counts divided by the data collection time interval as the flow rate. However, it should be noted that the reason Equation 55 could be as accurate as Equation 50 could be because of the homogeneous vehicles in the NGSIM dataset used in this study.

$$v = \frac{V_{detector}}{O_{time} \times T} \qquad \textbf{Equation 55}$$

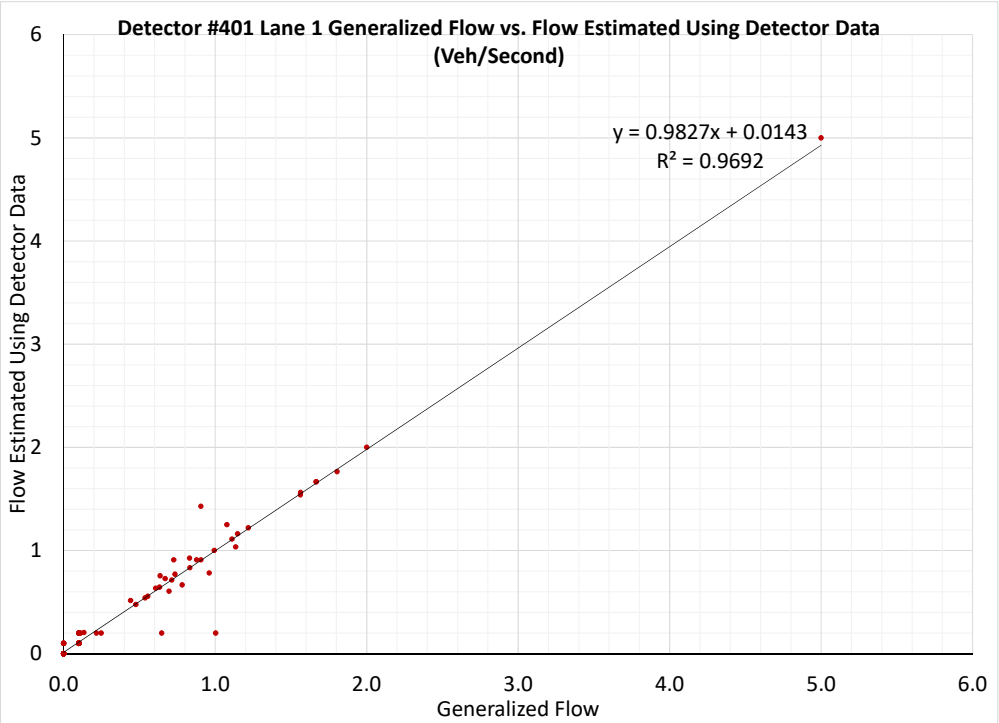

Figure 39 Detector Set #401 Lane 1 Generalized Flow vs. Flow Estimated Using Detector Data Without Vehicle Lengths
(Plotted using NGSIM data at stop bar)

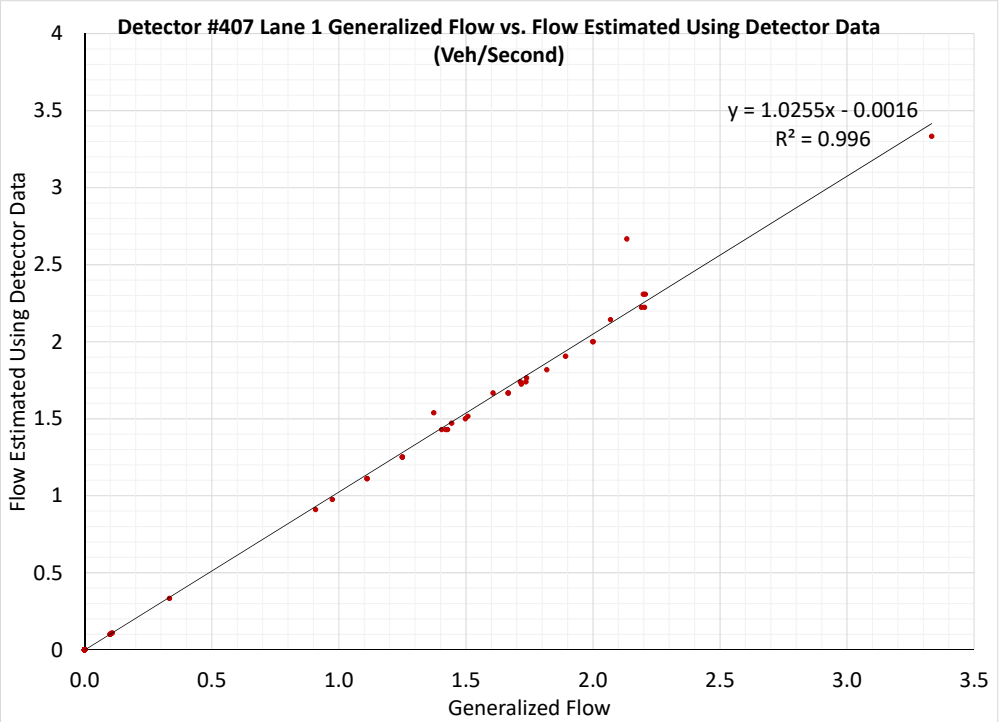

Figure 40 Detector Set #407 Lane 1 Generalized Flow vs. Flow Estimated Using Detector Data Without Vehicle Lengths (Plotted using NGSIM data at stop bar)

5.3.2 Speed

It can be seen that Equation 45 and Equation 52 are the same. The generalized space mean speed data in time-space regions as defined in Figure 36 are identical to the generalized space mean speed data in the time-space region as defined in Figure 26. This is anticipated based on the definition that the generalized space mean speed is defined as the total distance traveled by all vehicles in the time-space region divided by the total time spent by all vehicles in the time-space region.

As shown in Figure 28 and Figure 29, Figure 36 presents the correlation between the generalized space mean speed and the detector harmonic mean speed is very strong. Given the defined time-space region at the detector has a very small length (about 28 feet in the NGSIM dataset), the difference between the detector harmonic mean speed and the space mean speed should be very small, if any difference exists. The stop bar data are more scattered than the midblock data, because vehicles frequently decelerate, stop and accelerate due to signal phasing changes and queueing at the signalized intersection.

5.3.3 Density

Density cannot be directly measured by detectors. The generalized density has no linear relationship with the detector density that is calculated by Equation 51 assuming all vehicles completely crossing the detection zone during the data collection time period. It is assumed that

during the data collection time period, when crossing the detection zone, the average distance traveled by vehicles is $\frac{\sum_{i=1}^{n} y_i}{n}$ and equal to $L_t + L_d$, the time weighted average vehicle length plus the detection zone length L_d.

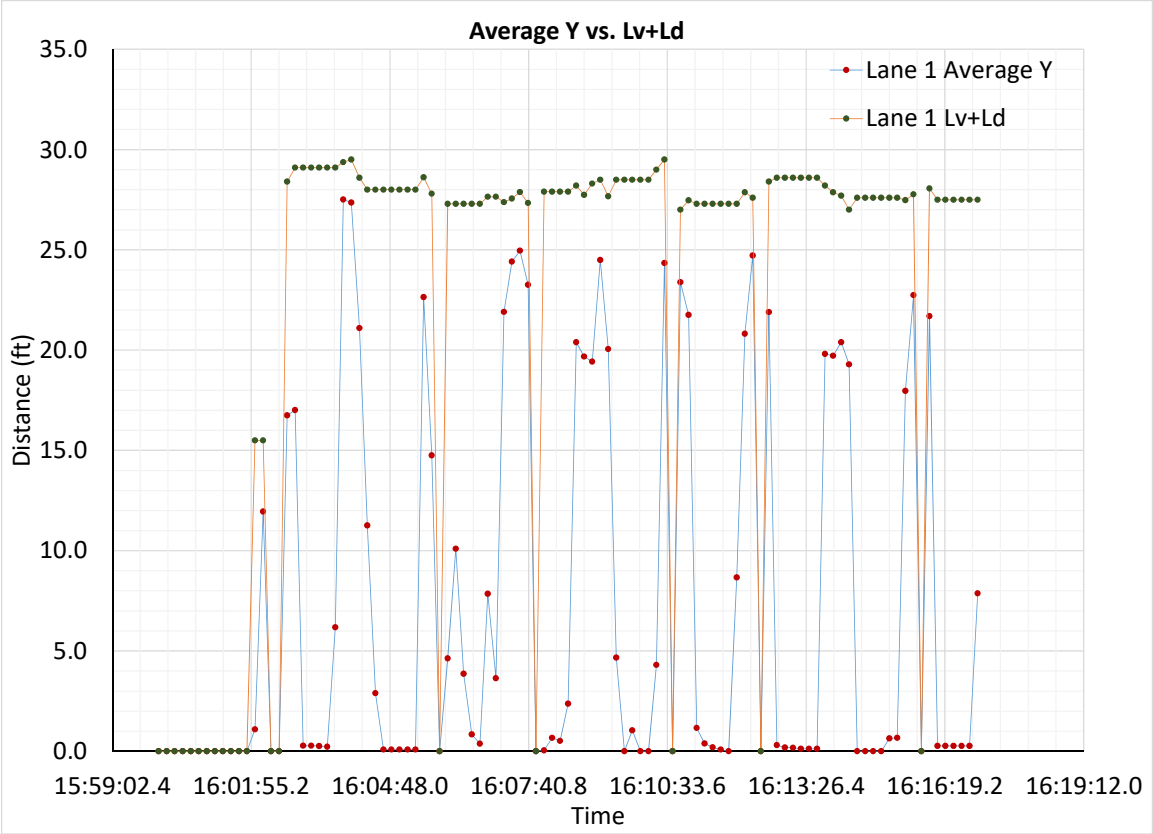

Figure 41 Detector Set #401 Lane 1 Average Distance Traveled vs. $L_t + L_d$ (Plotted using NGSIM data at stop bar)

In Figure 41, the average distance traveled by vehicles at the stop bar detector during one data collection time period is plotted with the corresponding time weighted average vehicle length. The time weighted average vehicle length is calculated using the NGSIM dataset. Significant difference exists between the two sets of values, which is more significant at the stop bar and less significant at midblock. Given some vehicles may not completely cross the detector during the

data collection time period, the generalized density estimated directly from Equation 51 is very inaccurate. Equation 51 assumes all vehicles travel the distance of $L_t + L_d$, even vehicles completely stop during the data collection time period. An alternative approach is necessary.

Considering the fundamental relationship, $v = ds$, applies to all types of traffic conditions and all shapes of time-space regions, including signalized arterials as shown by Figure 27, the generalized density can be estimated using, $d = \frac{v}{s}$. Given the generalized flow rate estimated using the detector data is $\frac{V_{detector}}{O_{time} \times T}$, the generalized density can be calculated using Equation 56. $S_{detector}$ is the detector harmonic mean speed.

$$d = \frac{V_{detector}}{S_{detector} \times O_{time} \times T} \qquad \textbf{Equation 56}$$

Figure 42 and Figure 43 show the results estimated using Equation 56, at both the stop bar and the midblock. The x axis presents the generalized density generated using the NGSIM dataset and the y axis presents the ratio of $\frac{V_{detector}}{O_{time} \times T}$ to the detector harmonic mean speed. In the time-space regions as defined in in Figure 36, Equation 56 provides an accurate approach to estimate the generalized density using the detector data.

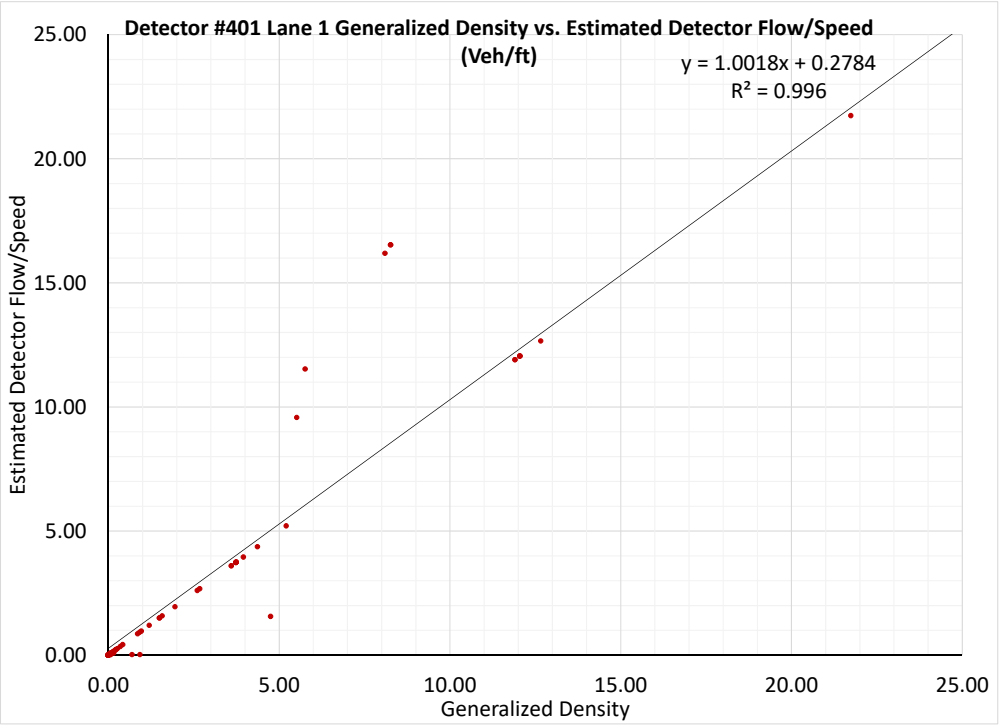

Figure 42 Detector Set #401 Lane 1 Generalized Density vs. Estimated Detector Flow/Detector Speed (Plotted using NGSIM data at stop bar)

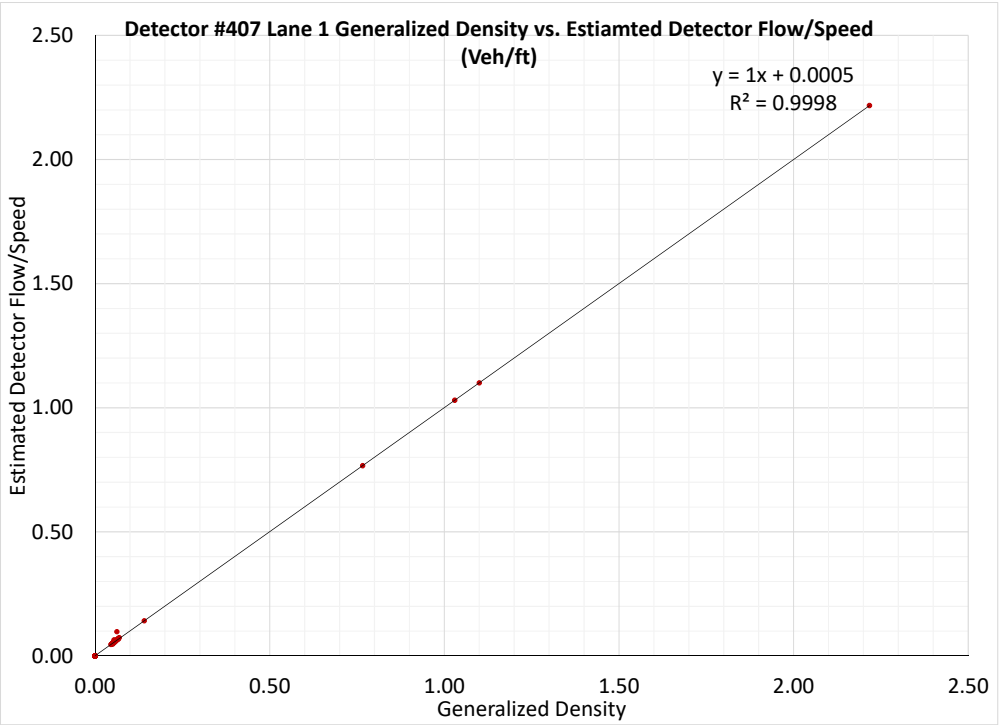

Figure 43 Detector Set #407 Lane 1 Generalized Density vs. Estimated Detector Flow/Detector Speed (Plotted using NGSIM data at midblock)

5.4 Traffic Flow Intensity

Detectors aggregate the individual vehicle data measured during the data collection time period to the aggregated detector volume, speed and time occupancy. In time-space diagrams, detectors only provide actual measurements in the time-space regions as defined in Figure 36. The most common approach currently used in research and practice is to analyze the detector data in the time-space region as the rectangular $Region\ ABCD$ defined in Figure 26. This approach involves to average the measurements when detectors are occupied by vehicles with measurements when detectors are not occupied.

For example, comparing Equation 55 with Equation 43, it is interesting to see that the two equations estimate the generalized flow rate in different time-space regions. Equation 43 estimates the generalized flow rate as if vehicles would evenly spread across the data collection time period when crossing the detection zone. Equation 55 estimates the generalized flow rate only during the time when the detector is occupied by vehicles. Equation 55 produces much more accurate results than Equation 43 does.

However, Equation 55's generalized flow rate does not represent the actual number of vehicles that have crossed the detection zone during the analysis time period. It only indicates the number of vehicles that would have crossed the detection zone if the traffic condition has

remained the same as the traffic condition measured when detectors are occupied by vehicles, throughout the entire data collection time period.

In some traffic flow theory literatures, the generalized traffic flow rate is also called as intensity. From here on in this dissertation, Equation 55's generalized flow rate will be referred to as the intensity of the traffic flow. This traffic flow intensity measurement is critical for this dissertation's objective to develop methodologies that can be used for real-time traffic operations.

When Equation 50, Equation 51 and Equation 52 developed in Section 5.3, the assumption made is that vehicles completely cross the detector during one data collection time interval. In addition, the average physical vehicle length and the time weighted average vehicle length data are not always available during real-time operations. Equation 50 is simplified to Equation 55 and Equation 51 is transformed to Equation 56. Although Equation 55 and Equation 56 provide accurate results as shown by the analysis of the NGSIM dataset, it can be argued that it is because the percentage of heavy vehicles is very low in the NGSIM dataset. It is necessary to derive the equations without relying on the assumption and the vehicle length data.

In the rectangular $Region\ EFGH$ in Figure 36, there is one vehicle during time t_i. The traffic flow rate in $Region\ EFGH$ is $\frac{1}{t_i}$. The traffic flow rate for all time-space regions combined can be seen as the time weighted average of each region's flow rate, calculated as Equation 57.

$$v = \sum_{i=1}^{n} \left(\frac{1}{t_i} \times \frac{t_i}{O_{time} \times T} \right) = \sum_{i=1}^{n} \left(\frac{1}{O_{time} \times T} \right) = \frac{V_{detector}}{O_{time} \times T}$$

Equation 57

Similarly, in the rectangular $Region\ EFGH$ in Figure 36, there is one vehicle during time t_i. The density in $Region\ EFGH$ is $\frac{1}{y_i}$. y_i is the distance vehicle i traveled in the time-space region during time t_i and equals to $S_i \times t_i$, where S_i is vehicle i's speed in the time-space region. The density for all time-space regions combined can be seen as the time weighted average of each region's density, calculated as Equation 58. In Equation 58, $\frac{N}{\sum_{i=1}^{n} \left(\frac{1}{S_i} \right)}$ is the detector harmonic mean speed, $S_{detector}$ and N is the detector vehicle counts, $V_{detector}$.

$$d = \sum_{i=1}^{n} \left(\frac{1}{S_i \times t_i} \times \frac{t_i}{O_{time} \times T} \right) = \sum_{i=1}^{n} \left(\frac{1}{S_i} \times \frac{1}{O_{time} \times T} \right)$$

$$= \frac{\sum_{i=1}^{n} \left(\frac{1}{S_i} \right)}{O_{time} \times T} = \frac{\frac{N}{S_{detector}}}{O_{time} \times T} = \frac{V_{detector}}{S_{detector} \times O_{time} \times T}$$

Equation 58

Equation 57 and Equation 58 provide another way to derive the formulas to estimate the traffic flow intensity and the corresponding density without assuming vehicles completely crossing the detector or using the vehicle lengths as inputs. The traffic flow density will be used as an important input to the models developed in the next chapter.

6 QUEUE LENGTH AND TRAVEL TIME ALONG SIGNALIZED LINK

This chapter starts with attempts to make improvements to the input-output technique for queue estimation along signalized links. Based on analyses of the theoretical and experiential cumulative input-output diagrams, also known as the Newell Curves (92), two major improvements are proposed to improve the performance of the input-output technique. The improvements will be tested using two sets of field data, the NGSIM data and metered on-ramp data. Based on the traffic flow intensity and the improved queue estimation technique, a simple approach will be developed and evaluated for the signalized link travel time estimation.

6.1 Input-Output Technique for Queue Estimation

Various theories to model queueing at signalized intersections have been extensively studied, including input-output models, shock wave models, signal processing models, and probabilistic models. However, most of these queueing models are very complex, and were developed and analyzed using microscopic traffic simulations. Carefully performed empirical studies and models suitable for real-time operation purposes are very rare. Furthermore, most of these queueing models estimate the queue lengths using input-output techniques when vehicle queues do not extend beyond the input or advanced detector.

Input-output techniques are often used in research and practice because of their simplicity to implement and providing reasonable queue length estimates with balanced volumes. However, the performance of the input-output technique estimation is not always satisfactory. In addition,

generally, input-output techniques are facing two challenges, how to handle long queues extending beyond the input detector and how to remove accumulated errors over time. Utilizing field queue length, detector vehicle counts and time occupancy, this dissertation focuses on improving the performance of the input-output technique and attempts to reduce the input-output technique accumulated errors over a long time period. Improvements to handle long queues extending beyond the input detector is not discussed in this dissertation and is a future research topic. This dissertation will improve the Kalman filter model to estimate long queues extending beyond the input detector.

As shown below, Equation 10 described in Section 2.2.2.3 is the common formula of the input-output calculation.

$$Q_n = Q_{n-1} + N_{in} - N_{out} \qquad \textbf{Equation 10}$$

where

Q_n = number of queued vehicles in the current time interval (veh),
Q_{n-1} = number of queued vehicles in the previous time interval (veh),
N_{in} = vehicle counts entering the signalized link during a data collection time interval like 10 seconds (veh), and
N_{out} = vehicle counts exiting the signalized link during the same time interval (veh).

6.1.1 Cumulative Input-Output Diagram

The cumulative input-output diagram, also known as the Newell Curve, provides a graphical representation of input-output techniques for queue estimation and is often used to describe the queueing process at traffic signals (92). Figure 44 shows an example of the theoretical cumulative input-output diagram at an isolated traffic signal. The traffic signal can be considered as a pulsed service provider that provides a high service rate during green phases and

periodically stops servicing during red phases. The vehicle arrival curve simulates the constant arrival of vehicles during both red and green phases. The vehicle departure curve indicates the queueing during red phases and the queue discharging during green phases. In Figure 44, the queue is cleared during the green phase and there is no residual queue left at the end of the green phase. The total aggregated delay incurred by all vehicles on a signalized intersection approach is determined as the total area between the arrival and departure curves. At a specific time, the difference between the arrival curve and the departure curve along the Y axis is the number of vehicles in the queue. Using input-output techniques to estimate the queue length is actually to calculate the difference between two curves along the Y axis in a cumulative input-output diagram.

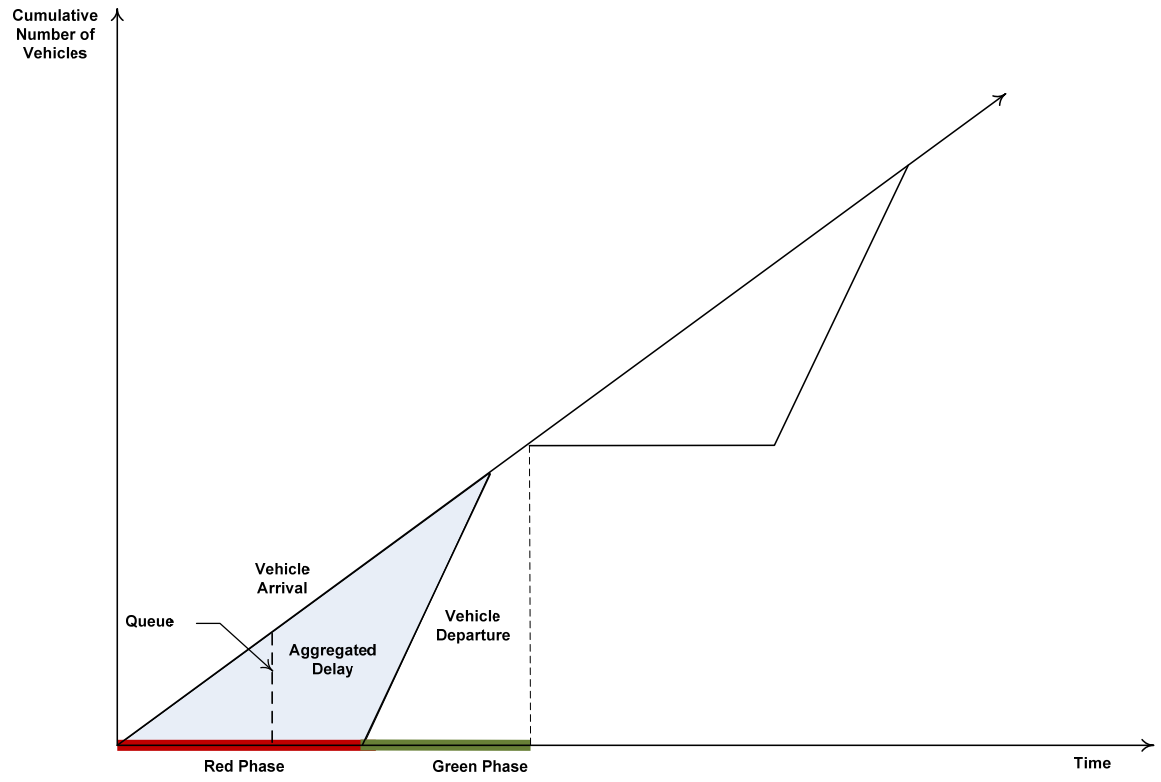

Figure 44 Cumulative Input-Output Diagram at Signalized Intersection

When the input-output technique is applied in research and in practice, two assumptions usually made are that vehicles do not change lanes after crossing the input detectors and the first-in-first-out principle applies. However, this is often not the case, since vehicles do change lanes and the first vehicle entering the link may not be the first vehicle to exit the link. The consequence is that the input-output calculation introduces estimation errors. Figure 45 shows the cumulative input-output diagram plotted using the NGSIM data, with Detector Set #401 Lane 2 located at the stop bar as the output detector and Detector Set #407 Lane 2 located close to midblock as the input detector.

A detailed review of the NGSIM vehicle trajectory data reveals that there are queueing at this intersection during the red phases and the queues can be cleared during most of the green phases. In addition, the field cumulative input-output diagram shown in Figure 45 presents three major aspects that are different from the theoretical cumulative input-output diagram shown in Figure 44. The first aspect is the cumulative vehicle count difference between the output detector and the input detector increases significantly over a 16-minute time period. The difference reaches 61 vehicles at the end of the 16-minute time period, which cannot be explained as the number of vehicles in the queue and apparently is the accumulated estimation error increased over a longer time period.

The second difference is that the departure curve is almost always above the arrival curve, which means the vehicle departure rate is faster than the vehicle arrival rate and no queues should be present even during the red phases. This is contrary to the field condition, since vehicle queues do exist during every cycle.

The third difference is that the departure curve does not indicate red phases. During red phases, the curve should be flat presenting vehicles stop and the cumulative number of vehicles does not increase as one or two vehicles stop on top of the output detector. However, the arrival curve does show the alternating pattern of red and green phases.

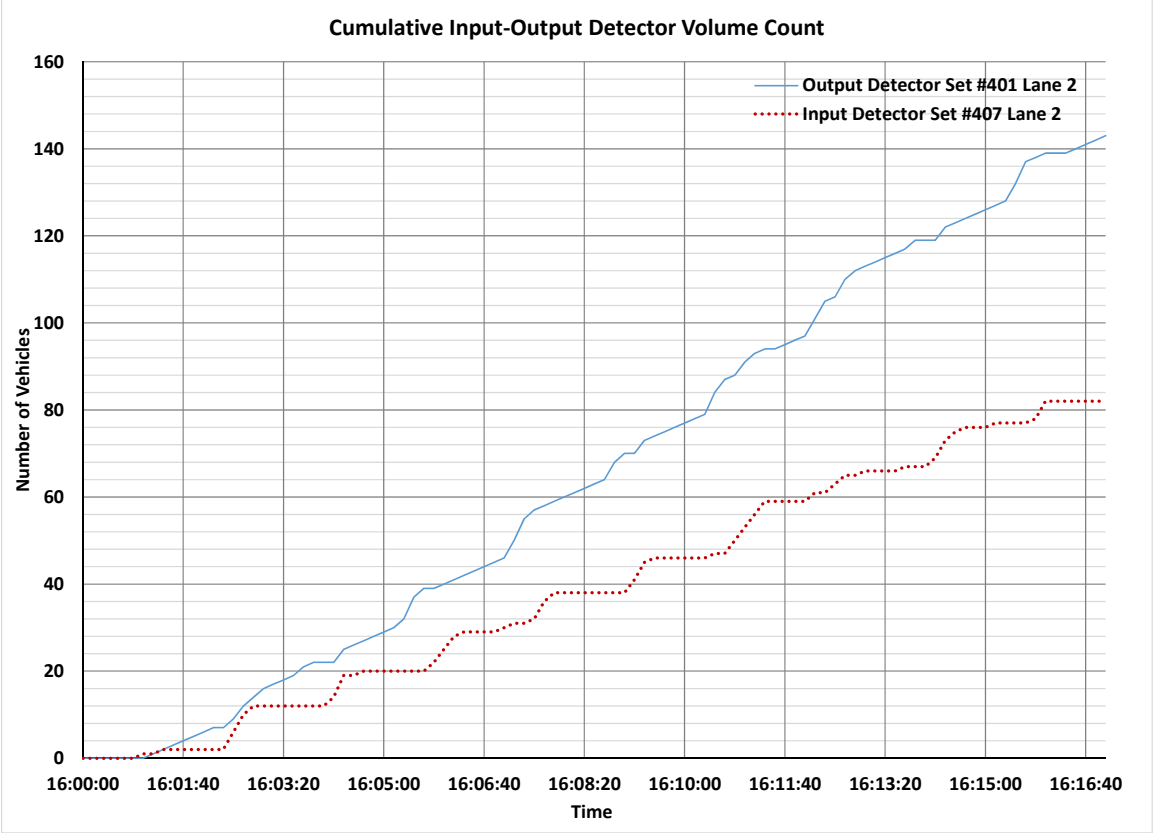

Figure 45 Cumulative Input-Output Diagram
(Plotted using NGSIM data)

6.1.2 Queueing in Time Space Diagram

Input-output techniques estimate the number of vehicles between the input and output detectors, regardless the vehicles are moving or not. Figure 46 shows the trajectories of vehicles traveling

along a link during three data collection time periods in a time-space diagram. Note in Figure 46, vehicles are traveling from top to bottom. Each data collection time period can be defined as a time-space region. Using the number of vehicles within the region to represent the traffic condition in the region can be very time-sensitive, given the number of vehicles constantly changes during the data collection time period. For example, between 16:02:30 and 16:02:40, there are two vehicles traveling along the link at 16:02:30, but there are five vehicles traveling along the link at 16:02:40. In addition, volume counts from the input and output detectors cannot accurately and consistently indicate the number of vehicles within the region. This is because vehicles may enter the defined time-space region from the left side and exit the defined region through the right side, which can be explained as these vehicles may not cross the input detector or the output detector during the data collection period.

As a result, to avoid introducing additional errors, a specific time during each data collection time period should be identified to collect the queue length data. In this dissertation, the number of vehicles traveling along the link is recorded at the end of each data collection time period so that all vehicles crossing the input detector or the output detector during the data collection time period can be accounted for consistently.

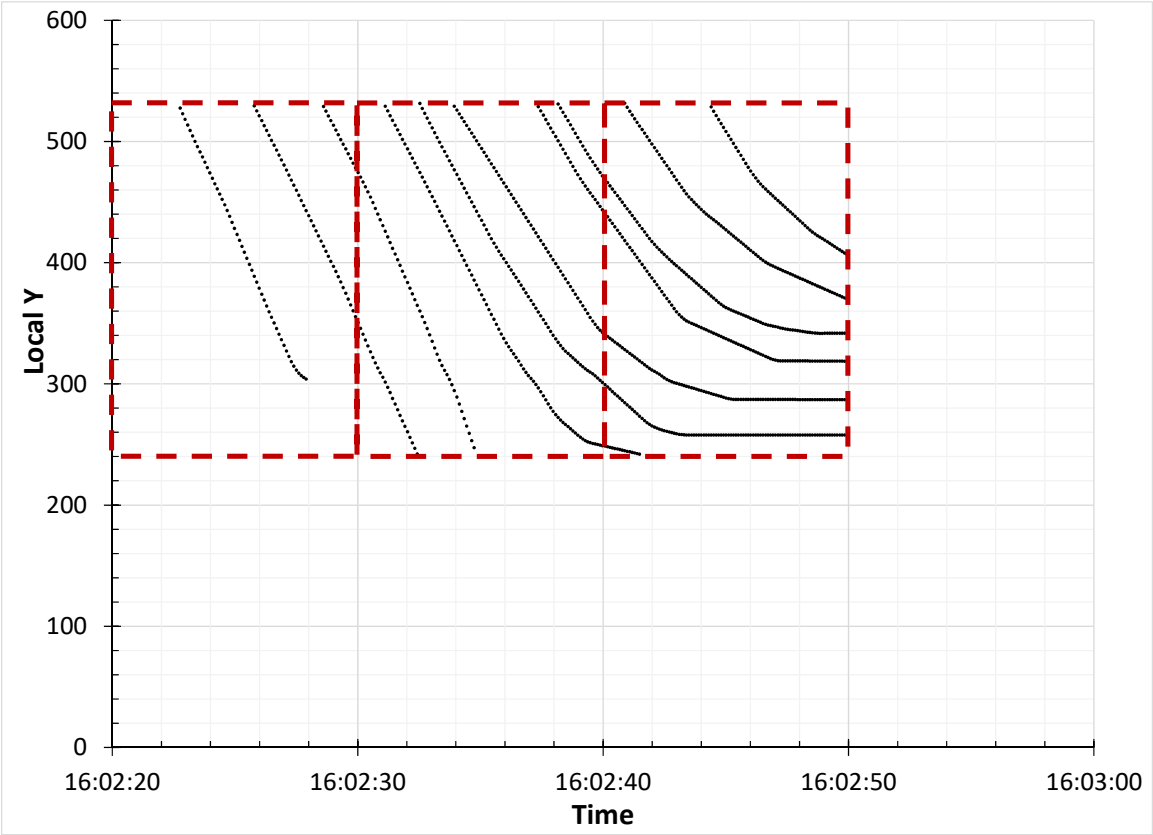

Figure 46 Vehicle Trajectories during Three Data Collection Time Periods (Plotted using NGSIM data)

6.1.3 Vehicle Count Adjustment Using Time Occupancy

The detector volume or vehicle count is the number of vehicles crossed the detection zone in the data collection time interval. A vehicle is detected or counted by a detector, when any part of the vehicle activates the detection zone. This is an industry standard way to collect detector vehicle counts and is accurate for most detection technologies. When a vehicle fully stops on top of the detector during the data collection time period, the vehicle count is one, the speed is zero and the time occupancy is 100% during the time period. However, there is no vehicle actual movement during the time period. For example, if a vehicle fully stops on top of the output detector and vehicles still cross the input detector to enter the link during a data collection time period, there

should be no vehicles exiting the link. In this case, the input-output technique underestimates the queue length by one vehicle, assuming the vehicle stopped on top of the output detector has left. If the vehicle stops on top of the detector for several data collection time periods, the input-output technique would underestimate the queue length by several vehicles, assuming one vehicle exits during one data collection time period. This underestimation has a larger impact to the estimation if a short time interval is used, as the queue length will be reduced by one for each time interval.

In order to improve the input-output estimation, the detector vehicle counts including stopped vehicles should be identified. There are many ways to filter the vehicle counts. For example, the detector time occupancy or speed can be used to adjust the vehicle counts when vehicles stop on top of the detector. A speed threshold can be selected such that when the speed is below the speed threshold, the vehicle counts will not be used as inputs or outputs for the estimation. A time occupancy threshold can also be selected such that when the time occupancy is above the threshold, the vehicle counts will not be used as inputs or outputs for the estimation. This study uses time occupancy to adjust the vehicle counts used by the input-output technique.

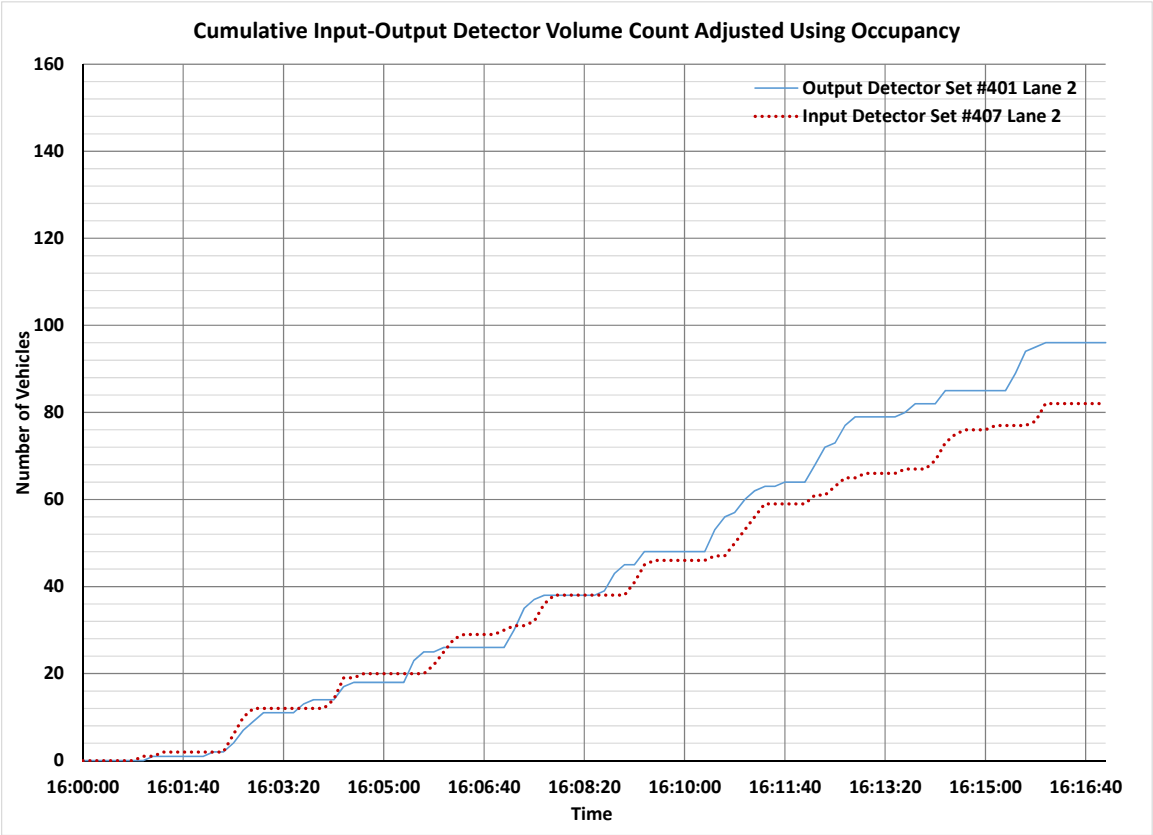

Figure 47 Cumulative Input-Output Diagram Plotted Using Adjusted Vehicle Counts (Plotted using NGSIM data)

Figure 47 shows the cumulative input-output diagram plotted using the same detector data as those used by Figure 44, except the vehicle counts are adjusted based on a time occupancy threshold. If the time occupancy of the input detector or the output detector is above 75% during the data collection time period, then the vehicle count used by the input-output technique will be adjusted to zero. Compared to Figure 44, the departure curve in Figure 47 shows both red and green phases. Figure 48 shows the ground truth queue, the queue estimated by the input-output technique using the vehicle counts adjusted based on time occupancy, and the queue estimated by the input-output technique using the raw vehicle counts without any adjustments. The estimation is improved significantly when vehicle counts are adjusted based on time occupancy.

The Root Mean Squared Errors (RMSE) of the queue estimated using the adjusted vehicle counts is 0.71 vehicles and the RMSE of the queue estimated using the raw vehicle counts without any adjustments is 2.23 vehicles.

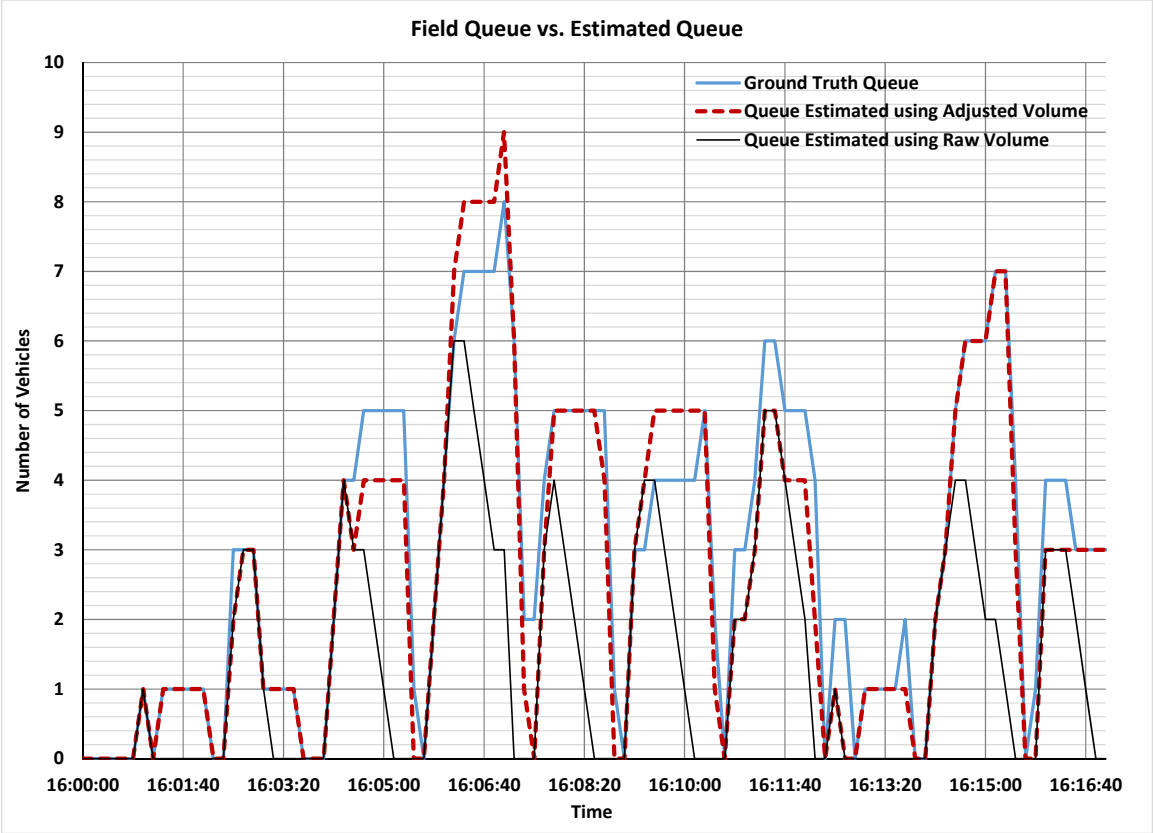

Figure 48 Comparison between Ground Truth Queue and Estimated Queues (Queue Estimated using the NGSIM Data Set)

The time occupancy threshold used in this study is selected by minimizing the RMSE between the estimated queue and the ground truth queue. The time occupancy threshold is not 100% is because vehicles are not always fully stopped during the data collection time period. In order to determine the time occupancy threshold, more research efforts are necessary to be performed with extensive data from various locations and various time periods.

Table 5 Time Occupancy Thresholds and Coefficients for Metered On-ramp Data

Location	Time Period	Input Detector Time Occupancy Threshold	Output Detector Time Occupancy Threshold	Kalman Filter Coefficient (K)	
				With Adjusted Volume	With Raw Volume
Capital Drive	March 14 AM	16%	16%	0.02	0.26
	March 14 PM	12%	19%	0.05	0.02
	March 15 AM	17%	11%	0.10	0.19
	March 16 AM	15%	19%	0.02	0.27
	March 16 PM	14%	11%	0.17	0.00

As a comparison, similar adjustments are also made to adjust the input and output loop detector vehicle counts at the Capital Drive on-ramp in the metered on-ramp data set. The occupancy thresholds selected are shown in Table 5. The occupancy threshold values used to adjust the on-ramp data are much lower than those occupancy threshold values used to adjust the signalized arterial data. This can be explained as the traffic flow along the on-ramps is constantly moving, while the traffic flow along the signalized arterials stops completely during the red phase. In addition, the metered on-ramp data set data collection time interval is 20 seconds, while the NGSIM virtual detector dataset has 10-second data collection time intervals. It is more likely to have both stopped and moving vehicles within one data collection time interval when longer data collection time intervals are used. When the input detector occupancy threshold values are higher than the output detector occupancy threshold values, it means vehicle queues have backed up to the output detector locations.

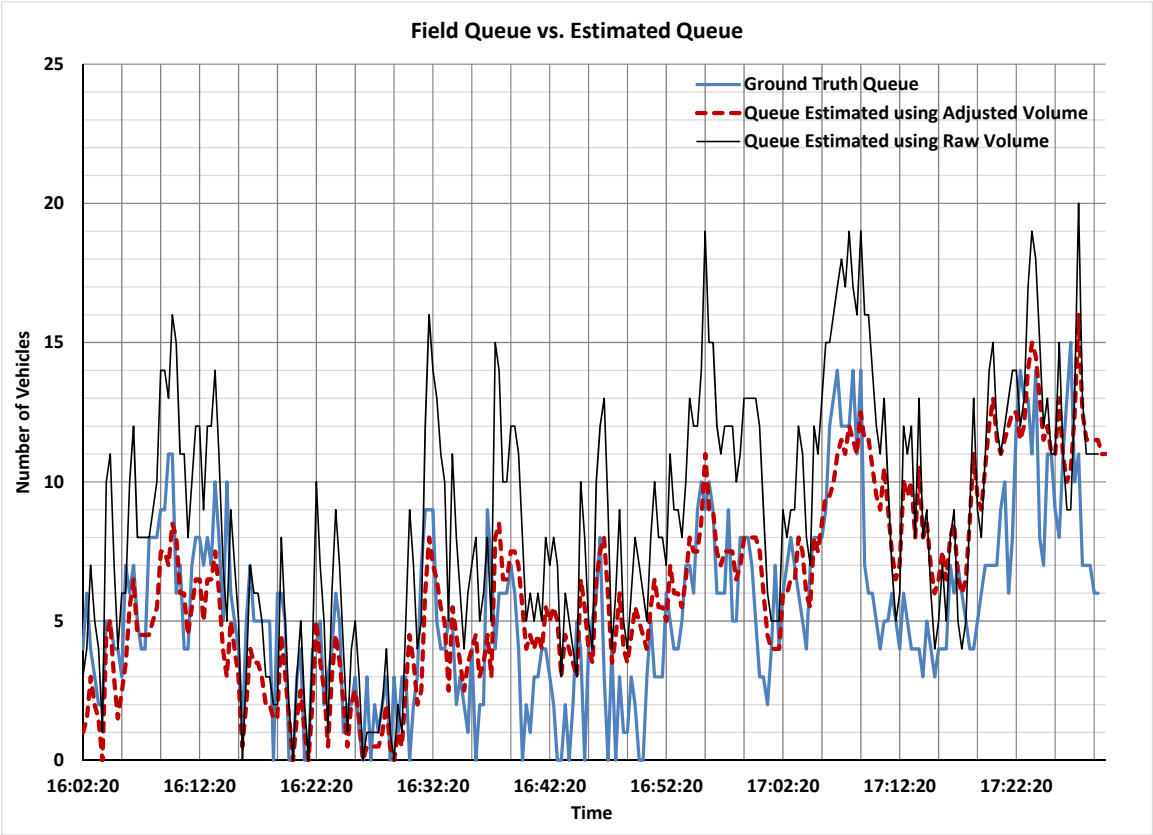

Figure 49 Comparison between Ground Truth Queue and Estimated Queues (Queue Estimated using the Metered On-ramp Data Set)

Figure 49 shows an example of the comparison between the on-ramp ground truth queue and the queue estimated by the input-output technique. With the vehicle counts adjusted based on time occupancy threshold values, the input-output technique estimation performs much better than the estimation using raw vehicle counts. Table 6 lists Root Mean Squared Errors for four methods analyzed. For comparison, with this specific set of data (37), the RMSE values of the queues estimated using the Kalman Filter model developed by Vigos et al. (32) are also included in Table 6. The input-output technique using the adjusted vehicle counts has similar performance as the results estimated by the Kalman Filter model. The performance of the Kalman Filter model is significantly improved when the vehicle counts are adjusted based on time occupancy

thresholds. It should be noted that the occupancy threshold values shown in Table 5 are selected by minimizing the RMSE between the queue estimated using the input-output technique and the ground truth queue. If the occupancy threshold values are optimized for the Kalman Filter model, the model will perform constantly better and the RMSE values will be slightly lower. Table 5 also lists the Kalman Filter coefficients used.

Table 6 Root Mean Squared Errors of Estimated Vehicle Queues

Location	Time Period	RMSE			
		Input Output	Input Output with Adjusted Volume	Kalman Filter	Kalman Filter With Adjusted Volume
Capital Drive	March 14 AM	10.10	6.21	7.37	2.60
	March 14 PM	4.54	2.73	3.48	0.86
	March 15 AM	10.53	7.27	6.38	2.24
	March 16 AM	11.73	8.29	8.14	1.04
	March 16 PM	7.04	7.48	7.18	1.13

6.1.4 Input-Output Technique Reset Mechanism

The departure curve in Figure 47 is able to show patterns of the red phase and the green phase alternating. However, when the analysis period extends longer, the error still starts to accumulate and the departure curve remains above the arrival curve. The error may be caused by lane changing movements or vehicles entering or exiting the link between the input and output detectors. If the cumulative number of exiting vehicles is more than the cumulative number of entering vehicles, the queue would be cleared. When there is no vehicle queue present, the departure curve and the arrival curve should intersect, meaning all vehicles entered have exited and the cumulative number of exiting vehicles is equal to the cumulative number of entering

vehicles. This specific time can be used as a correction point to remove the errors accumulated by the input-output technique over a certain time period.

In this dissertation, when the cumulative number of exiting vehicles is more than the cumulative number of entering vehicles, the cumulative number of exiting vehicles is set to the value of the cumulative number of entering vehicles at the end of the last data collection time period. Figure 50 displays the cumulative input-output diagram with the departure curve reset multiple times. As a result, the modified cumulative input-output diagram matches the pattern of the theoretical cumulative input-output diagram shown in Figure 44. The queue estimated using the modified cumulative input-output diagram has a RMSE of 0.68 vehicles, which is further improved the estimation comparing to the estimation only using the adjusted vehicle counts, which has a RMSE of 0.71 vehicles. However, further analysis is necessary to determine whether the improvements have statistical significance. This dissertation does not consider the initial queue in the analysis. Ignoring the initial queue introduces initial estimation errors. However, after the first reset point, the initial queue no longer plays any roles in the estimation results, as the queue has cleared and the cumulative number of exiting vehicles is set to the value of the cumulative number of entering vehicles.

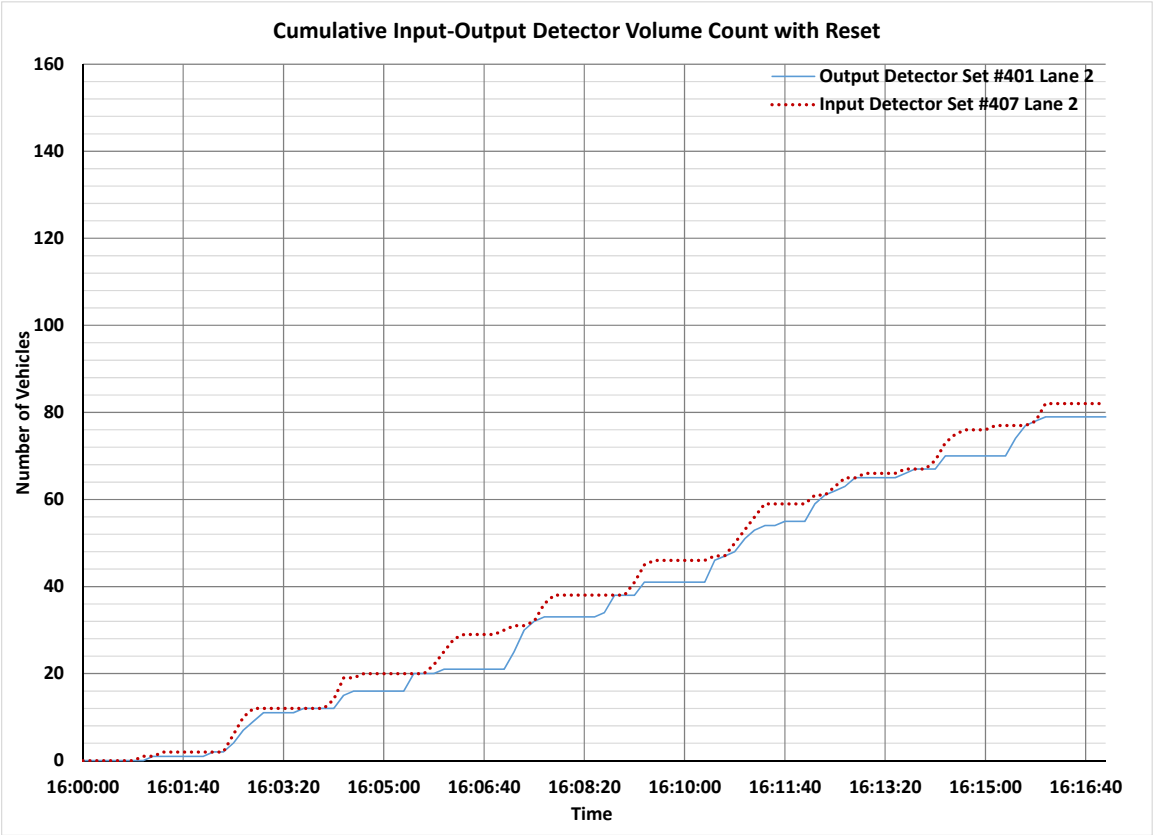

Figure 50 Cumulative Input-Output Diagram Plotted with Correction Points (Plotted using NGSIM data)

In Figure 51 and Figure 52, X axis is the ground truth queue and Y axis is the estimated queue. With a R^2 value of 0.9238, the estimation using the adjusted vehicle counts along with multiple correction points produces much better results than the estimation using just the raw vehicle counts, which has a R^2 value of 0.466.

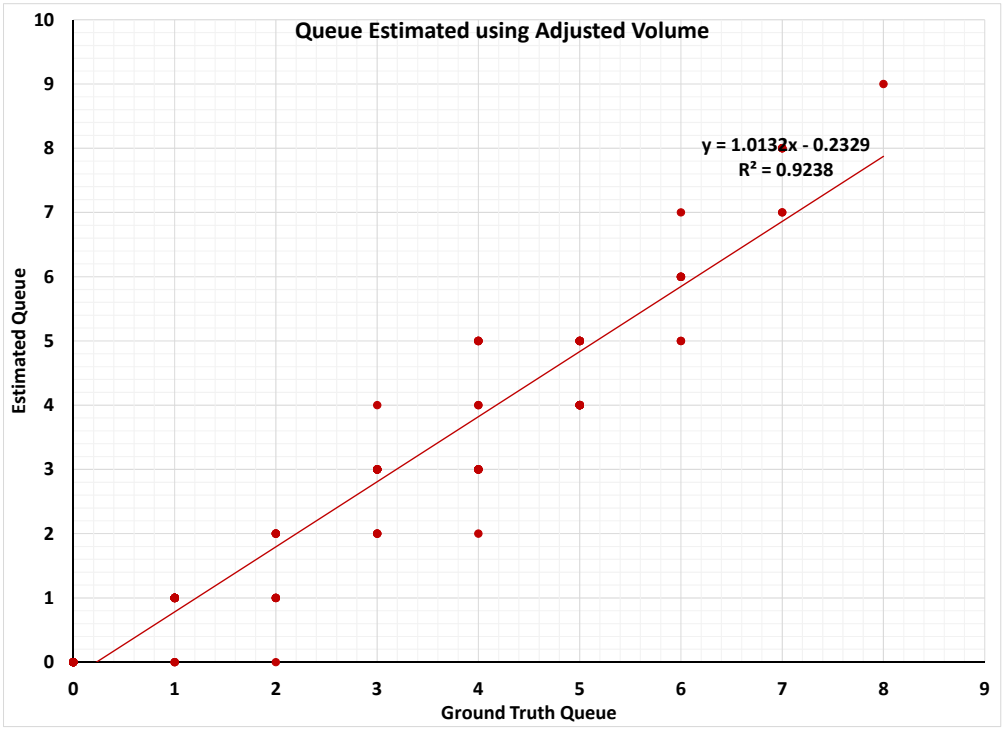

Figure 51 Ground Truth Queue vs. Queue Estimated Using Adjusted Volume (Plotted using NGSIM data)

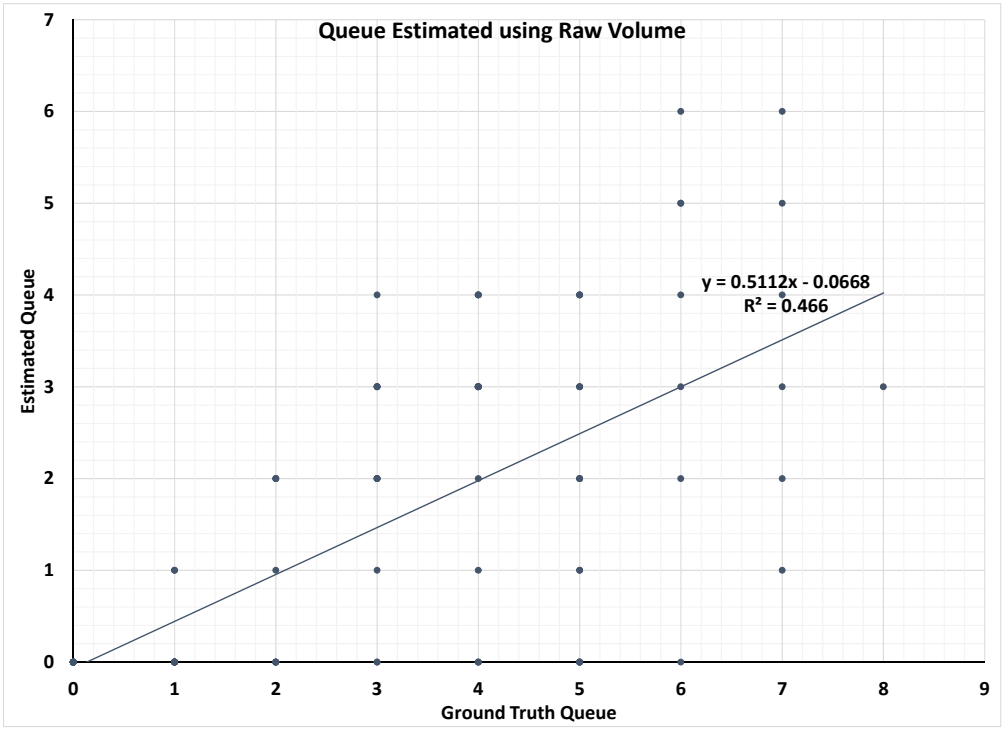

Figure 52 Ground Truth Queue vs. Queue Estimated Using Raw Volume (Plotted using NGSIM data)

6.2 Travel Time Estimation

As discussed in Chapter 5, the traffic flow intensity at detectors can be accurately estimated by using the detector volume counts divided by the detector time occupancy multiplied by the data collection time interval. In addition, the vehicle queue length between the input detector and the output detector can be estimated using the improved input-output technique with the detector volume data adjusted based on the detector time occupancy data.

According to the conservation equation, the total number of vehicles exiting a roadway segment equals to the total number of vehicles entering the roadway segment plus the number of vehicles traveling along the roadway segment. Depending on the length of the roadway segment and the traffic flow conditions, vehicles may enter and exit the roadway segment within the same data collection time period, or it may take several data collection time periods. If the initial queue exists, it should be included in the estimation to minimize errors.

In Figure 53, vehicles are traveling from the input detector to the output detector along the link. Using the first in, first out (FIFO) method, vehicles enter the link at the input detector first will leave the link at the output detector first. When the output detector vehicle counts is greater than or equal to the input detector vehicle counts plus the initial queue along the link, it can be considered that vehicles entering the link at the input detector have completely crossed the link and exited at the output detector. This process may take several data collection time periods.

The number of data collection periods elapsed is the average vehicle travel time from the input detector to the output detector. Because the detector data are collected and aggregated every data collection time period, the travel time estimated using this method can only be accurate to the data collection interval.

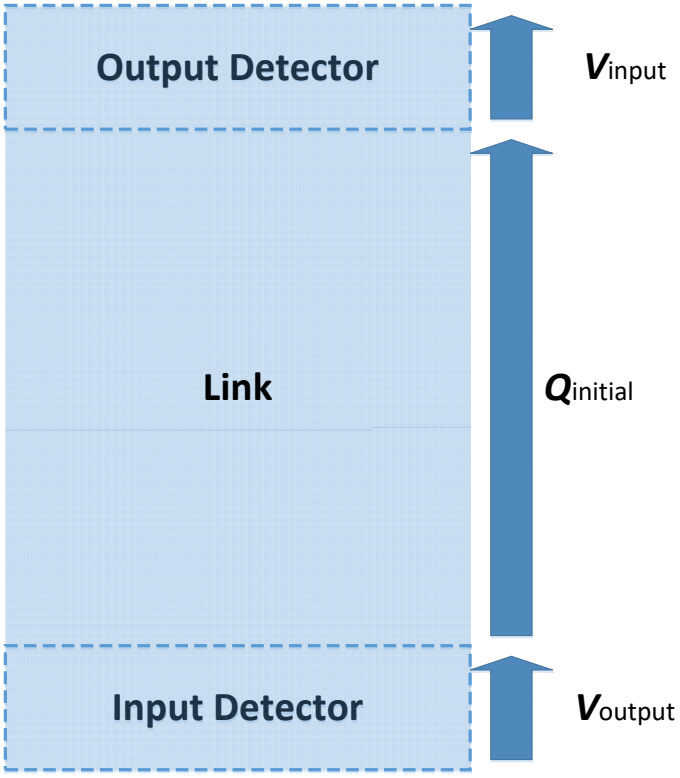

Figure 53 Link and Detector Flow

In Equation 59, $Q_{initial}$ is the number of vehicles traveling along the link at the beginning of the analysis time period. V_{input} is the traffic flow intensity at the input detector at the beginning of the analysis time period. $V_{output\,T_i}$ is the traffic flow intensity at the output detector during each data collection time period T_i. Equation 59 estimates the number of data collection time periods n spent by vehicles entering at the input detector to exit at the output detector. The number of data collection periods n multiplied by the data collection interval T is the average vehicle travel

time. As discussed in Chapter 5, the traffic flow intensity is used because it is more accurate than using the equivalent hourly volume of the detector vehicle counts as the generalized flow rate.

The travel time estimated using Equation 59 takes the approach delay into account. The National Cooperative Highway Research Program (NCHRP) Project 3-79 (30) defines the approach delay of a vehicle as the delay time incurred due to deceleration, stop time and acceleration until the vehicle crosses the stop bar.

$$\sum_{i=1}^{n}\left(V_{output\ T_i} \times T\right) \geq \left(V_{input} \times T\right) + Q_{initial} \qquad \textbf{Equation 59}$$

where

$Q_{initial}$ = the number of vehicles traveling along the link at the beginning of the analysis time period (number of vehicles),
T = time interval of detector data collection (seconds),
V_{input} = traffic flow intensity at input detector at the beginning of the analysis time period (vehicles per second), and
$V_{output\ T_i}$ = traffic flow intensity at output detector of data collection time period T_i (vehicles per second).

Figure 54 shows the field travel time and the estimated travel time for each 10-second data collection time period. The field travel time is generated from the NGSIM dataset. The travel time of a vehicle is measured from the moment the vehicle front enters the input detector to the moment the vehicle rear leaves the output detector. The vehicle travel time is highly dependent on the vehicle departure time. In addition, the travel time data usually present as a distribution of values falling within a certain range. As discussed in the literature review chapter, many methods have been studied to filter the outliers and aggregate the travel time values into a single

number. This dissertation uses the arithmetic average of the travel time values of all vehicles crossing the input detector during the data collection time interval.

The estimated travel time are calculated as the number of the data collection time periods that vehicles are travelling within the link. A link is defined in this study as the roadway segment between two virtual detectors, from downstream detector downstream edge to the upstream detector upstream edge.

As shown in Figure 54, the estimated travel time changes follow the field travel time changes very closely. Considering the data collection time period is 10 seconds, it is anticipated that the estimated travel time has a 10-second difference from the field travel time. When comparing two sets of link performance measurements, it is important to compare each data point. It is also critical to compare the patterns of changes, because the two sets of data may not be synchronized given the link performance measurement is an average value within a defined time-space region.

In addition, in Figure 54, the vehicle queue length between the input detector and the output detector is estimated using the improved input-output technique with the detector volume data adjusted based on the detector time occupancy data. If the Kalman Filter model is used to estimate the queue length, the queue length estimation is more accurate. The RMSE value is 1.25 vehicles for the Kalman Filter model and the RMSE value is 1.29 vehicles for the input-output technique. However, the travel time estimated in Figure 54 does not change, by using Equation 59 with the Kalman Filter model estimated queue length as the initial queue input. The impacts of the initial queue will need further analysis for evaluating the model sensitivity.

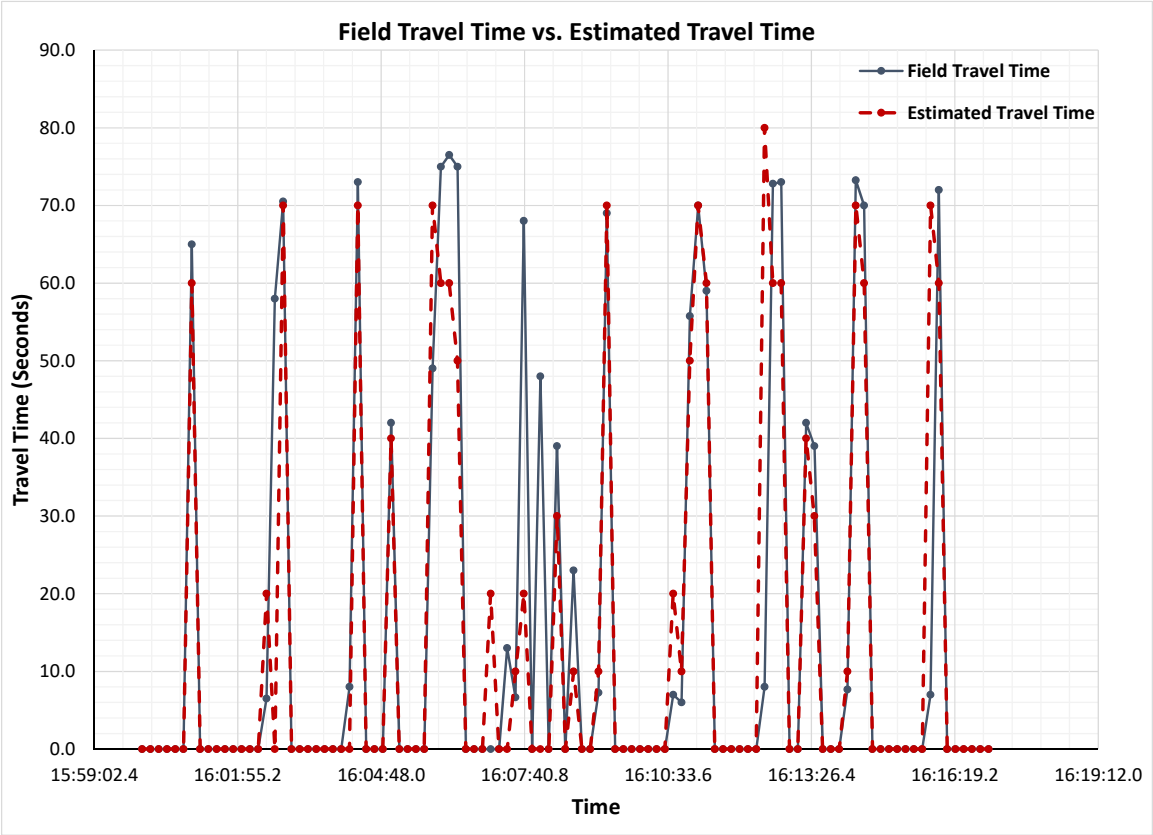

Figure 54 Link 401-407 Lane 1 Field Travel Time and Estimated Travel Time Using Equation 59
(Plotted using NGSIM data)

6.2.1 Comparison with NCHRP Project 3-79 Model

The NCHRP Project 3-79 (30) estimated the total delay for vehicles in the queue during the previous cycle as the total area below the queue polygon. The queue polygon was created by calculating the difference between the cumulative departure profile and the cumulative arrival profile. The polygon defines the number of vehicles in the queue at any time in the cycle. The average delay per vehicle is calculated as the total delay for all vehicles divided by the total number of vehicles crossed the input detector during the cycle.

The same method is used to estimate the average delay per vehicle per data collection time period in this study. Figure 55 shows the comparison among the field travel time, the travel time estimated using Equation 59 and the travel time estimated using the NCHRP Project 3-79 delay model. The NCHRP Project 3-79 travel time is estimated as the average delay per vehicle per data collection time period plus the free flow running time along the link. In Figure 55, the free flow running time along Link 401-407 is about 7.5 seconds. On a per data collection time period basis, Equation 59 performs much better than the NCHRP Project 3-79 delay model. The RMSE of the Equation 59 estimation is about 14.18 seconds and the RMSE of the NCHRP Project 3-79 delay model estimation is about 42.22 seconds.

On a per cycle basis, the maximum delay time estimated by the NCHRP Project 3-79 delay model is close to the field travel time. The maximum delay time tends to appear in the middle of the cycle, after the green phase starts and the queue starts to dissipate. The NCHRP Project 3-79 delay model estimation describes the magnitude of the delay during the cycle, but it cannot accurately identify the specific time during the cycle when the maximum delay happens. Given travel time is highly dependent on the time of departure, Equation 59 provides more accurate estimations of both the magnitude of the delay and the temporal distribution of the delay.

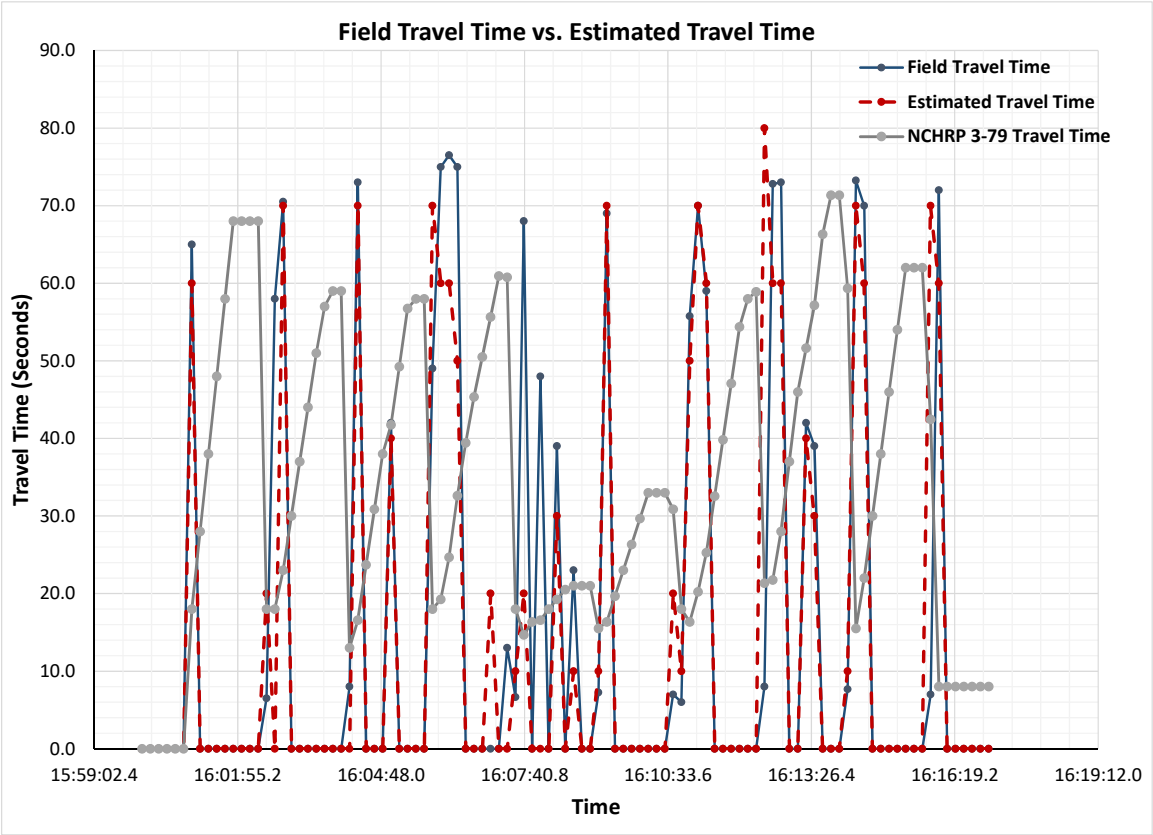

Figure 55 Link 401-407 Lane 1 Field Travel Time, Estimated Travel Time Using Equation 59 and Estimated Travel Time Using NCHRP Project 3-79 Model (Plotted using NGSIM data)

6.2.2 Comparison with Little's Law

As a comparison, Figure 56 shows the travel time estimated using Little's Law. Little's Law is one of the most famous and useful laws in queueing theory, known as Equation 60, which describes that the average number of vehicles in the queue L equals to the arrival rate λ multiplied by the average time W vehicles spent in the queueing system. In this case, the queue L is the number of vehicles between the input and output detectors. The arrival rate λ is the input detector traffic flow intensity. The average time W is the vehicle average travel time along the link.

$$L = \lambda W$$

Equation 60

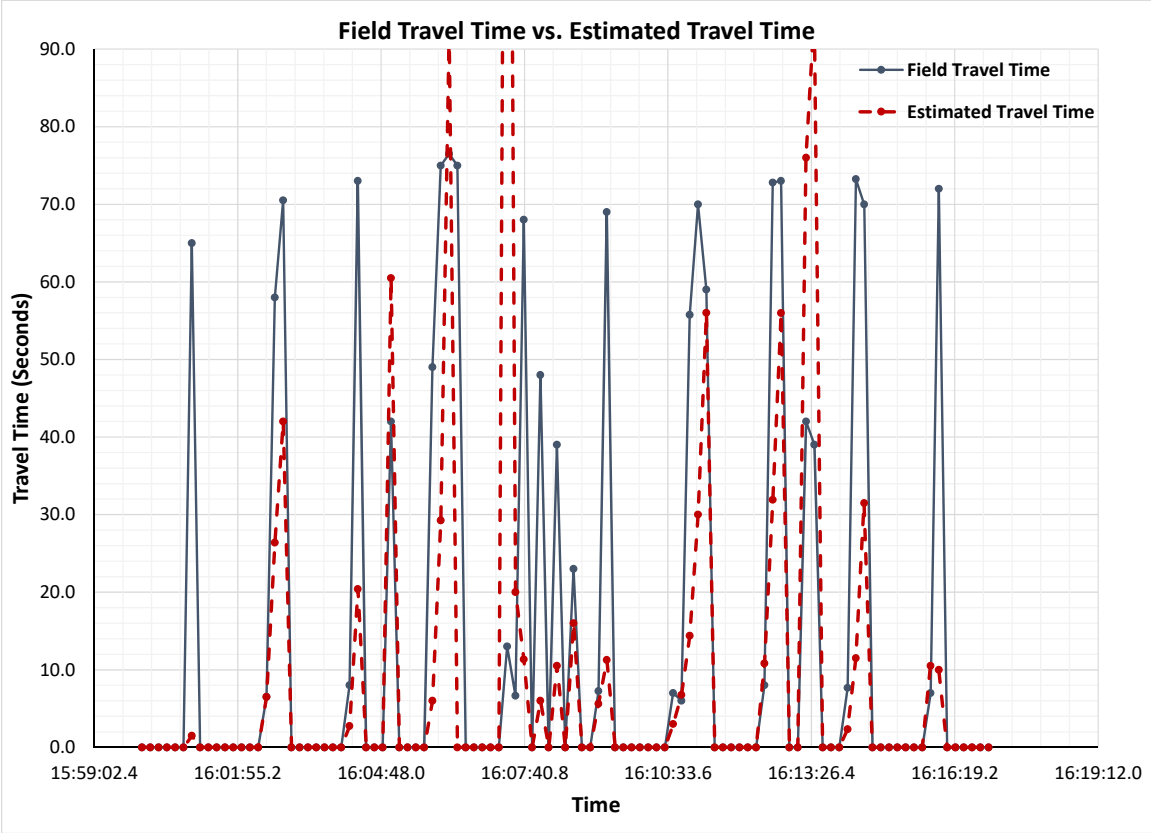

Figure 56 Link 401-407 Lane 1 Field Travel Time and Travel Time Calculated Using Little's Law
(Plotted using NGSIM data)

Comparing Figure 54 with Figure 56, the travel time estimated using Equation 59 performs much better than the estimation using Little's Law. Figure 54 has a RMSE value of 14.18 seconds and Figure 56 has a RMSE value of 28.84 seconds. Generally, in queueing models, it is assumed that vehicles do not occupy space and vehicle spatial locations are usually not considered.

6.2.3 Close Look at Individual Vehicle Travel Time

A close look at the field travel time of vehicles travelling along the link reveals that it is very challenging to estimate the travel time vehicles spent crossing a link, which is very dependent on the time when the vehicle enters the link. The exact time a vehicle entering the link cannot be accurately captured by the 10-second detector data. In Figure 57, there are six vehicles entering the link during the 10-second data collection time period. One vehicle does not have valid data. One vehicle had a green phase and four vehicles stopped at the signal during the red phase. Figure 58 shows the details of the vehicle trajectories. The averaged field travel time is about 58 seconds and the estimated travel time using Equation 59 is about 70 seconds.

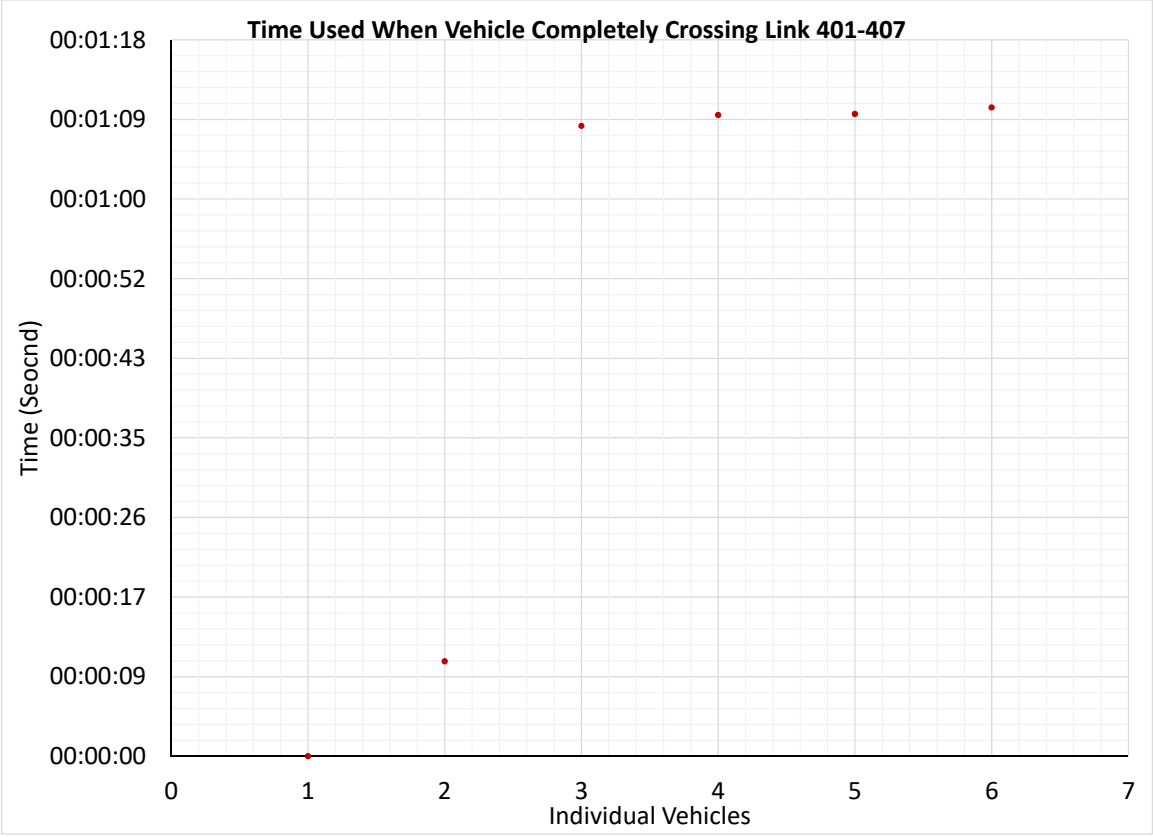

Figure 57 Field Travel Time of Vehicles Travelling along Link 401-407 between 16:02:30 and 16:02:40

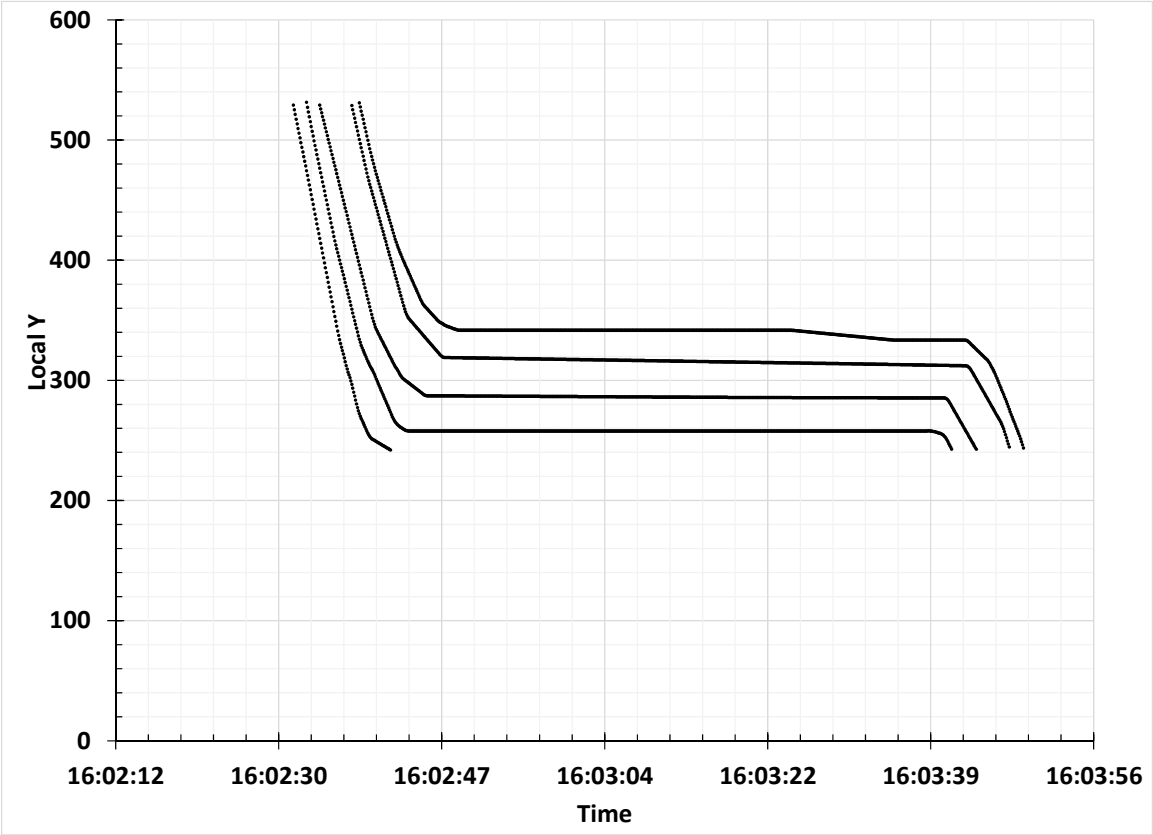

Figure 58 Trajectories of Vehicles Entering Link 401-407 between 16:02:30 and 16:02:40

Equation 59 provides a simple approach to estimate travel time along a signalized link that can be used for real-time traffic operations. It only uses the detector volume and time occupancy data. It does not rely on signal timing data to estimate the control delay or a delay model to estimate the queueing delay. In addition, neither roadway geometry nor vehicle length data are used.

7 CONCLUSION

Aiming to solve real-time traffic operation problems in the real world, this dissertation attempts to develop simple and direct approaches to estimate the vehicle queue length and travel time along signalized arterial links for real-time traffic operations. The approaches developed minimize modeling assumptions for implementation and utilize detector data that are commonly available like detector volume, speed and time occupancy.

With smart phone users everywhere and connected/automated vehicles emerging, vehicle trajectory data will become widely available for traffic operation agencies. This dissertation is the first to demonstrate a process using vehicle trajectory data to generate detector volume, speed and time occupancy data, along with the generalized flow rate, density and space mean speed data. This approach improves detector data accuracy, and minimizes detector over-counting and miss-counting issues. The detection zone can be of any shape or size and at any location along the trajectory. In addition, the data collection time interval is flexible.

7.1 Detector Volume, Speed and Time Occupancy

The relationships among detector volume, speed and time occupancy along signalized arterials are analyzed theoretically and experientially. They are different from the relationships of the freeway data. The signalized arterial data are more scattered because traffic flow on signalized arterials is periodically interrupted by traffic signals and vehicles go through deceleration, stop and acceleration constantly. However, if the generalized definitions of flow rate, density and space mean speed are used, the fundamental relationship, $v = ds$, holds valid in a signalized

arterial environment. Figure 27 demonstrates the fundamental relationship plotted using field signalized arterial data, which has not been seen in any of the literatures reviewed.

In addition, within the defined time-space rectangular $Region\ ABCD$ as shown in Figure 26 and assuming vehicles completely crossing the detector during the data collection period, the generalized density and the detector time occupancy has a relationship of $d = \frac{O_{time}}{L_v+L_d}$. This means if the percentage of heavy vehicles is very low, the scatter diagram of the generalized density and the detector time occupancy will present a strong linear correlation. The main reason that the perfect linear correlation is seldom seen in most previous studies is because most studies don't have the generalized density data available and usually use the ratio of detector volume to detector speed as the estimated detector density.

Simply converting detector volume counts within one data collection time period to use as the generalized flow rate will introduce estimation errors. There are two major reasons. In Equation 43, if vehicles don't completely cross the detector during the data collection time period, the total distance traveled by all vehicles divided by the detection zone length L_d plus the average physical vehicle length L_v, $\frac{\sum_{i=1}^{n} y_i}{(L_v+L_d)}$, will not equal to the number of vehicles n. In this case, the generalized flow rate will not be $\frac{n}{T}$. Furthermore, converting detector volume counts to use as the generalized flow rate always assumes that vehicles would evenly spread across the data collection time period when crossing the detection zone. This study provides a practical method to identify the minimum data collection time period needed to collect the accurate field flow rate data.

Traffic flow intensity is introduced and defined within the time-space regions as defined in Figure 36. It represents the number of vehicles that would have crossed the detection zone if the traffic condition has remained the same as the traffic condition measured when detectors are occupied by vehicles, throughout the entire data collection time period. Traffic flow intensity is calculated as $v = \frac{V_{detector}}{O_{time} \times T}$. It provides much more accurate description of the traffic flow condition than directly using the detector volume counts divided by the data collection time interval.

Future research is needed to develop the arterial fundamental diagrams to describe the relationships among the detector volume, speed and time occupancy, and the generalized flow rate, space mean speed and density along signalized urban arterial links.

7.2 Vehicle Queue Length

Based on analyses of the theoretical and field cumulative input-output diagrams, two major improvements are proposed to improve the performance of the input-output technique. The first improvement is to adjust the vehicle counts using time occupancy thresholds to take into account the condition that a vehicle stops on top of the detector. In this dissertation, when the time occupancy is above the threshold, the vehicle counts will not be used as inputs or outputs for the estimation. The second improvement is to reset the value of the number of entering vehicles, whenever the cumulative number of exiting vehicles is more than the cumulative number of entering vehicles. Both improvements produce estimation results far better than the estimation

without using the proposed improvements. Especially, the performance of the Kalman Filter model is significantly improved when the vehicle counts are adjusted based on time occupancy thresholds.

In addition, based on the analysis of the time-space diagram, the queue length should be recorded at the end of each data collection time period so that all vehicles crossing the input detector or the output detector during the data collection time period can be accounted for consistently.

Further research is needed in order to determine the optimum value of the threshold values used to adjust the vehicle counts. In order to prove the statistical significance of the proposed improvements, more research efforts utilizing field data from various locations and various time periods are necessary. In addition, input-output techniques can be further improved to handle long queues extending beyond the input detector.

7.3 Travel Time

A simple conservation law approach is developed to estimate travel time using widely available detector volume, speed and time occupancy data. Inputs used include the traffic flow intensity at input and out detectors, plus the initial vehicle queue. The estimated travel time is tested with the field travel time data generated using the NGSIM data to evaluate the performance of the estimation. The estimated travel time changes follow the field travel time changes very closely. The developed model is also compared with the NCHRP Project 3-79 model and the Little's Law queueing theory model. The developed model performs much better for per short interval travel

time estimation. Considering the data collection time period is 10 seconds, it is anticipated that the estimated travel time has a 10-second difference from the field travel time.

The proposed approach only uses the detector volume and time occupancy data. It does not rely on signal timing data to estimate the control delay or a delay model to estimate the queueing delay. In addition, neither roadway geometry nor vehicle length data are used. Further research is needed to estimate travel time along a signalized link, where the input detector is located at the mid-link location. Further research is also needed to estimate travel time along an arterial route, composed of multiple signalized links.

8 REFERENCES

1. *Highway Capacity Manual (HCM) 2000*. Transportation Research Board, National Research Council, Washington, D.C., 2000, Chapter 15.
2. Federal Highway Administration Office of Operations "Operations Performance Measurement". http://www.ops.fhwa.dot.gov/perf_measurement/index.htm, visited July 5, 2011.
3. Wu, J., Jin, X., Horowitz, A. Comparison of Queue Estimation Models at Traffic Signals. Accepted for presentation at the 18th World Congress on Intelligent Transportation Systems, 2011.
4. *Traffic Detector Handbook—Second Edition*. Institute of Transportation Engineers, Washington, D.C., 1990.
5. Riggio, P., Wu, J. Lower Manhattan Construction Command Center Intelligent Transportation System Detector Beta Test Report. JHK Engineering, P.C., New York, April 2009.
6. Turner, S., Eisele, W., Benz, R., Holdener, D. *Travel Time Data Collection Handbook*. Texas Transportation Institute, March 1998.
7. Click, S, Boden, E. Real Time Traffic Signal Delay Estimation using State-of-the-Practice Detection Technology: A Simulation Proof-of-Concept. In the 89th Annual Meeting of the Transportation Research Board. CD-ROM. TRB, National Research Council, Washington, D.C., January 2010.
8. Boden, E, Click, S. Real Time Traffic Signal Delay Estimation using State-of-the-Practice Detection Technology. In the 90th Annual Meeting of the Transportation Research Board. CD-ROM. TRB, National Research Council, Washington, D.C., January 2011.
9. Geroliminis N., Skabardonis, A. Queue Spillovers in City Street Networks with Signal-Controlled Intersections. In the 89th Annual Meeting of the Transportation Research Board. CD-ROM. TRB, National Research Council, Washington, D.C., January 2010.
10. Wu, X., Liu, H., Geroliminis, N. An empirical analysis on the arterial fundamental diagram. *Transportation Research Part B, Vol. 45, Issue 1*, Elsevier Ltd., United Kingdom, 2011, pp. 255-266.
11. Zhang, H. M. Link-Journey-Speed Model for Arterial Traffic. In *Transportation Research Record: Journal of the Transportation Research Board, No. 1676*, TRB, National Research Council, Washington, D.C., 1999, pp. 109-115.
12. SRF Consulting Group, Inc. Ramp Queue Detection Final Report. SRF Consulting Group, Inc, January 2009.
13. Green, M., Fontaine, M., Smith, B. Investigation of Dynamic Probe Sample Requirements for Traffic Condition Monitoring. . In *Transportation Research Record:*

Journal of the Transportation Research Board, No. 1870, TRB, National Research Council, Washington, D.C., 2004, pp. 55-61.

14. Hellinga, B., Fu, L. Reducing bias in probe-based arterial link travel time estimates. *Transportation Research Part C, Vol. 10, Issue 4*, Elsevier Ltd., United Kingdom, 2002, pp. 257-273.

15. Kwong, K., Kavaler, R., Rajagopal, R., Varaiya, P. Arterial travel time estimation based on vehicle re-identification using wireless magnetic sensors. *Transportation Research Part C, Vol. 17, Issue 6*, Elsevier Ltd., United Kingdom, 2009, pp. 586-606.

16. Haoui, A., Kavaler, R., Varaiya, P. Wireless magnetic sensors for traffic surveillance. *Transportation Research Part C, Vol. 16, Issue 3*, Elsevier Ltd., United Kingdom, 2008, pp. 294-306.

17. Sun, C., Arr, G., Ramachandran, R.P. Vehicle Reidentification as Method for Deriving Travel Time and Travel Time Distributions: Investigation. In *Transportation Research Record: Journal of the Transportation Research Board, No. 1826*, TRB, National Research Council, Washington, D.C., 2003, pp. 25-31.

18. Abdulhai, B., Tabib, S.M. Spatio-temporal inductance-pattern recognition for vehicle re-identification. *Transportation Research Part C, Vol. 11, Issues 3-4*, Elsevier Ltd., United Kingdom, 2003, pp. 223-239.

19. Wasson, J., Sturdevant, J., Bullock, D. Real-Time Travel Time Estimates Using Media Access Control Address Matching. *ITE Journal*, June 2008, pp. 20-23.

20. Quayle, S., Koonce, P., DePencier, D., and Bullock, D. Arterial Performance Measures Using MAC Readers: Portland Pilot Study. In the 89th Annual Meeting of the Transportation Research Board. CD-ROM. TRB, National Research Council, Washington, D.C., January 2010.

21. "Wireless Connections and Bluetooth Security Tips", https://www.fcc.gov/consumers/guides/how-protect-yourself-online, visited November 11, 2016.

22. Clark, S., Grant-Muller, S., Chen, H. Cleaning of Matched License Plate Data. In *Transportation Research Record: Journal of the Transportation Research Board, No. 1804*, TRB, National Research Council, Washington, D.C., 2002, pp. 1-7.

23. TransCore ITS, LLC. http://www.transcore.com/, visited April 27, 2011.

24. Hellinga, B. Automated Vehicle Identification Tag-Matching Algorithms for Estimating Vehicle Travel Times: Comparative Assessment. In *Transportation Research Record: Journal of the Transportation Research Board, No. 1774*, TRB, National Research Council, Washington, D.C., 2001, pp. 106-114.

25. Herrera, J., Work, D., Herring, R., Ban, X., Jacobson, Q., Bayen, A. Evaluation of traffic data obtained via GPS-enabled mobile phones: The Mobile Century field experiment. *Transportation Research Part C, Vol. 18, Issue 4*, Elsevier Ltd., United Kingdom, 2010, pp. 568-583.

26. Hellinga, B., Izadpanah, P., Takada, H., Fu, L. Decomposing travel times measured by probe-based traffic monitoring systems to individual road segments. *Transportation Research Part C, Vol. 16, Issue 6*, Elsevier Ltd., United Kingdom, 2008, pp. 768-782.

27. Kuhne, R., Michalopoulos, P. *Revised Monograph on Traffic Flow Theory, Chapter 5, Continuum Flow Models*. https://www.fhwa.dot.gov/publications/research/operations/tft/, visited July 30, 2016.

28. Rouphail, N., Tarko, A., Li, J. *Revised Monograph on Traffic Flow Theory, Chapter 9, Traffic Flow at Signalized Intersections*. https://www.fhwa.dot.gov/publications/research/operations/tft/, visited July 30, 2016.

29. Webster, F. Traffic signal settings. *Road Research Technical Paper 39*. Road Research Laboratory, Her Majesty's Stationery Office, London, 1958.

30. Sharma, A., Bullock D., Bonneson, J. Input-Output and Hybrid Techniques for Real-Time Prediction of Delay and Maximum Queue Length at Signalized Intersections. In *Transportation Research Record: Journal of the Transportation Research Board, No. 2035*, TRB, National Research Council, Washington, D.C., 2007, pp. 69-80.

31. NCHRP Project 3-79 Report. *Measuring the Performance of Automobile Traffic on Urban Streets*. TRB, National Research Council, Washington, D.C., 2008.

32. Vigos, G., Papageorgiou, M., Wang, Y. Real-time estimation of vehicle-count within signalized links. *Transportation Research Part C, Vol. 16, Issue 1*, Elsevier Ltd., United Kingdom, 2008, pp. 18-35.

33. Wu, J., Jin, X., Horowitz, A. Methodologies for Estimating Vehicle Queue Length at Metered On-Ramps. In *Transportation Research Record: Journal of the Transportation Research Board, No. 2047*, TRB, National Research Council, Washington, D.C., 2008, pp. 75-82.

34. Papageorgiou, M., Vigos, G. Relating time-occupancy measurements to space-occupancy and link vehicle-count. *Transportation Research Part C, Vol. 16, Issue 1,* Elsevier Ltd., United Kingdom, 2008, pp. 1-17.

35. Lee, J., Jiang, R., Chung, E. A Kalman Filter Based Queue Estimation Algorithm Using Time Occupancies for Motorway On-ramps. In the 92nd Annual Meeting of the Transportation Research Board. CD-ROM. TRB, National Research Council, Washington, D.C., January 2013.

36. Vigos, G., Papageorgiou, M. A Simplified Estimation Scheme for the Number of Vehicles in Signalized Links. *IEEE Transactions on Intelligent Transportation Systems, Vol. 11, Issue 2*, Piscataway, NJ, 2010, pp. 312-321.

37. Wu, J., Jin, X., Horowitz, A., Gong, D. Experiment to Improve Estimation of Vehicle Queue Length at Metered On-Ramps. In *Transportation Research Record: Journal of the Transportation Research Board, No. 2099*, TRB, National Research Council, Washington, D.C., 2009, pp. 30-38.

38. Lighthill, M., Whitham, G. On kinematic waves. I. Flood movement in long rivers. *Proceedings of the Royal Society of London. Series A, Mathematical and Physical Sciences, Vol. 229, No. 1178*, Piccadilly, London, 1955, pp. 281-316.

39. Lighthill, M., Whitham, G. On kinematic waves. II. A theory of traffic flow on long crowded roads. *Proceedings of the Royal Society of London. Series A, Mathematical and Physical Sciences, Vol. 229, No. 1178*, Piccadilly, London, 1955, pp. 317-345.

40. Richards, P. Shock waves on the highway. *Operations Research, Vol. 4, No. 1*, 1956, pp. 42–51.

41. Stephanopoulos, G., Michalopoulos, P., Stephanopoulos, G. Modelling and analysis of traffic queue dynamics at signalized intersections. *Transportation Research Part A, Vol. 13A, Issue 5*, Elsevier Ltd., United Kingdom, 1979, pp. 295-307.

42. Michalopoulos, P., Stephanopoulos, G. An application of shockwave theory to traffic signal control. *Transportation Research Part B, Vol. 15, Issue 1*, Elsevier Ltd., United Kingdom, 1981, pp. 35–51.

43. Liu, H., Wu, X., Ma, W., Hu, H. Real-time queue length estimation for congested signalized intersections. *Transportation Research Part C, Vol. 17*, *Issue 4*, Elsevier Ltd., United Kingdom, 2009, pp. 412-427.

44. Wu, X., Liu, H., Gettman, D. Identification of oversaturated intersections using high-resolution traffic signal data. *Transportation Research Part C, Vol. 18*, *Issue 4*, Elsevier Ltd., United Kingdom, 2010, pp. 626-638.

45. Liu, H., Ma, W., Wu, X., Hu, H. Real-time estimation of arterial travel time under congested conditions. *Transportmetrica*, Volume 6, Issue 3, 2010.

46. Viti, F., van Zuylen, H.J. Modeling Queues at Signalized Intersections. In *Transportation Research Record: Journal of the Transportation Research Board, No. 1883*, TRB, National Research Council, Washington, D.C., 2004, pp. 68-77.

47. Viti, F., van Zuylen, H.J. Probabilistic models for queues at fixed control signals. *Transportation Research Part B, Vol. 44, Issue 1,* Elsevier Ltd., United Kingdom, 2010, pp. 120-135.

48. Van Zuylen, H.J., Viti, F. The Dynamics and the Uncertainty of Queues at Fixed and Actuated Controls: A Probabilistic Approach *Journal of Intelligent Transportation Systems, Volume 13, Issue 1*, Taylor & Francis Group, LLC., United Kingdom, 2009, pp.39–51.

49. Viti, F., van Zuylen, H.J. A probabilistic model for traffic at actuated control signals. *Transportation Research Part C, Vol. 18, Issue 3,* Elsevier Ltd., United Kingdom, 2010, pp. 299-310.

50. Zheng, F., van Zuylen, H.J. Uncertainty and Predictability of Urban Link Travel Time: A Delay Distribution Based Analysis. In the 89th Annual Meeting of the Transportation Research Board. CD-ROM. TRB, National Research Council, Washington, D.C., January 2010.

51. Sanchez, R., Horowitz, R., Varaiya, P. Analysis of queue estimation methods using wireless magnetic sensors. In the 90th Annual Meeting of the Transportation Research Board. CD-ROM. TRB, National Research Council, Washington, D.C., January 2011.

52. Prikryl, J., Kocijan, J. An Empirical Model of Occupancy-Queue Relation. 12th International Federation of Automatic Control (IFAC) Symposium on Control in Transportation Systems, Redondo Beach, CA, September, 2009.

53. Comert, G., Cetin, M. Queue length estimation from probe vehicle location and the impacts of sample size. *European Journal of Operational Research, Vol. 197, Issue 1,* Elsevier Ltd., United Kingdom, 2009, pp. 196–202.

54. Ban, X., Hao, P., Sun, Z. Real time queue length estimation for signalized intersections using travel times from mobile sensors. *Transportation Research Part C, Article in Press,* Elsevier Ltd., United Kingdom, 2011.

55. Cheng, Y., Qin, X., Jin, J., Ran, B. An Exploratory Shockwave Approach for Signalized Intersection Performance Measurements Using Probe Trajectories. In the 89th Annual Meeting of the Transportation Research Board. CD-ROM. TRB, National Research Council, Washington, D.C., January 2010.

56. Cheng, Y., Qin, X., Jin, J., Ran, B., Anderson, J. Cycle by Cycle Queue Length Estimation for Signalized Intersections Using Sampled Trajectory Data. In the 90th Annual Meeting of the Transportation Research Board. CD-ROM. TRB, National Research Council, Washington, D.C., January 2011.

57. Muck, J. Using detectors near the stop-line to estimate traffic flows. *Traffic Engineering and Control 43*, 2002, pp. 429–434.

58. Akcelik, R., Besley, M. Queue Discharge Flow and Speed Models For Signalised Intersections. Proceedings of the 15th International Symposium on Transportation and Traffic Theory, Elsevier Ltd., United Kingdom, 2002.

59. Skabardonis, A., Geroliminis N. Real-time estimation of travel times on signalized arterials. *Proceedings 16th International Symposium on Transportation and Traffic Theory*, Elsevier Ltd., United Kingdom, 2005, pp. 387–406.

60. Skabardonis, A., Geroliminis, N. Real-time Monitoring and Control on Signalized Arterials. *Journal of Intelligent Transportation Systems, Volume 12, Issue 2*, Taylor & Francis Group, LLC., United Kingdom, 2008, pp.64–74.

61. Heidemann, D. Queue length and delay distributions at traffic signals. *Transportation Research Part B, Vol. 28, Issue 5,* Elsevier Ltd., United Kingdom, 1994, pp. 377–389.

62. Akcelik, R., Rouphail, N. Estimation of delays at traffic signals for variable demand conditions. *Transportation Research Part B, Vol. 27, Issue 2,* Elsevier Ltd., United Kingdom, 1993, pp. 109–131.

63. Kimber, R., Hollis, E. Traffic Queues and Delays at Road Junctions. *Transport and Road Research Laboratory Report 909*. Transport and Road Research Laboratory, United Kingdom, 1979.

64. Dion, F., Rakha, H., Kang, Y. Comparison of delay estimates at under-saturated and over-saturated pre-timed signalized intersections. *Transportation Research Part B, Vol. 38, Issue 2,* Elsevier Ltd., United Kingdom, 2004, pp. 99-122.

65. Wang, H., Hobeika, A. Travel Time Estimation on Arterial Streets. In the 89th Annual Meeting of the Transportation Research Board. CD-ROM. TRB, National Research Council, Washington, D.C., January 2010.

66. Noroozi, R., Hellinga, B. A Method to Estimate the Distribution of Average Vehicle Delay at Signalized Intersections. In the 90th Annual Meeting of the Transportation Research Board. CD-ROM. TRB, National Research Council, Washington, D.C., January 2011.

67. Li, J., Rouphail, N., Tarko, A., Velichansky, L. Overflow Delay Model for Signalized Arterials. . In *Transportation Research Record: Journal of the Transportation Research Board, No.1555*, TRB, National Research Council, Washington, D.C., 1996, pp. 1-8.

68. Zheng, F., van Zuylen, H.J. Modeling Urban Travel Time Variability by Analyzing Delay Distribution for Signalized Urban Trips. In the 90th Annual Meeting of the Transportation Research Board. CD-ROM. TRB, National Research Council, Washington, D.C., January 2011.

69. Lei, H., Zhou, X., List, G., Taylor, J. http://www.tandfonline.com/doi/full/10.1080/23311916.2014.990672, visited December 5, 2016.

70. Daganzo, C. The cell transmission model: A dynamic representation of highway traffic consistent with the hydrodynamic theory. *Transportation Research Part B, Vol. 28, Issue 4,* Elsevier Ltd., United Kingdom, 1994, pp. 269-287.

71. Daganzo, C. The cell transmission model, part II: Network traffic. *Transportation Research Part B, Vol. 29, Issue 2,* Elsevier Ltd., United Kingdom, 1995, pp. 79-93.

72. Munoz, L., Sun, X., Horowitz, R., Alvarez, L. Traffic density estimation with the cell transmission model. In the proceedings of the American Control 2003 Conference, Colorado, June 2003.

73. Colyar, J., Rouphail, N. Measured Distributions of Control Delay on Signalized Arterials. In *Transportation Research Record: Journal of the Transportation Research Board, No. 1852*, TRB, National Research Council, Washington, D.C., 2003, pp. 1-9.

74. Akcelik, R., Besley, M., Roper, R. Fundamental Relationships for Traffic Flows at Signalised Intersections. Research Report ARR 340. ARRB Transport Research Ltd, Vermont South, Australia, 1999.

75. Fu, L., Hellinga, B. Delay Variability at Signalized Intersections. In *Transportation Research Record: Journal of the Transportation Research Board, No. 1710*, TRB, National Research Council, Washington, D.C., 2000, pp. 215-221.

76. Liu, H. Travel Time Prediction for Urban Networks. Ph.D. Dissertation, Delft University of Technology, September 2008.

77. Liu, H., van Zuylen, H., van Lint, H., and Salomons, M. Predicting Urban Arterial Travel Time with State-Space Neural Networks and Kalman Filters. In *Transportation Research Record: Journal of the Transportation Research Board, No. 1968*, TRB, National Research Council, Washington, D.C., 2006, pp. 99-108.

78. Qian, B., Lee, J., Chung, E. Algorithm for Queue Estimation with Loop Detector of Time Occupancy in Off-Ramps on Signalized Motorways. In *Transportation Research Record: Journal of the Transportation Research Board, No. 2278*, TRB, National Research Council, Washington, D.C., 2012, pp. 50-56.

79. Cassidy, M., Coifman, B. Relation among average speed, flow, and density and analogous relation between density and occupancy. In *Transportation Research Record: Journal of the Transportation Research Board, No. 1591*, TRB, National Research Council, Washington, D.C., 1997, pp. 1-6.

80. Kim, Y., Hall, F. Relationships between occupancy and density reflecting average vehicle lengths. In *Transportation Research Record: Journal of the Transportation Research Board, No. 1883*, TRB, National Research Council, Washington, D.C., 2004, pp. 85-93.

81. Hall, F. *Revised Monograph on Traffic Flow Theory, Chapter 2, Traffic Stream Characteristics*. https://www.fhwa.dot.gov/publications/research/operations/tft/, visited July 30, 2016.

82. *Wavetronix SmartSensor HD User Guide*. http://www.wavetronix.com/en/support/downloads/494-smartsensor-hd-user-guide, visited July 18, 2016.

83. Edie, L. C. Discussion of Traffic Stream Measurements and Definitions. *Proceedings of Second International Symposium on the Theory of Traffic Flow*, Paris, France, 1965, pp. 139–154.

84. Edie, L. C. *Flow theories*, in *Traffic Science*, D. C. Gazis, Editor. John Wiley and Sons, Inc., New York, 1974, pp. 8–20.

85. Daganzo, C. *Fundamentals of Transportation and Traffic Operations*. Emerald Group Publishing Limited, 1997.

86. Next Generation Simulation (NGSIM). http://ops.fhwa.dot.gov/trafficanalysistools/ngsim.htm, visited April 3, 2016.

87. Home of the Next Generation Simulation Community. http://gateway.path.berkeley.edu/ngsimdocs/, visited April 3, 2016.

88. *Improved Simulation of Stop Bar Driver Behavior at Signalized Intersections*. Report No. N10-07. http://www.webpages.uidaho.edu/niatt/research/final_reports/klk712_n10-07.pdf, visited April 3, 2016.

89. Punzo, V., Borzacchiello, M., Ciuffo, B. On the assessment of vehicle trajectory data accuracy and application to the Next Generation SIMulation (NGSIM) program data. *Transportation Research Part C, Vol. 19, Issue 6*, Elsevier Ltd., United Kingdom, 2011, pp. 1243-1262.

90. *Evaluation of Ramp Meter Effectiveness for Wisconsin Freeways, A Milwaukee Case Study*. Report No. 0092-45-17. http://www.topslab.wisc.edu/its/rampmetering/milwaukee_ramp_meter.pdf, visited October 29, 2016.

91. *Highway Capacity Manual (HCM) 2010*. Transportation Research Board, National Research Council, Washington, D.C., 2010, Volume 1, Chapter 4.

92. Newell, G. F. *Applications of Queueing Theory, Second Edition*. Chapman and Hall, New York, 1982.

9 CURRICULUM VITAE

Jingcheng Wu, PE, PTOE

Education

Master of Science, Civil Engineering, University of Wisconsin – Milwaukee, 2001

Bachelor of Engineering, Design of General Planning and Transportation Engineering, Xi'an University of Architecture & Technology, 1998

Professional Experience

HDR, ITS Project Manager, Ft. Lauderdale, FL, 2012 – present

AECOM, Senior Systems Engineer, Sunrise, FL, 2011-2012

TransCore, Principle Engineer, New York, NY, 2006-2011

TransCore, ITS Engineer, Milwaukee, WI, 2001-2006

Publications

1. Improving Input-Output Technique for Queue Estimation along Signalized Links. In the 96th Annual Meeting of the Transportation Research Board. CD-ROM. TRB, National Research Council, Washington, D.C., January 2017.
2. Comparison of Queue Estimation Models at Traffic Signals. Presented at the 18th World Congress on ITS, 2011.
3. Urban Arterial Performance Measurement — Proof of Concept. Presented at the 18th World Congress on ITS, 2011.
4. Propensity to Telecommute: Exploring the National Household Travel Survey. In the 90th Annual Meeting of the Transportation Research Board. CD-ROM. TRB, National Research Council, Washington, D.C., January 2011.
5. Experiment to Improve Estimation of Vehicle Queue Length at Metered On-Ramps. In *Transportation Research Record 2099*, TRB, National Research Council, Washington, D.C. 2009, pp. 30-38.
6. Transferability of Time-of-Day Choice Modeling for Long-Distance Trips. In the 88th Annual Meeting of the Transportation Research Board. CD-ROM. TRB, National Research Council, Washington, D.C., January 2009.
7. Reforming Ramp Meter Queue Override. Presented at the 15th World Congress on ITS, 2008.
8. Methodologies for Estimating Vehicle Queue Length at Metered On-Ramps. In *Transportation Research Record 2047*, TRB, National Research Council, Washington, D.C. 2008, pp. 75-82.
9. Experimental Measurement of Diversion Due to Ramp Meters. In *Transportation Research Record 1985*, TRB, National Research Council, Washington, D.C. 2006, pp. 188-197.

10. Evaluation of Ramp Meter Effectiveness for Wisconsin Freeways, a Milwaukee Case Study. *Federal Highway Administration Report No. 0092-45-17*. October 2004.
11. Distributed Concept in ATMS Software. 2003 IEEE Intelligent Transportation Systems Proceedings, vol. 2, pp. 1295-1298. October 2003.